TECHNISCHE UNIVERSITÄT WIEN
Vienna University of Technology

MASTER'S THESIS

Concrete Faced Sand-Gravel Dams, Stressed Deformation Analysis and Case Studies about Preliminary Design of Sarigüzel Dam.

Thesis for the Master of Science

Thesis Adviser: Univ.Prof. Dipl.-Ing. Dr.techn. Peter Tschernutter
[Institute of Hydraulic Engineering and Water Resources Management]
[Vienna University of Technology]

Second Advisor: Dr.-Ing. Ronald Haselsteiner
[Fichtner GmbH & Co. KG, Turkey]

A Thesis Submitted to Vienna University of Technology
Faculty of Civil Engineering

By

Author: Hans-Martin Leitner

Matriculation number: 0326313

5721 Piesendorf, Hauserberg 413

Vienna, the 1st of October, 2010   Signature

Abstract

This paper highlights the differences, developments and up-to date principles for design, zoning and construction of concrete faced rockfill dams and concrete faced sand gravel fill dams. Design and fundamentals of five dams in operation is presented herein. Special emphasis is put on deformation behavior and analyses of concrete faced dams. Therefore, the stress strain behavior of rockfill is illustrated and compared to the stress strain behavior shown by the well known Mohr-Coulomb and the so called Hardening Soil model, an advanced Duncan-Chan model.

For a better understanding on the deformation behavior and analyses of the preliminary design of Sarigüzel dam, showing the differences of Mohr-Coulomb and Hardening Soil model. For the analyses the software package Plaxis 2D was applied.

Furthermore, special features in numerical modeling the stress strain behavior of stiff rockfills in contrast to weak rockfills is highlighted.

Acknowledgement

Table of Content

Table of Figures

List of Tables

List of Abbreviations

CFRD	Concrete faced Rockfill Dam
CFSGD	Concrete faced Sand Gravel Dam
HEPP	Hydro Electric Power Plant
IWP&DC	International Water Power & Dam Construction
USSD	United States Society on Dams
USBR	United States Bureau of Reclamation
AS	Australian Standard
SDVR	Smooth drum vibratory roller
USCS	Unified soil classification system
MC	Mohr – Coulomb
DC	Duncan – Chan
HS	Hardening soil
SPT test	Standard penetration test
HS SG	Hardening Soil Sand Gravel
MC SG	Mohr-Coulomb Sand Gravel
HS WR	Hardening Soil Weak Rockfill
MC WR	Mohr-Coulomb Weak Rockfill

1 Executive Summary

This paper highlights the differences of concrete faced rockfill dams and concrete faced sand gravel dams, both of them enjoying, increasing popularity in recent years. Developments and actual principles in design, zoning and construction are summarized herein. Special emphasis is put on deformation analysis of concrete faced dams. Therefore the natural stress strain behavior of rockfills is illustrated and compared to the stress strain behavior reproduced by two constitutive models. Advantages and disadvantages in accurately reproducing natural rockfill behavior by the well known Mohr-Coulomb model and the so called Hardening Soil model (an advanced model, close to Duncan-Chan model) are presented. These two constitutive models are incorporated in Plaxis 2D software package, utilized in all analysis.

The information gained from the former mentioned, is applied to deformation analysis about the preliminary design of Sarigüzel dam, impounding the river ceyhan, located in turkey. Sarigüzel dam is provided as an 82m high CFSGD constructed on 30m deep alluvial disposals. Part of the research work was to study the impact of the two above mentioned constitutive models on the dam's deformation behavior as well as the influence of varying parameter sets.

To adjust the design and deformation analysis of Sarigüzel dam, an extensive study about similar dams in operation was undertaken. Design and deformation behavior of five CFSGD is presented herein.

A further aspect of this thesis was to highlight differences in numerically modeling the stress strain behavior of stiff rockfills (i.e. alluvial sand gravel, quarried rockfill obtained from high strength rock) in contrast to weak rockfills (i.e. quarried rockfill obtained from low strength rock < 30 MN/m^2). Again the impact of MC and HS model is researched for weak rockfill analysis.

2 Introduction

As economical and technical feasible dam sites reduce all over the world. Building dams on sites of complicated technical character will only meet economical feasibility, if construction costs are lowered drastically. The engineers challenge is to do so without lowering a dam's safety level. CFRDs enjoy increasing popularity in recent years, because they meet both demands. However, suitable rockfill obtained from quarried high strength rock is not always available in economic distances, while in many cases alluvial deposits exist in abundance very close to site. Alluvial deposits do have their own weakness as discussed later, but one of their advantages is the low cost exploitation from borrow pits. One further method, helping to lower construction costs, is to construct the dam's embankment directly on alluvial deposits, ensuring the impermeability by cut off walls connected to the concrete slab. While CFRDs rely on their unsaturated downstream shoulder, sandy gravel fill material does not always show free draining character. Hence, a new dam design came up, accounting for sand gravel fill's specific properties.

3 Scope and Outline

Scope of this thesis was to gain better understanding of CFSGDs in general with special emphasis put on its deformation behavior and its characteristics in modeling deformations. The finite element method is utilized to do so. The probability of face slab cracking as well as rupturing of joints is calculated and evaluated.

Wetting effects are not part of the finite element analysis. Due to the rounded particle shape and the saturated conditions, alluvial sand gravel fill is not significantly influenced by wetting. As this thesis deals with the preliminary design of Sarigüzel dam, there is a lack of information about the cut off wall's technical properties. As a consequence, the probability of cracks potentially occurring cannot be estimated.

4 Concrete Faced Rockfill and Sand-Gravel Dams

4.1 General

Concrete Faced Rockfill Dams (CFRDs) became most popular in recent years. Decisions in what type of dam should be applied are normally economical decisions and no safety decisions. However, modern CFRDs meet both demands. Cooke and Sherard (1987), and Fitzpatric et al. (1985) discussed Factors, leading to CFRDs as most economic alternative.

- Small quantities of embankment fill because of steep slopes leading to cost reduction.
- Time independent embankment construction and grouting measures.
- Advantages in humid climate. Embankment filling during winter and rain periods leads to fast construction and further cost reduction.
- High values of leakage do not affect stability, because of the materials free draining character.
- Non availability of suitable earthfill.

According to Pritchard (2008) further advantages are:

- No piping.
- Safer river diversion.
- Easy to find equipment.
- Use of almost all types of rock.

According to ICOLD (2005) CFRDs provide many features in design, construction and schedule. Some of them are listed in extracts here.

Design:

- Due to the fact that the entire rockfill is behind the impervious membrane, CFRDs reach factors of sliding safety up to 7 and sometimes higher.
- No pore water pressure can build up in case of seismic loading, due to the rock fill's free draining character. CFRDs stay inherent safe in case of an earthquake.

- Failure mechanisms for CFRDs are limited to two mechanisms.
  - Erosion by overtopping.
  - Piping of residual or sedimentary soils in the foundation.
- Little instrumentation for safety monitoring (only surveillance monitoring, i.e. leakage and concrete face movements).

Construction and Schedule:

- Less haul road lengths due to the permission of ramps within the dam body.
- Construction works for plinth and grout curtain do not interfere embankment rising.

A differentiation between "classical" rockfill and sand gravel fills has to be made: Classical rockfill is normally obtained from quarries by blasting, resulting in particles of angular shape. Due to high contact forces, angular shaped particles tend to grain breakage, resulting in a lower deformation modulus. Furthermore angular shaped grains tend to large collapse settlements on wetting, especially when low strength (weak) rockfill is used. Both effects are undesirable. In general high deformations lead to high leakage.

In contrast, sand gravel fill has many favorable properties. As there are:

- Sand gravel material is a cost effective alternative, because it is obtained from borrow pits.
- Due to the particles rounded shape, very high moduli may be reached.

But there are also a few drawbacks:

- CFSGDs may require additional drainage zones, if the fill material is not free draining, which is the case usually.
- Construction in winter is limited, because adding water is necessary during compaction and the materials high fines content in some cases.

4.2 CFRDs Worldwide

Increasing numbers of CFRDs all over the world show, that this dam type is economic in dry climate too. Figure 1 shows the number and distribution of CFRDs worldwide. The people's republic of china is heading the statistics in number and since 2003 also in dam height with Shuibuya the tallest CFRD in the word. There are prefeasibility studies for even higher CFRDs up to 340m (Rumei).
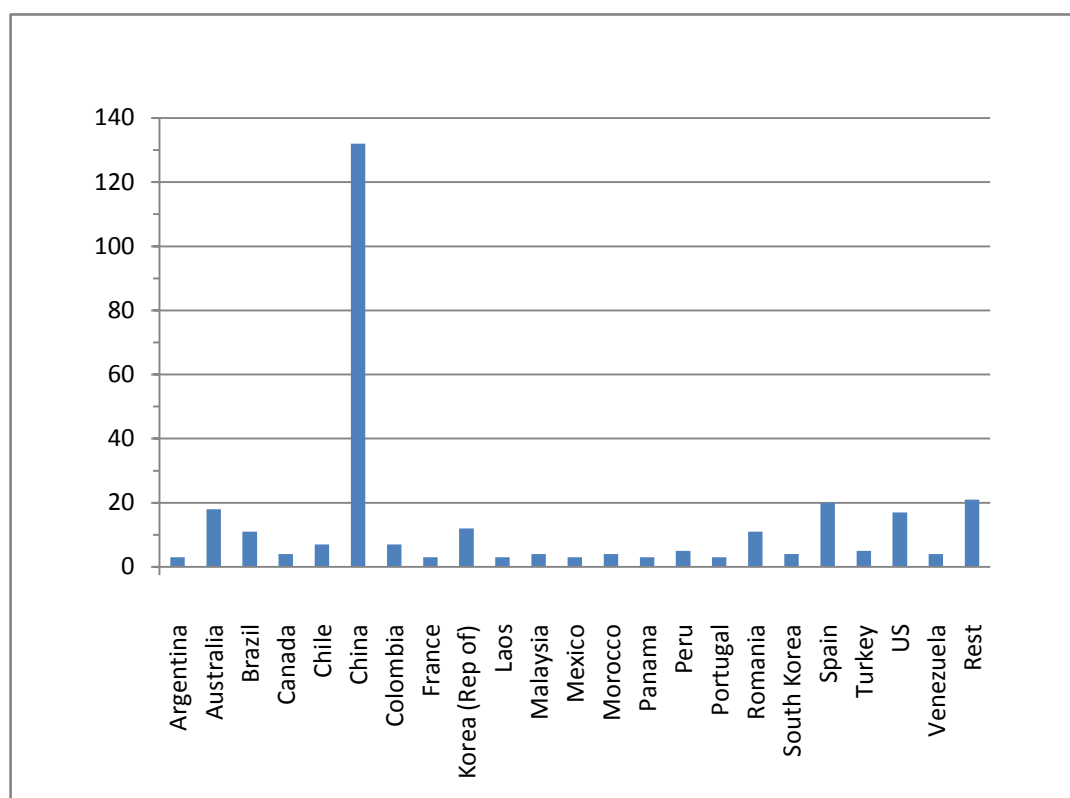
Figure 1 CFRDs worldwide.

Figure 2 shows the number of completed CFRDs and the average dam height plotted against the axis of time. While the number of finished dams doubled from 1980 the average dam height remained approximately constant. The trend in maximum dam height is obvious. Only used for heights lower than 150m in the past, CFRDs play in the upper league since the early 1980s, heading for new records in dam construction.
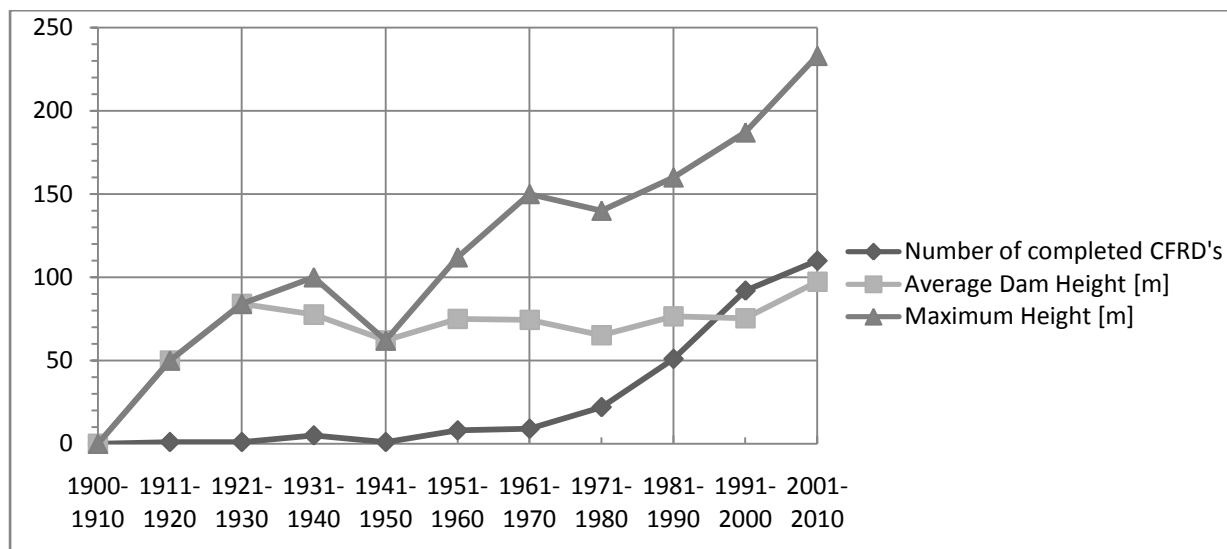
Figure 2 Number of completed CFRDs, average and maximum height observed in the last 110 years.

4.3   Concrete Faced Sand-Gravel Dams (CFSGDs) in practice

CFSGDs seem to enjoy increasing popularity all over the world, as many planed dams will be of this type. Dams currently in operation are: Aquamilpa (Mexico), Puclaro (Chile), Salvajina (Colombia), Gollilas (Colombia), Santa Juana (Chile), Wuluwati (China), Tankeng (China), Siping (China), Gudongkou (China), Heiquan (China), Chahanwusu (China), Nalan (China), Grotty (Australia) . Some of the above mentioned, are displayed as case studies in chapter: 9 CFSGDs - Case Studies taken from Literature.

It should be noted, that the notation "sand gravel" as used for embankment dams worldwide, is apparently not restricted to gradations limited by the unified soil classification system (USCS). In many cases dams denoted as CFSGD show grain size distributions that are typically rockfill gradations, but were obtained from alluvial deposits. Thus highly affecting the permeability and of course the dams zoning.

Excluding Gouhou and Aquamilpa dam, most CFSGDs have performed very well. Due to its high deformation modulus, most dams show small to very small leakage rates (compared to other CFRDs).

According to Wang and Qu, (2000) sand gravel fill has its own weakness. The gradation curves of different borrow pits vary strongly, which will result in an inhomogeneous embankment. Due to the natural deposition of alluvial soils, its grain size distribution often lacks of several grain sizes, making the seepage stability a further disadvantage. Fur-

thermore, sand gravel fill tends to intense segregation during spreading, which will again increase the embankment's heterogeneousness.

4.4 State of the Art for Concrete Faced Dams

An extensive summary in the history of CFRD development can be found in Fell et al. (2005). In this chapter only a brief summary shall be given. Development of CFRDs is mainly based on an empirical approach. In the early stages of CFRD construction, dumped and sluiced rockfill was used without compaction in lifts up to 50m. All CFRDs build before 1967 are of dumped rockfill (IWP&DC Yearbook 2009).

Dumping in such lifts lead to segregation, high deformation during impounding and resulted in cracks of the concrete sealing. Nowadays the rockfill material is placed in lifts of 0.3-2m depending on the dam's particular zone. Compaction work is typically done by a 10 to vibratory steel drum roller by a number of 4 to 8 passes. Due to the concrete face's casting, the upstream slope is normally fixed to V1:H1.5 (vertical to horizontal direction). The downstream slope is typically ranging from V1:H1.4-1.6, concerning on the used material's parameters. (Fell et al. 2005)

To give a short review on international literature concerning CFRD development, the following books shall be named: *Geotechnical Engineering of Dams* (Fell et al., 2005); *Concrete face rockfill dams: design, construction and performance*. (Cooke and Sherard, 1987); *Design of concrete faced rockfill dams*. (Fitzpatric et al., 1985); Recent *experience on design, construction and performance of CFRD dams*. (Marulanda and Pinto, 2000); *Concrete face rockfill dams. Construction features*. (Materon and Mori, 2000); *Rockfill dams with concrete facing. State-of-the-art*. International Committee on Large Dams, Paris. Bulletin 70. (ICOLD, 1989); *Concrete Face Rockfill Dams Concepts for Design and Construction*. Draft. (ICOLD, 2005).

4.5 Further Trends

There is a trend in building CFRDs on residual alluvial soils, resulting in a very economic dam design. However, even if the dam is built on alluvial soils, the plinth structure, in most cases, is constructed on suitable rock. Thus, making additional excavation and water retaining measures necessary for plinth construction. However, a cut off wall linked to the plinth structure lowers costs and construction time and consequently enjoys in-

creasing popularity.

The curb construction method of is now applied in nearly every new CFRD design, providing several improvements in construction costs and schedule.

Unfortunately there is a trend to accept high leakage values (up to several hundreds of liters per second), especially for high and very high dams.

A relatively new trend in joint design is, not to conduct the reinforcement trough the compression joints and to fill the joint with compressible materials (wood, rubber).

As pointed out in chapter: 4.2 CFRDs Worldwide, there is a trend to increase the maximum height of CFRDs. Due to the sand gravel's high deformation modulus, face slab deformations reduce in contrast to quarried rockfill. Consequently, it is assumed, that sand gravel fill will play a major role in super high CFRD construction.

5   Design Criteria and Principles

Figure 3 shows a longitudinal upstream view of a typical concrete facing. Figure 4 shows the main section of a typical CFRD. Figure 5 shows the section of a CFSGD. Its zoning varies strongly in international literature. This is thought to be due to the fact that CFSGDs are a relatively young dam type and its development is still on the way.
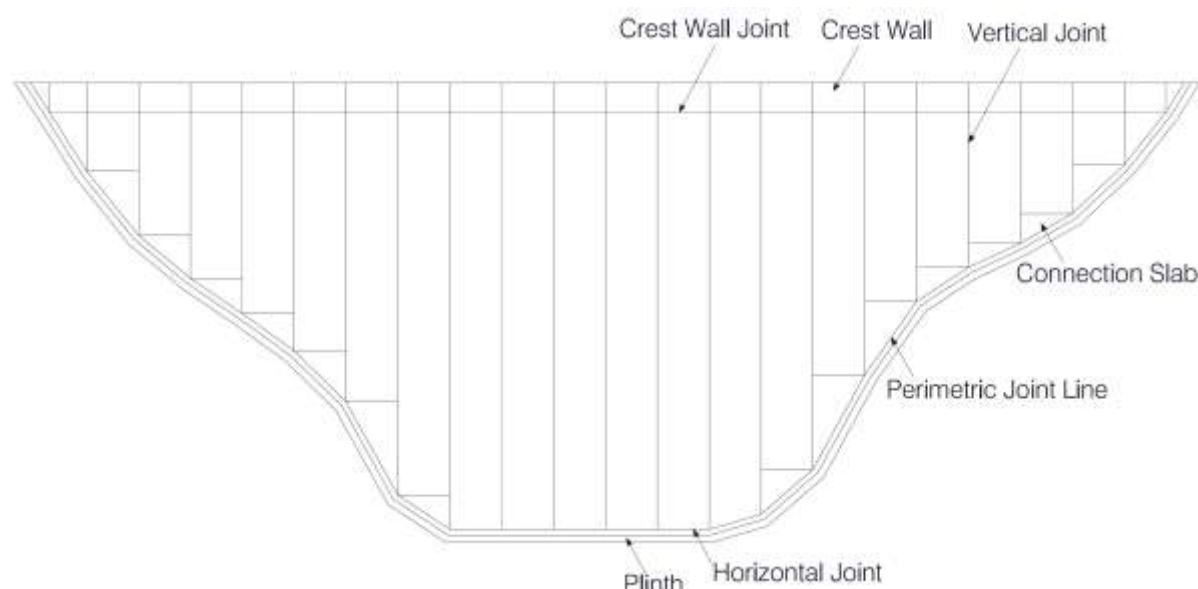
Figure 3 CFRD design, concrete face slabs and joint arrangement (adapted from ICOLD 1989a).
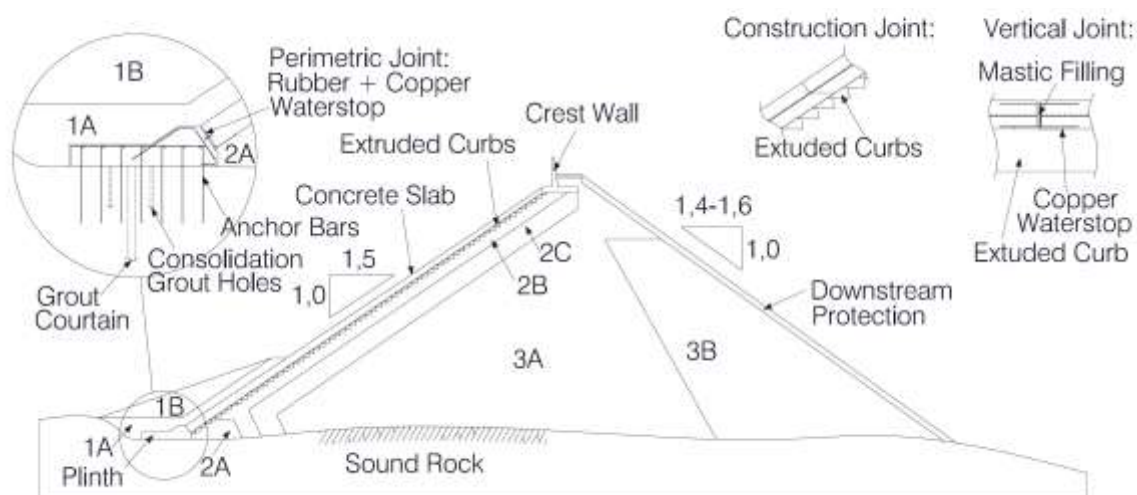
Figure 4 CFRD design, zoning (adapted from ICOLD 1989a).

Zones in Figure 4 are named as follows:

- 1A Selfhealing material.

- 1B Protection of selfhealing material.

- 2A Plinth support.

- 2B Cushion zone.

- 2C Transition material.

- 3A Upstream main fill material.

- 3B Downstream fill material.
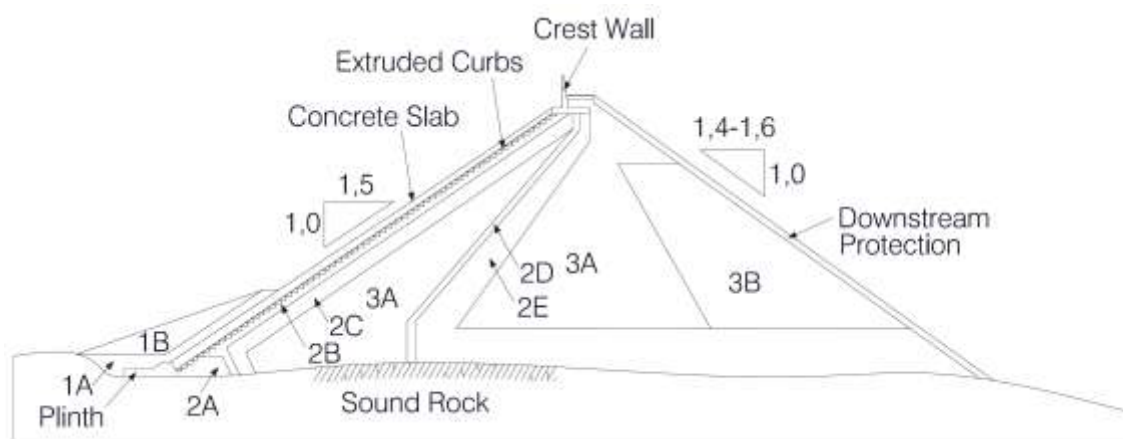
Figure 5 Typical CFSGD zoning (adapted from ICOLD 1989a).

Zones presented in Figure 5 are named as follows:

- 1A to 3B same notation as in Figure 4.

– 2D Filter zone.

– 2E Drainage zone.

Properties and specifications of all zones are discussed in chapter: 5.3 Zoning and Specifications.

5.1 Loads & Load cases

According to USSD (2007, p. 2):
> The stability of the upstream and downstream slopes of the dam embankment is analyzed for the most critical or severe loading conditions that may occur during the life of the dam. These loading conditions typically include:
> 1) End of Construction — when significant pore pressure development is expected either in the embankment or foundation during construction of the embankment.
> 2) Steady-State Seepage — when the long-term phreatic surface within the embankment has been established.
> 3) Rapid (or Sudden) Drawdown — when the reservoir is drawn down faster than the pore pressures can dissipate within the embankment after the establishment of steady-state seepage conditions.
> 4) Earthquake — when the embankment is subjected to seismic loading.

According to Wang, Y., and Qu, L., (2000), CFRDs constructed of classical rockfill (i.e. high compressive strength and free draining quarried material) even high leakage values do not affect stability, high leakage in this case is only an economical problem.

In CFSGD design seepage control is a more important part. Seepage control and zone stability is the main focus in design, due to the low scour resistance and the higher fines content of alluvial soils. They suggest that seepage control ….." should be carried out in the following order: first, prevention; second, limitation; third, drainage." (p. 428).

- Prevention: appropriate design and construction of face, plinth, joints and the grouting.

- Limitation: by the cushion zone in case joint rupturing.

- Drainage: lowering of the dam body's phreatic level by high permeable drainage zones with upstream protective filter zones, if necessary.

5.2 Required Factors of safety

Required factors of safety vary in guidelines all over the world. In general the "global" factor of safety depends on actual load conditions, but as discussed below, these factors do also vary due to site conditions, dam type and may in-/decrease due to measurements, specially taken to increase the accuracy in parameter determination. Table 1 shows required factors of safety, according to USBR.

Table 1 Required factors of safety (USSD 2007, p.23).

Agency	Loading Condition	Stress Parameter	F.S.
USBR	End of Construction – Pore pressures in embankment and foundation with laboratory determination of pore pressure and monitoring during construction	Effective	1.3
	End of Construction – Pore pressures in embankment and foundation with no laboratory determination and no monitoring during construction.	Effective	1.4
	End of Construction – Pore pressures in embankment only with or without field monitoring and no laboratory determination	Effective	1.3
	End of Construction	Undrained (Total)	1.3
	Steady-State Seepage from Active Pool	Effective	1.5
	Operational – Max Pool Level	Effective or Undrained	1.5
	Operational – Rapid Drawdown from Normal Pool	Effective or Undrained	1.3
	Operational – Rapid Drawdown from Max Pool		1.3
	Unusual		1.2

Fell et al. (2005) suggest to use varying factors of safety, by in- or decreasing a minimum acceptable factor of safety due to site dependent conditions. Table 2 shows the suggested minimum (i.e. baseline) factors of safety. Table 3 shows the recommended changes to the baseline factor of safety.

Table 2 Baseline recommended minimum acceptable factors of safety and load conditions (Fell et al., 2005, p 471).

Slope	Load condition	Reservoir characteristic	Minimum factor of safety
Upstream and downstream	End of construction	Reservoir empty	1.3
Downstream	Steady state seepage	Reservoir at normal maximum operating level (Full Supply Level)	1.5
Downstream	Maximum flood	Reservoir at maximum flood level	1.5, free draining crest zones, 1.3 otherwise
Upstream	Drawdown	Rapid drawdown to critical level	1.3

Note: These factors of safety apply to design of new high consequence of failure dams, on high strength foundations, with low permeability zones constructed of soil which is not strain weakening, using reasonably conservative shear strengths and pore pressures developed from extensive geotechnical investigations of borrow areas, laboratory testing and analysis of the results and using the methods of analysis detailed above. It is assumed there will be monitoring of deformations by surface settlement points during construction and during operation of the dams.

Table 3 Factors which influence the selection of factors of safety, and their effect on the baseline minimum factor of safety (Fell et al., 2005, p. 471).

Factor	Description	Recommended change to the baseline minimum factor of safety
Existing (vs new) Dam	A lower factor of safety may be adopted for an existing dam which is well monitored and performing well	0 to −0.1
Soil or weak rock foundation	A higher factor of safety may be needed to account for the greater uncertainty of the strength	0 to +0.2 for effective stress +0.1 to +0.3 for undrained strength analyses
Strain weakening soils in the embankment or foundation	A higher factor of safety may be needed to account for progressive failure, and greater displacements if failure occurs	0 to +0.2
Limited (little or no good quality) strength investigation and testing, particularly of soil and weak rock foundations	A higher factor of safety should be used to account for the lack of knowledge	+0.1 to +0.3 for effective stress analyses, +0.3 to +0.5 for undrained strength analyses
Contractive soils in the embankment or foundation	A higher factor of safety may be needed to account for the greater uncertainty in the undrained strength	+0.1 to +0.3 for undrained strength

Note: These figures are given for general guidance only. Experienced Geotechnical Professionals should use their own judgement, but note the principles involved in this table.

Table 4 shows required factors of safety suggested by the Austrian Commission on Reservoirs and Dams. In general, all factors are global factors of safety. Thus, standing in contrast to Eurocode 7, where a semi-probabilistic concept is suggested (i.e. one factor increasing the load and one factor decreasing the material parameters). Whilst other Eurocodes have established in practice, Eurocode 7 is still in discussion in soil engineering society. One point of discussion is that a semi-probabilistic concept does not always lead to safe side results. This is the case if a non linear stress-strain relations is applied, a common practice in soil engineering. Hence, global factors of safety are still in use in dam construction.

Table 4 Required factors of safety (Austrian Commission on Reservoirs and Dams)

Type of Load	Loading Conditions	Factor of Safety
Ordinary	Stages during construction, excavation stages; consolidation stages prior to first filling; operating conditions including water levels up to the planed reservoir level; special loads if affecting the dam.	1.3
Extraordinary	Extraordinary operating conditions as rapid draw down, maximum reservoir level and earth quake loading.	1.2
Extreme	Conditions as: damaged upstream sealing; earth quake combined to maximum reservoir level.	1.1

5.3 Zoning and Specifications

5.3.1 Seepage Control

The big advantage of CFRD is that dam safety is not affected even by very high leakage values. However, this advantage is only given, if very coarse material is used as main embankment fill and the dam's zoning is consistent with the filling material's general properties.

If unprocessed alluvial sand gravel fill or very weak rockfill (obtained from schist, slate or shale) is used as fill material, additional drainage zones have to be provided to control the seepage conditions and to avoid the build up of critical pore water pressures within the embankment's downstream shoulder. This is discussed in chapter: 5.3.1.6 Drainage Zone.

In general, applied seepage control measures are:

- Concrete facing
- Joints
- Zone 2B – cushion zone
- Zone 2C – transition zone
- Plinth structure
- Zone 2A – plinth support material
- Drainage (2E) and upstream filter (2D) Zone

The zones 2B and 2C are discussed in chapter: 5.3.2 Special Zoning, even if they do also perform seepage control tasks.

5.3.1.1 Concrete Slab

The concrete facing is the impermeable part of the dam. The casting process is shown in Figure 6. It is typically casted in vertical slabs with slip foams that are pulled upwards by winches (Figure 6a+e). Reinforcement work is shown in Figure 6b. Slab widths are normally ranging from 6m to 18m. Panel widths of 15 m are common practice.

According to ICOLD (1989a) and Cooke (2000) the slab thickness is normally set to 0.3m+0.002H (H= water head in m) for high dams (h >100m) or may also be constant varying from 0.25m to 0.3m for smaller dams. The concrete is slumped with chutes or delivered in a bucket (Figure 6c+d). Yan L. (no date) indicates that the former may lead

to aggregate segregation and loss of water the later is more desirable to provide a constant quality but is also linked with higher costs. Strength varies from 20MPa to 24MPa at 28 days, if higher values are reached shrinkage cracking is likely (ICOLD 1989).
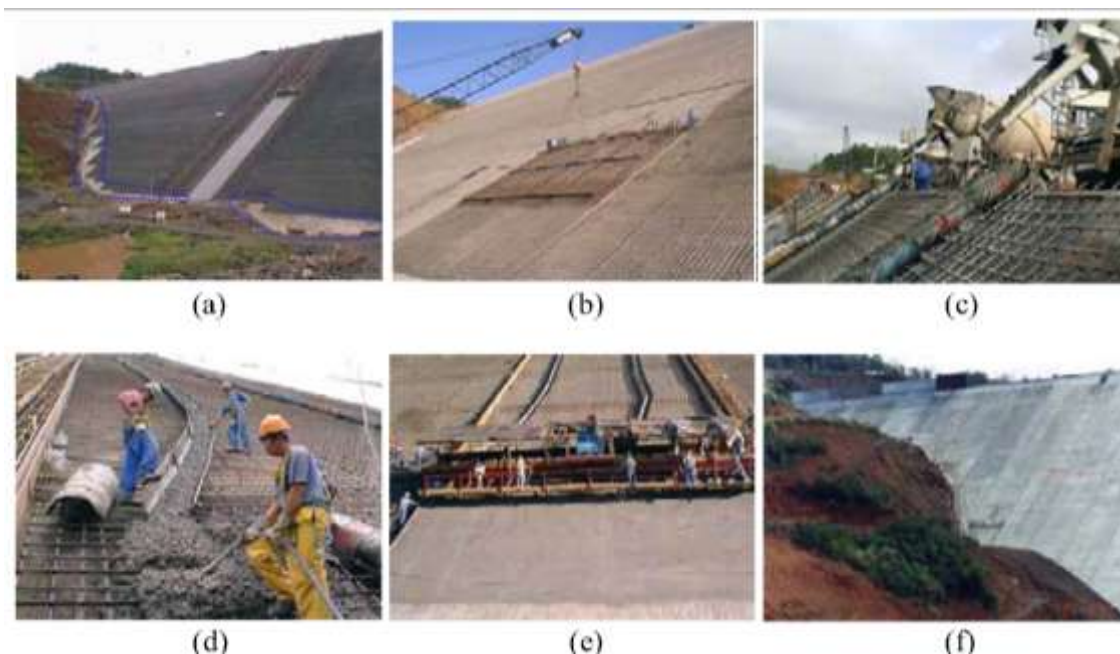
Figure 6 Construction of the concrete face. (Frutuoso da Silva 2007, p. 12)

To ensure impermeability special concrete mixtures are used to reduce inappropriate heat development or shrinking affects (e.g. fly ash, low heat Portland cement, non shrinkage admixtures). In dry climate special attention should be paid to drying up during setting of concrete. For example the surface of Wuluwati dam was covered with wet straw bags and cotton blankets combined with water sprinkling as curing method (Liyi, A. no date). Reinforcement is applied to avoid large crack widths due to shrinking and heat development (Fell et al, 2005). The amount of used reinforcing steel varies in literature. In general it ranges from 0.3% to 0.5% in both directions and is applied to the slabs axis in most cases. For more specific information the reader is guided to Fell et al. (2005) or ICOLD (2005).

5.3.1.2 *Plinth*

Fell et al. (2005 p. 613-616) wrote:

> The principal purpose of the plinth (or "toe slab") is to provide a "watertight" connection between the face slab and the dam foundation. The plinth is usually founded on strong, non erodible rock which is groutable, and which has been carefully excavated and cleaned up with a water jet to facilitate a low permeability cutoff. For these conditions the Plinth width is of the order of 1/20 to 1/25 of the water depth (ICOLD, 1989b; Cook and Sherard, 1987).....The minimum width has generally been 3 m,.....The minimum plinth thickness is usually between 0.3 m and 0.4 m,....The plinth is usually anchored to the rock with grouted dowels, which are generally 25 mm to 35 mm diameter, reinforcing steel bars, 3 m to 5 m long and are installed at 1.0 m to 1.5 m spacing.....The plinth is reinforced to control cracking due to temperature and to spread out and minimize cracks which may tend to develop from any bending strains from grouting.

As typical design example, Fell et al. (2005) pictures the plinth of Mangrove Creek dam (Figure 7).
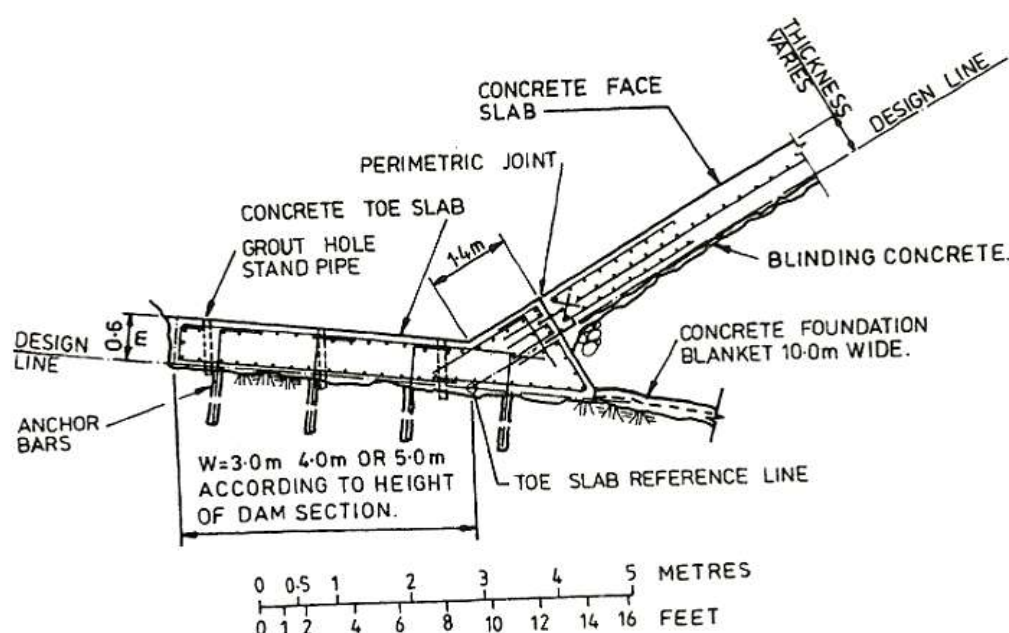
Figure 7 Plinth design of Mangrove Creek Dam (Mackenzie and McDonald, 1985)

In the majority of cases concrete casting is done manually but sometimes slip foams may be economical, especially if the plinth geometry is simple (Figure 8).

Figure 8 Plinth casting by slip foams. (Frutuoso da Silva 2007, p. 11)

According to ICOLD (2005) haul roads, crossing the plinth alignment, result in irregular settlements and consequently may lead to cracks in the face slab. However, this might be necessary, if fill material can only be obtained from borrows or quarries located upstream of the site.

5.3.1.3 Joints

In nowadays CFRD construction 6 different types of Joints are applied, of which the last two are optional:

– Perimetric Joint

– Vertical Compression Joint

– Vertical Contraction Joint

– Horizontal Construction Joint

– Horizontal Contraction Joint

– Connection between Face Slab and Crest Wall

Latterly, due to extensive joint rupturing of several very high CFRDs, rapid modifications in joint design can be observed. These damages made it necessary to improve joint design and construction. At the time of writing this thesis, it can be said: The development is still on the way. The following lines can only give a brief summary. Joint details are shown for some of the case studies in chapter: 9 CFSGDs - Case Studies taken from Literature.

Generally, according to the joint's type, two or three watertight "defense lines" are applied (Fell et al. 2005):

– Primary: Copper or Stainless Steel:

  "W" or "F" shaped copper or stainless steel water stop, between the concrete slab and a mortar or sand asphalt pad.

– Secondary: Central Bulb:

  Water stop made of rubber, hypalon or PVC, located in the slab's axis.

– Thirdly: Filled Sheets:

  Normally used for higher dams. The joint is filled with mastic or fly ash and covered with stainless steel or hypalon sheets situated on the joints upstream surface. The sheets are fixed by steel angles and are anchored to the concrete slab.

Recent design developments tend to soft joints (i.e. compression joints with inlays, without conducting the reinforcement through the joint). Soft vertical joints, in the central part of the facing, shall reduce horizontal stresses, by absorbing horizontal stains. Soft vertical joints are nowadays a clear designers` choice especially for high CFRDs in narrow valleys. The joints compressibility is given by wooden inlays. Soft horizontal joints may help to reduce vertical slab stresses. However, in contrast to soft vertical joints, soft horizontal joints are no clear designers' choice. (Pritchard 2008)

5.3.1.4   Zone 1A – self healing material

Zone 1A (Figure 4 and Figure 5) consists of earthfill with great amount of silty sand to seal potential cracks or joint openings. Originally it was designated to cover only the perimetric joint and plinth, which is empirically the weakest point of the sealing (Fell et al. 2005). The fill is dumped and compacted only by truck traffic. Generally the trend is to raise zone 1A (and 1B) up to an elevation of 0.4% - 0.5% of maximum dam height, to protect the facings critical, high deformation area (Pritchard 2008). As Pritchard (2008) reports, this practice leads to extra vertical stress in the face slabs and is therefore in suspicion to cause further cracking. Cooke and Sherard (1987) advise against that practice, because zone 2D acts as filter to silty sand, which is spread over the slab in case of leakage, anyway. However, they do advise to use a zone 1A restricted to the plinth area.

5.3.1.5   Zone 1B – self healing protection

Zone 1B (Figure 4 and Figure 5) consists of random fill that shall ensure stability and protection of Zone 1A. (Fell et al. 2005)

5.3.1.6 Drainage Zone 2E

According to ICOLD (2005) even high leakage rates do not affect safety of CFRD because of the embankment's free draining character, resulting in an unsaturated downstream shell. As the use of weak, weathered rock or dirty sand and gravel (7% - 12% < 0,074mm) is suitable too, special zoning has to be adopted. Due to the low permeability of the above mentioned materials after compaction, high permeable drainage zones have to be applied (Figure 5).

Fell et al. (2005) point out that the lack of a drainage zone in Gouhou dam design induced the failure of its embankment which mainly consisted of dirty (i.e. high fines content) sandy gravel. The failure was caused by poor design and construction of the crest wall connection joint. However, the dam would probably not have failed if a suitable chimney- and underdrain would have been provided in design.

ICOLD (2005) point out that:

The drain should be placed well back from the upstream face and should have sufficient drainage capacity to ensure that the shell downstream from the drain cannot become saturated under any circumstances. The chimney drain has to be connected to an equally draining zone at the base of the embankment that will discharge freely to tail water (Hacelas, et al, 1985; Cooke, 1960; Vithalani and Beene, 1976; Good, et al, 1985; Amaya and Marulanda, 1985). If the drain is placed immediately under the concrete face, then defects in the face slab, rather than the drainage capacity of the underlying rockfill, is the main factor controlling leakage rates. The appropriate design leakage rates cannot be realistically established since the size and frequency of cracks in the concrete face are difficult to predict. If a semi pervious zone is introduced between the face slab and the chimney drain, the permeability of the semi-pervious zone imposes an upper limit on leakage rates, even if the concrete face slab is badly cracked. Where required, a layer of filter-transition of appropriate grading (Mackenzie and McDonald, 1980; Hacelas and Ramirez, 1985) can be placed over the abutments to prevent piping of fines into the dam, to allow free drainage of the abutment, and to prevent saturation of the dam body.

5.3.1.7 Filter zone 2D

If 3A material is sensible to suffusion, a filter zone (Figure 5) should be provided up-stream of the drainage, to protect the drainage zone from clocking. For example, a 1,5m (horizontal) wide upstream filter was provided in Siping dam (90m high, China).

5.3.2   **Special Zoning**

5.3.2.1 Concrete Crest Wall

The main advantage of applying a concrete crest wall is the reduction of dam volume and consequently a reduction of construction costs (Fell et al. 2005). The vertical wall reduces the wave surge and in addition the total required dam height. Nowadays, apply-ing a crest wall is a clear designer's choice.

5.3.2.2 Extruded Curbs

Extruded curbs became state of the art in recent years. The method's advantages are mainly economical ones. Extruded curbs compensates the time intensive compaction of the cushion zone, avoids its erosion due to intensive rainfall runoff and provides a con-struction surface for further processes (Fell at al., 2005). Figure 9 shows filling of the extruder machine. Further information about the extruded curb method can be found in Resende and Materon (2000).

Figure 9 Curb casting (Frutuoso da Silva 2007, p. 10)

Because of extensive leakage of several very high CFRDs in recent time, the curb ele-ments were in suspicion to cause large cracks and to lead to concrete spalling (Campos Novos, Barra Grande, Mohale Dam). It was assumed that the high friction between slab and curb elements induced these failures during impounding.

Pritchard (2008) reports that in some recently built dams, bond breaker products (bitu-men, plastic sheets or sand asphalt) were used between the concrete slabs and the curb

elements in order to reduce friction. However, stress measuring evidenced that the former mentioned measures can not reduce the friction. Dam engineers discussed the problem at the 3rd Symposium on CFRDs, held in October 2007 and concluded that the arguments against that practice are not convincing. They do not advise to give up this practice.

5.3.2.3   Zone 2A – plinth support

The application of a zone 2A (Figure 4 and Figure 5) is quite a new approach and was a result of operating experience. Limits of its gradation can be found in Table 5. Under normal conditions the perimetric joint detail always was a part of failure, resulting in high leakage rates. Fell et al. (2005) point out that on the one hand, zone 2A shall support the facing and reduce its deformation and on the other hand it should act as a filter to the material used in zone 1A, ensuring a "self healing function". To meet the filter criterion, zone 2A consists of silty fines with a maximum grain size of 19 to 37 mm. A high modulus is achieved by well compaction in 20cm lifts. Due to the negative effect of differential settlements, a modulus much higher than achieved by the surrounding rockfill should be avoided.

ICOLD (2005) furthermore recommends limiting the horizontal width of zone 2F from 1 to 2 meters instead of 3m as commonly applied. This would reduce bending stresses in the concrete panel and prevent the slab of cracking in the order of 10m above the perimetric joint. Such a 1m wide zone 2A is sufficient in providing a filter. Zone 2A's material is equal in quality to concrete aggregate.

Table 5 Gradation Limits of Zone 2A (ICOLD 2005, p.8-8).

US Standard Sieve	Size in mm	Percent passing, by weight	
		Aquamilpa Mexico (Zone 2F)	Alternative Gradation
1 ½ "	38.1	100	100
¾"	19.1	60-80	85-100
No. 4	4.76	32-60	50-75
No. 16	1.19	20-43	25-50
No. 50	0.297	12-26	10-25
No. 200	0.074	5-12	0-5

5.3.2.4 Zone 2B – cushion zone

The cushion zone (Figure 4 and Figure 5) is thought to be the most important zone in a CFRD. Referring to Fell et al. (2005), zone 2B's material is obtained from processed rock-fill or alluvial disposals, graded from silt to coarse size. Zone 2B has to meet several demands:

– Ensuring the concrete slabs uniform support.

A high modulus is achieved by a compaction in thin layers of 40 to 50cm thickness and an adequate number of roller passes. 4 to 8 passes of a 10to SDVR are usual (Fell et al. 2005). If no curb elements are used, the surface has to be compacted by vibratory rollers in an additional procedure. The winches are pulled up by lifting jacks (Figure 9). Afterwards, shotcrete is spread on the surface to provide a firm face for reinforcing work.

– Meet filter requirements with zone 2C.

– A high content of silty fines, to reduce permeability.

Sherard (1985b) points out, that the amount of leakage is more a function of the transition zone's permeability, than of a crack's aperture. Sherard recommends a zone 2B of 4 to 5m width.

– Internal stability in case of face slab cracking.

A grading as indicated by Sherard (1985b, Table 6) meets the criterion of semi-permeability (10^{-6} m/sec) and internally stability. Furthermore, an internal stable zone 2B avoids settlements due to eroded fines.

– Acting as filter to silty sand that might get spread over the face in case of observed abnormal leakage. Gradations, presented in Table 6 will hold back silty sands that get washed into it and will consequently seals the crack (Fitzpatric et al.1985, Sherard 1985b, Cooke 2000). This method has been used successfully in several cases.

Table 6 Desirable Specification for Zone 2B. (Fell et al. 2005, p. 596)

Size (mm)	Sherard (1985b) % finer	ICOLD (1989a) % finer	Amaya & Marulanda (2000) % finer
75	90–100	90–100	90–100
37	70–95	70–100	70–100
19	55–80	55–80	65–100
4.76	35–55	35–55	40–55
0.6	8–30	8–30	10–22
0.075	2–12	5–15	4–8

Figure 10 Compaction of zone 2B   (Frutuoso da Silva 2007, p. 19)

ICOLD (2005) suggests a horizontal width of zone 2B in the order of 2 – 4m and a quality hat should be close to the quality of concrete aggregate.

ICOLD (2005) furthermore highlights problems that appeared with a zone 2B gradation as suggested in Table 6. Due to its large fines content, the gradation is of brittle nature. Settlements during construction lead to a bulging outwards of the upstream surface and may produce cracks in zone 2B.

At Tianshengqiao dam, vertical cracks with widths up to 100mm and depths up to 3m were observed. The effect tightens with:

- Great variation of all zones' deformation characteristics.
- Staged construction with ahead running upstream shell construction.

By reason of the above mentioned problems, a modified bulletin 70 gradation is presented in ICOLD (2005), mainly reducing the fines content, (Table 7).

Table 7 Modified bulletin 70 gradation limits of zone 2B (ICOLD 2005. p.8-11).

US Standard Sieve	Size in mm	Percent passing, by weight
3"	76.2	100
1 ½ "	38.1	70-100
¾"	19.1	55-80
No. 4	4.76	35-60
No. 16	1.19	18-40
No. 50	0.297	6-18
No. 200	0.074	0-7

5.3.2.5   Zone 2C – transition zone

The transition zone (Figure 4 and Figure 5) has to meet the filter requirements for zone 2B and 3A. The zone acts, as its name indicates, as transition between the two zones stated above. It is either obtained from a suitable quarry (borrow) or grizzly run material and should be of "free draining" character. Compaction work and layer thickness is similar to zone 2B (Fell et al. 2005).

Sandy gravel obtained from alluvial deposits often shows a gradation close to the limits of cushion zone 2B. If the filter criterion is met between 2B and 3A, providing a transition zone is redundant.

5.3.2.6 *Zone 3A and Zone 3B*

Figure 4 and Figure 5. As reported by Fell et al. (2005), a great number of rock types have been successfully used as rockfill material. Cook (1984) gave an easy rule of thumb: "If blasted rock is strong enough to support construction trucks and the 10 ton vibratory roller when wetted, it may be considered to be suitable for use in compacted rockfill." ICOLD (2005) describes: "The embankment of CFRD may consist of hard strong basalts, granites, greywackes and dolomites; or the softer, weaker claystones, siltstones, sandstones, and the poorly cemented limestones; or alluvial sands, gravels, cobbles and boulders".

Fell et al. point out three desirable properties of rockfill:

– Free draining.

That's the biggest advantage of CFRDs. No "modern" CFRD built of free draining rockfill has ever failed. In case of intense rupturing of the facing, water is drained without affecting safety or causing damage. Cooke (1984) recommends a limitation of fines for truly free draining rockfill. He gives: less than 50% shall pass 25 mm sieve, less than 6% shall be silt or clay particles and less than 10% finer than 0.075 mm. If the free draining character is not ensured, he advises drainage zones in dam design. This is maybe the case for weak or weathered rock types as: sandstone, siltstone, argillite, schist and shale (Fell et al. 2005). Fell et al. point out that, even though the material is called "free draining", water may pond on layers surface, due to segregation and grain breakage during compaction.

– High modulus after compaction.

The requirements for zone 3A are higher than for zone 3B, because the water load is largely transmitted by zone 3A. Layer thickness of zone 3A ranges from 0.6 m to 1.0 m, zone 3B is compacted in layers 1.5m to 2.0m thick. The layer thickness depends on the used material, thinner layers for gravels, thicker one for quarried rockfill. Oversize rock is normally pulled from zone 3A to 3B. Compaction is normally done by 10 ton vibratory steel drum rollers by 4 to 8 passes. (Fell et al. 2005) ICOLD (2005) suggests the use water in the order of 10% to 25% of the rockfill volume during construction.

In practice, if water is used at all, it is used for zone 3A. Zone 3B is normally com-

pacted without water.

If the main fill material consists of silty gravels, no water should be added during compaction. However, zone 3B should not have a significant lower (or different) deformation modulus than zone 3A. A vertical interface between 3A and 3B should be preferred. (Fell et al. 2005)

CFRD International Society (2008) recommends a interface not steeper than 1:0.2.

− Readily available.

Crushing, processing or screening the material increases excavation costs.

6 Stress-Strain-Behavior of Rockfill Material

6.1 General

Herein, the general behavior of rockfill materials is illustrated, including the typical curved Mohr envelope as well as hardening/softening and the behavior on wetting. One of the challenges in dam engineering is the determination of appropriate material parameters. In many cases adequate testing of materials used for embankments, is found to be to cost intensive. In fact one single or even several specimens cannot represent the whole embankment consisting of millions of cubic meters. In international literature, triaxial tests with specimen diameters of 30cm are often called "large scale" triaxial tests. However, even if the specimens diameters exceeds 100cm, oversize grains have to be removed resulting in a scalped or scaled down grain size distribution. Another problem in testing is to create a representative compaction. So material testing is a science on its own and in many cases it may be doubted, if these tests do really represent the natural behavior of embankments with respect to deformation analysis (Fell et al. 2005). But in fact these tests give an indication of how the material deforms and will enable the dam engineer to select appropriate parameters more accurately.

6.1.1 Hardening – Softening

Referring to Potts and Zdravkovic (1999), real soils show characteristic straining effects. At low deviatoric stresses, most soils show linear-elastic behavior (Figure 11). At high stress rates, before the peak stress is reached, hardening affects (i.e. tangent modulus

decreases with increasing stress) dominate the soils behavior. Hardening is manly dependent to the specimen's density (Marsal 1973). He goes on pointing out that dense gravel in one dimensional compression tests shows significant hardening whilst in loose states hardening does not occur.

If peak stress level is exceeded, some soils show significant softening effects (i.e. stress level decreases whilst strains increases).

From an engineering point of view, material that behaves in this brittle manner is of particular concern because, if strained beyond its initial yield point …. , its yield stress and capacity to resist load diminishes. Potts and Zdravkovic (1999 p. 134).
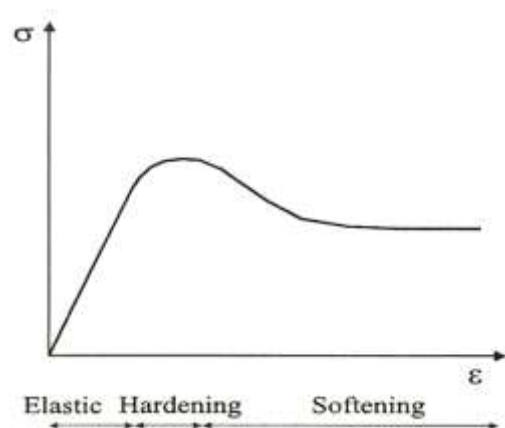
Figure 11 Illustration of real soil behavior (Potts and Zdravkovic 1999 p. 142)

Palmi and Sixtus (2007) report the unfavorable behavior of doloretic basalt rockfill in Mohale CFRD. Doloretic basalts come up with a peak modulus up to 100Mpa, but under increasing load conditions they tend to grain breakage, thus resulting in an overall low modulus amounting to only 30-40Mpa.
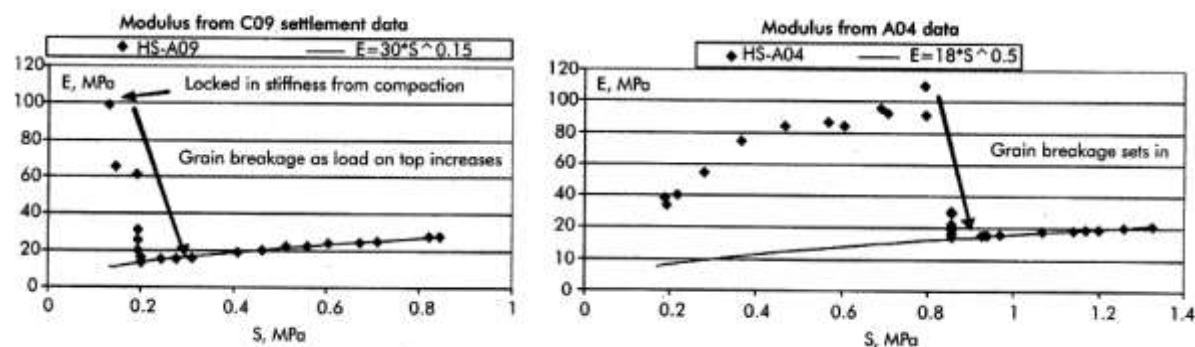
Figure 12 Settlement/load data and moduli, for poorly (left) and well (right) graded basalt (Palmi and Sixtus, 2007 p. 17).

6.2   Rockfill & Sand-Gravel Fills

6.2.1   Stress dependent Stiffness

Figure 13 shows triaxial test results on Oroville dam shell material with four different confining pressures A, B, C and D. Figure 13 shows that Young's modulus strongly varies with confining pressure. Furthermore it depicts the clearly nonlinear stress-strain relationship. With increasing stresses the soil's stiffness increases as long pore volume decreases (Potts and Zdravkovic, 1999).
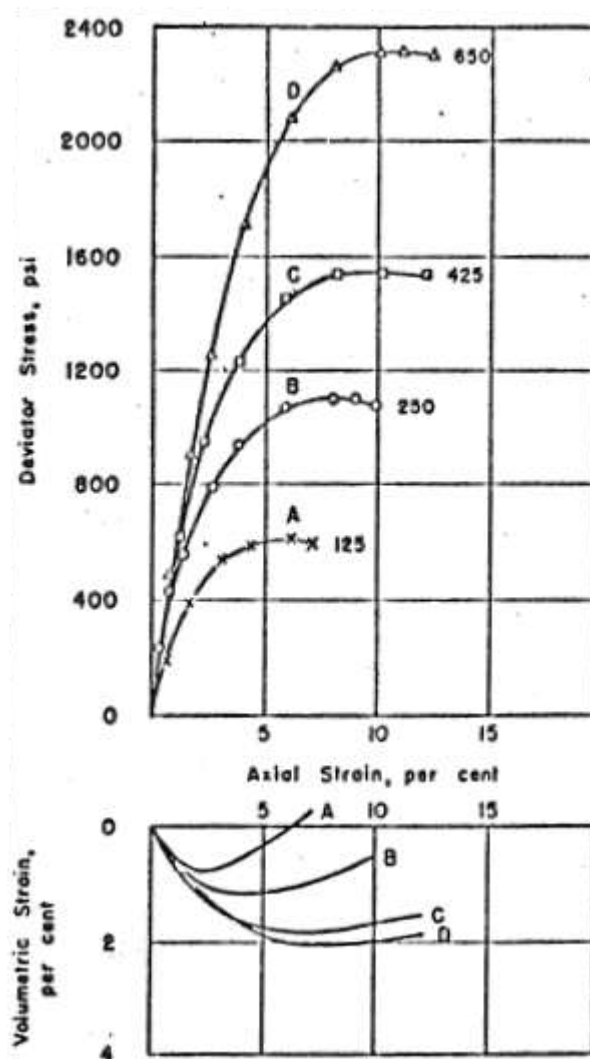
Figure 13 Stress-strain and volume change curves from triaxial tests on Oroville dam shell, silty sandy gravel (Hall and Gordon, 1963).

6.2.1.1   Factors affecting the stiffness

Hunter and Fell (2002) summarize factors affecting the deformation modulus:

6.2.1.1.1 Compaction:

Compaction has a significant effect on deformation modulus. The higher the compaction, the higher the resulting deformation modulus. Cook (1993, 1984) suggests to classify rockfill by compaction effort:

- Well compacted – 4 to 10 passes of a 10 - 15 to smooth drum vibratory roller (SDVR), layer thickness < 1m, water added.
- Reasonably to well compacted – 4 to 6 passes of a 10 - 15 to SDVR, layer thickness 1,2 to 1,6m, water added.
- Reasonable compacted – 4 passes of a 10 to SDVR, layer thickness 1,5 to 2m, no water added.

6.2.1.1.2 Particle shape:

Well compacted gravels (rounded) cause a higher modulus than well compacted quarried (angular, due to blasting) rockfills. By reason of stress concentration on sharp angled edges, the grains tend to break (Marsal 1973).

6.2.1.1.3 Intact rockfill strength:

Well compacted, very high strength rockfills cause greater modulus than medium to high strength rockfills.

6.2.1.1.4 Valley shape:

Due to cross valley arcing during construction and during impounding, the valley shape has a significant influence on the embankments deformation.

6.2.1.1.5 Particle size:

Decreasing deformation modulus with increasing d_{80} in case of well compacted very high and medium to high strength rockfills. Gravel fill has to be excluded from the d_{80} rule, because only a limited number of cases were available.

6.2.1.1.6 Gradation:

Uniform grading (low coefficient of uniformity) results in lower moduli (Marsal 1973). This is related to the lower number of contact points per particle, resulting in higher contact forces.

6.2.2 Dilatancy

Generally, heavily overconsolidated clays and dense sands tend to dilate (expand) on shearing, whereas lightly overconsolidated clays and loose sands tend to compress. However, loose sands may revert to a tendency to dilate as failure is approached. The tendency to dilate also depends on mean effective stress. At low levels there is a greater tendency to dilate, whereas at very high stress levels even dense sands compress (Figure 13, volumetric strains, curves A, B). Potts and Zdravkovic (1999 p. 127).

Douglas (2002) wrote that dilatation occurs till a critical confining pressure is exceeded (Figure 13, volumetric strains, curves C, D).

6.2.3 Stress Dependent Volumetric Straining

As obvious in Figure 13, the amount of volume change is dependent on confining pressure. At high confining pressures, rockfill material shows smaller volumetric straining than shown for lower confining stresses.

6.2.4 Curved Mohr Envelope

The shear strength envelope of rockfill material is of nonlinear nature (i.e. the friction angle decreases with increasing confining pressure, Figure 14).

If the friction angle is assumed to be constant in stability analysis, shallow slip surfaces are calculated as critical. However, due to the above mentioned, these slip surfaces do not occur in reality. This significantly affects stability analysis (Douglas 2002).
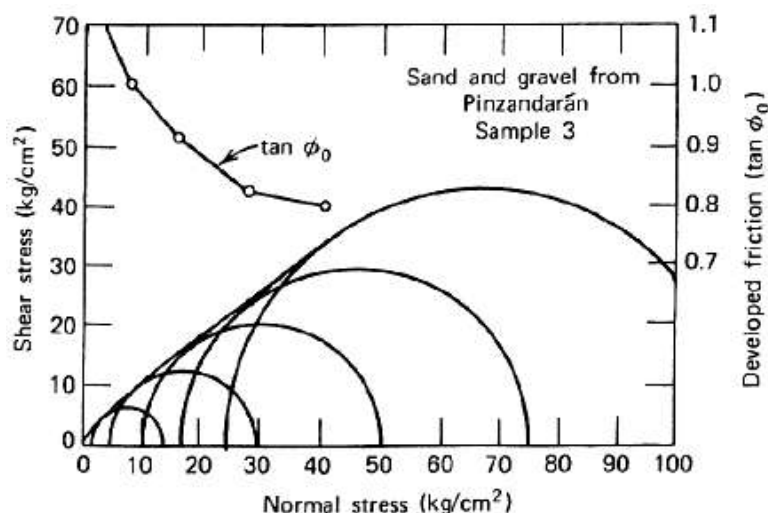
Figure 14 Curved Mohr envelope for Pinzandaran sand and gravel obtained from large scale triaxial testing (Marsal 1973 p. 166).

Douglas (2002) explains, "…as normal stress is increased dilatation is suppressed and therefore shear strength increase is reduced."

6.2.4.1 Factors affecting Shear Strength

Douglas (2002) summarized factors influencing the shear strength:

6.2.4.1.1 Confining pressure:

Shear strength decreases with increasing confining pressure.

6.2.4.1.2 Strength of intact rock:

Shear strength increases with increasing particle strength.

6.2.4.1.3 Density:

Shear strength increases with increasing density.

6.2.4.1.4 Uniformity coefficient:

Shear strength decreases with increasing uniformity. However, the uniformity does only have a minor effect on shear strength.

6.2.4.1.5 Grain size distribution:

In soils, having a d_{100} smaller than gravel size, the shear strength increases with increasing content of gravel. However, in soils where the gravel content is lower than 30-35% the shear strength is mainly controlled by the finer grain sizes. (USBR, 1961).

6.2.4.1.6 Particle shape:

Shear strength increases with the particle's angularity.

6.2.4.1.7 Diameter of tested specimen:

Shear strength decreases with increasing specimen diameter. Assuming a constant d_{max}/diameter ratio.

Shear strength increases with increasing d_{max}, if the specimen's diameter is held constant. Where d_{max} is the specimen's maximum grain size.

6.2.5 Creeping

Rockfill maerials show significant time dependent behavior. Most rockfill dams show ongoing crest settlements even decades after end of their construction. These long-term strains are linearly related with logarithm of time (Oldecop and Alonso 2007). According to Oldecop and Alonso (2007), creeping is caused by crack propagation in single particles, resulting in its breakage and ongoing redistribution of stresses. Figure 15 shows the vertical strain increasing with time when vertical stress is held constant in oedometer tests on slate.
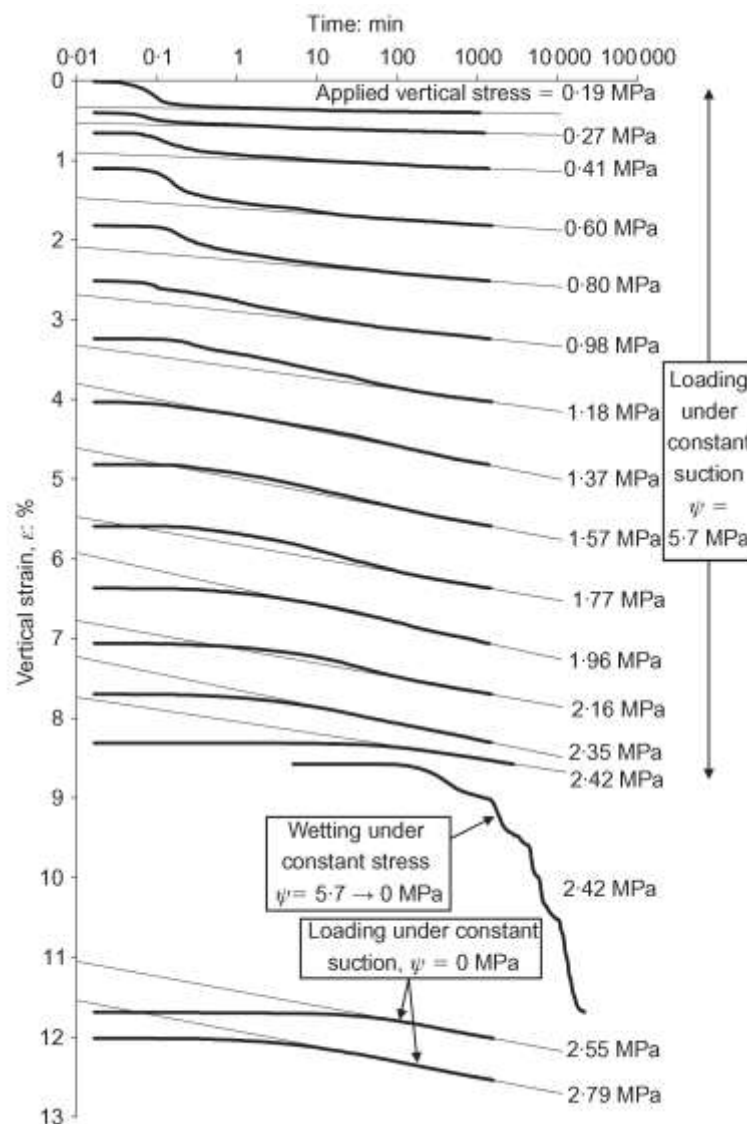
Figure 15 Time dependent behavior of gravel in one dimensional compression tests (Oldecop and Alonso 2007, p.291).

Referring to Hunter and Fell (2002), gravel shows significantly minor creeping deformation mainly by reason of the higher point area of contact, compared to angular shaped quarried rockfills. Thus, reducing the contact stresses.

6.2.6 Wetting

Most rockfill materials show considerable collapse settlements on wetting. There has been much effort to investigate this typical behavior of coarse granular embankment fills. Terzaghi (1960) pointed out, that the loss of strength is due to the breakage of highly stressed particles, where saturation speeds up this process. Figure 16 and Figure 17 show the results of triaxial tests on Pancrudo gravels (quarry run Cambric slate), once tested under conditions of 36% relative humidity and once under saturated conditions (Chavez and Alonso, 2003).
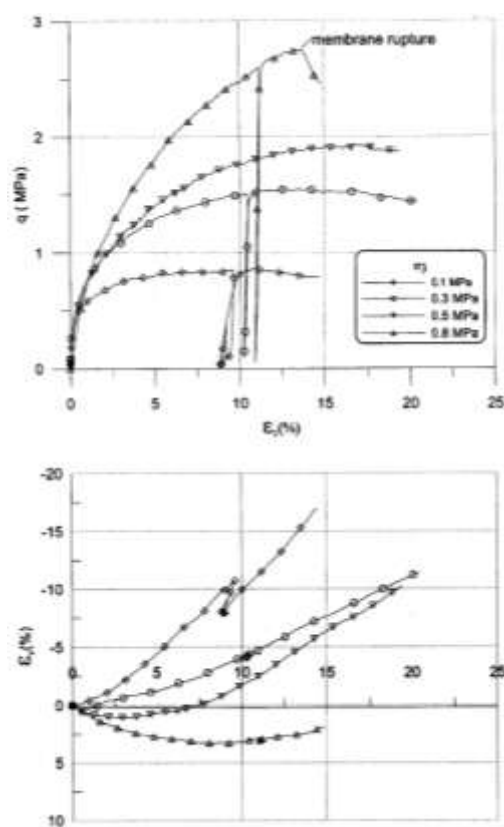
Figure 16 Triaxial test on Pancrudo gravel RH=36% (Chavez and Alonso 2003, p.219).
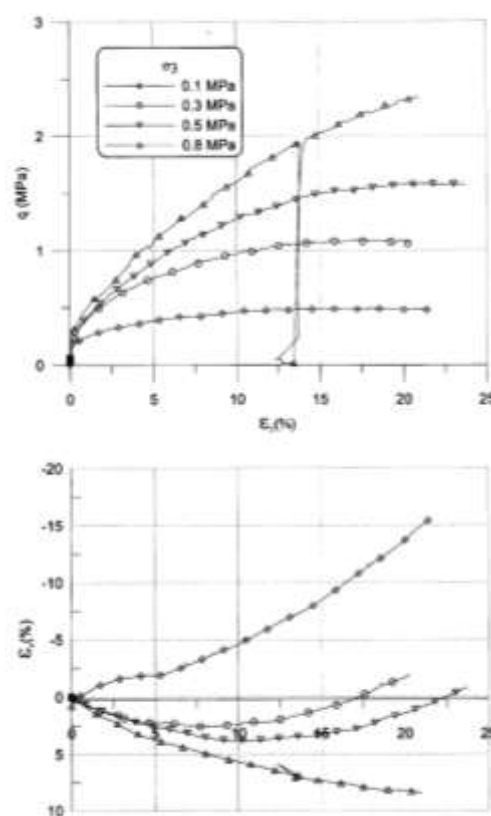
Figure 17 Triaxial test on Pancrudo gravel under saturated conditions (Chavez and Alonso 2003, p.219).

The specimen's strength reduction on wetting is obvious. If wetted, shear strength as well as stiffness reduce drastically. Chavez and Alonso (2003) point out that it is of special interest, that both specimens have very similar stress-strain behavior for low de-

viatoric stresses, but strongly differ with increasing stresses.

Alonso and Oldecop (2000) found out: If the stress level of dry rockfill is above the stress-strain path under saturated conditions, collapse settlements will occur and the abruptly appearing collapse strain is the difference of strain in saturated and dry conditions at the same stress level. Collapse settlements may occur without wetting if 100% humidity is present for a while. These settlements are of similar magnitude as occurring for wetting.

Fell et al. (2005) point out that especial quarried rockfill tends to collapse settlements when wetted through potential cracks in the facing, ruptured joints or by tailwater impoundment.

The magnitude of collapse settlements will reduce with increasing moisture content at placement (Nobari and Duncan 1972).

Gravels in general, due to its rounded shape, undergo smaller deformations (referring to wetting & creeping deformations). Whilst sound quarried rock and especially weathered quarried rock cause height deformations. Water head only has a little influence on slab deformation compared to the former. Rockfill obtained from sedimentary rock types, show significantly higher loss in strength than rockfill obtained from igneous or metamorphic rock types (Fell et al. 2005).

6.3   Constitutive Models

Potts and Zdravkovic (1999) point out, that:

> Due to the complex nature of soil it has not been possible, to date, to develop an
> elasto-plastic model that captures all the facets of real soil behavior and be defined
> by a limited set of input parameters that can be readily obtained from simple la-
> boratory tests.

In recent years, several new constitutive models for rockfill were published in litera-
ture, but most of them having the disadvantage not to be incorporated in commercial
software packages. Here three constitutive models shall be discussed, two of them
wide spread and well known in dam design and one of them, still relatively new for
dam design. Assets and drawbacks will be highlighted and compared.

6.3.1   Linear elastic – perfectly plastic

There are numerous linear elastic – perfectly plastic models describing the stress strain
behavior of soils. Commonly known are the Tresca model, von Mises model, Drucker –
Prager model and the wide spread Mohr – Coulomb criterion. Referring to software
packages for finite element analysis the Mohr – Coulomb model is the most utilized
model.

6.3.1.1   Mohr –Coulomb model

Mohr – Coulomb model (MC) requires 5 input parameters. Cohesion c, internal friction
angle φ, dilatancy ψ, young's modulus E and poison's ratio ν. The three former con-
trol plastic behavior, E and ν control the elastic behavior.

The following expressions specify the way MC-model is incorporated into Plaxis soft-
ware version 9.0 (Plaxis, 2005). In MC model the strain rate is separated into reversible
elastic and irreversible plastic strains. Figure 18 gives an idea of an elastic perfectly
plastic model.

$$\underline{\varepsilon} = \underline{\varepsilon}^e + \underline{\varepsilon}^p \qquad\qquad \underline{\dot{\varepsilon}} = \underline{\dot{\varepsilon}}^e + \underline{\dot{\varepsilon}}^p \tag{1}$$
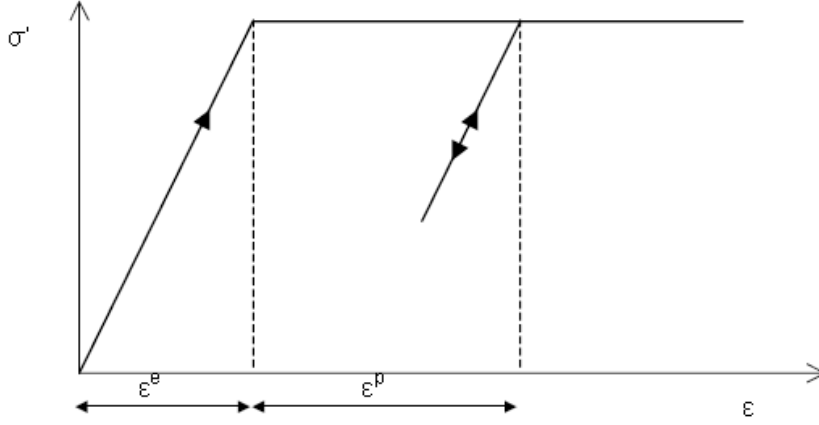
Figure 18 Basic idea of an elastic perfectly plastic model (Plaxis 2009, p. 3-2)

Substitution of (1) into Hooke's law, relates stress rates to elastic strain rates.

$$\dot{\underline{\sigma}}' = \underline{\underline{D}}^e \cdot \dot{\underline{\varepsilon}}^e = \underline{\underline{D}}^e \cdot (\dot{\underline{\varepsilon}} - \dot{\underline{\varepsilon}}^p) \tag{2}$$

Whether plastic strains occur or not, is controlled by the Mohr-Coulomb yield function, which is an extension of Coulomb's friction law (3).

$$\tau_f = c' + \sigma'_{nf} \cdot \tan \varphi' \tag{3}$$

Using the Mohr circles of stress from Figure 19, the Coulomb's friction law can be extended to the Mohr-Coulomb failure criterion (4).

$$\tau_f = \frac{(\sigma'_1 - \sigma'_3)}{2} = c' \cdot \cos \varphi' - \frac{1}{2} \cdot (\sigma'_1 + \sigma'_3) \cdot \sin \varphi' \tag{4}$$

The Mohr-Coulomb yield function can be written as:

$$f(\sigma', \lambda) = \frac{(\sigma'_1 - \sigma'_3)}{2} + \frac{1}{2} \cdot (\sigma'_1 + \sigma'_3) \cdot \sin \varphi' - c' \cdot \cos \varphi' \tag{5}$$

Where λ is the plastic multiplier:

$$\lambda = 0 \quad \text{if:} \quad f < 0 \quad \text{or:} \quad \frac{\partial f^T}{\partial \underline{\sigma'}} \cdot \underline{\underline{D}}^e \cdot \dot{\underline{\varepsilon}} \leq 0 \quad \text{(elasticity)}$$

$$\tag{6}$$

$$\lambda > 0 \quad \text{if:} \quad f = 0 \quad \text{and:} \quad \frac{\partial f^T}{\partial \underline{\sigma'}} \cdot \underline{\underline{D}}^e \cdot \dot{\underline{\varepsilon}} > 0 \quad \text{(plasticity)}$$

According to the classical theory of plasticity (Hill, 1950), plastic strain rates are proportional to the derivative of the yield function with respect to the stresses. This means that the plastic strain rates can be represented as vectors perpendicular to the yield surface. (Plaxis, 2009).

As shown in Figure 19. Instead of associated plasticity, where dilatancy is overestimated, Plaxis uses an additional yield function g to control the plastic strain rates. (Plaxis, 2009). The plastic potential function g is of the form:

$$g(\sigma') = \frac{(\sigma_1' - \sigma_3')}{2} + \frac{1}{2} \cdot (\sigma_1' + \sigma_3') \cdot \sin \psi \tag{7}$$

Plastic strain rates are of the form:

$$\dot{\underline{\varepsilon}}^p = \lambda \cdot \frac{\partial g}{\partial \underline{\sigma}'} \tag{8}$$

Smith and Griffith (1982), Vermeer and de Borst (1984) derived the following relation between effective stresses and elastoplastic strain rates:

$$\dot{\underline{\sigma}}' = \left(\underline{\underline{D}}^e - \frac{\alpha}{d} \cdot \underline{\underline{D}}^e \cdot \frac{\partial g}{\partial \underline{\sigma}'} \cdot \frac{\partial f^T}{\partial \underline{\sigma}'} \cdot \underline{\underline{D}}^e \right) \cdot \dot{\underline{\varepsilon}} \tag{9}$$

Where α is zero for elastic material behavior and equal to unity during plastic material behavior.

$$d = \frac{\partial f^T}{\partial \underline{\sigma}'} \cdot \underline{\underline{D}}^e \cdot \frac{\partial g}{\partial \underline{\sigma}'} \tag{10}$$
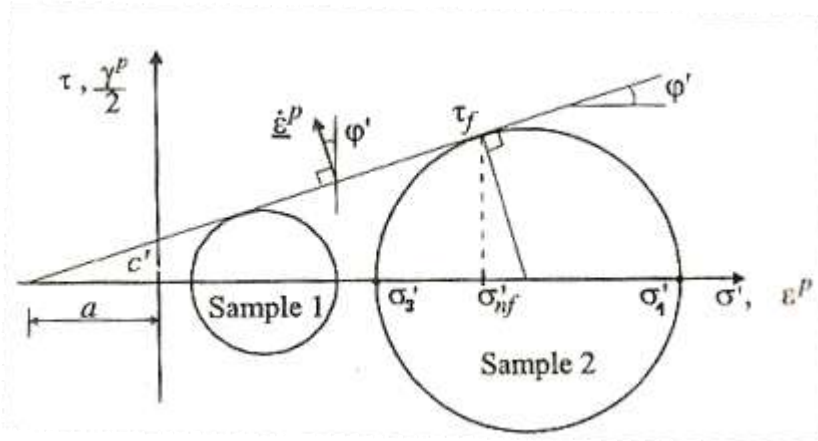
Figure 19 Mohr circles of effective stresses (adopted from Potts and Zdravkovic, 1999. p.152)

6.3.1.1.1   Assets and Drawbacks of MC-model

MC model is a wide spread constitutive model in soil mechanics. Its assets are low calculation time and use of commonly known parameters. However it is impossible to reflect real soil behavior as mentioned in chapter: 6.2 Rockfill & Sand-Gravel Fills. Real

soils show different stiffness for varying confining pressures, while MC-model describes the soil behavior assuming a constant value of stiffness. Furthermore MC-model does not allow for unloading / reloading effects. Potts and Zdravkovic (1999) point out one further drawback. Once plastic strains occur, the soil dilates forever. But real soils often reach constant volume condition for large strains.

The impact of assuming bilinear material behavior (i.e. neglecting partially hardening/ softening behavior) in constitutive models is dependent on estimated stress ranges (i.e. mainly dam height). In many cases (high strength rockfill and/or low embankment height) stresses won't exceed ranges where hardening occurs. Plaxis offers the opportunity of applying stress dependent stiffness (incremental modulus correction) in its advanced "Mohr-Coulomb" model. However, scope of this thesis is to compare the "normal" MC model, hence this option was not put to use herein.

6.3.2 Stress dependent hardening soil models

6.3.2.1 Duncan – Chan model

In recent years Duncan Chan model (DC) became the most commonly used constitutive model in finite element analysis of dam structures. Since Duncan Chan model is not part of the research work in this thesis, only a brief introduction is given. Scope of this part is to highlight the advantages and differences of Duncan Chan model to the former stated Mohr-Coulomb model and the later presented hardening soil model of Schanz. If further information is needed, the reader is guided to Kai and Duncan (1974).

One reason for the wide spread usage of DC might be, that there is plenty of data for dam fill materials available in international literature. A further reason and maybe the all dominant reason is the incorporated stress dependency of tangent modulus. Figure 20 shows the tangent modulus varying with confining pressure for Oroville dam shell material applying the DC constitutive model.
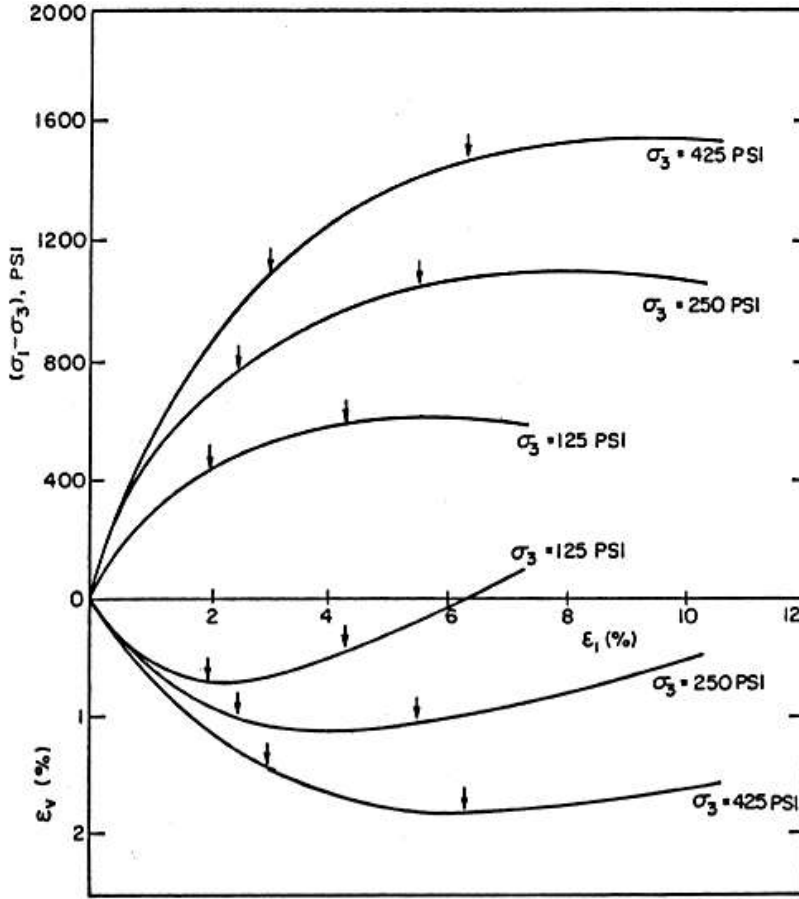
Figure 20 Replotted stress – strain and volume change curves of Oroville dam shell material using the Duncan – Chan model (Kai and Duncan 1974, p. 31).

DC model, in its version from 1974, needs 10 input parameters. These are: the bulk modulus for initial loading K, bulk modulus for un-/re loading K_{ur}, modulus exponent n, cohesion c, initial friction angle φ_0, reduction of friction angle $\Delta\varphi$ for a ten fold increase of confining pressure, failure ratio R_f, three poission's ratio parameters G, F and d. Kai and Duncan (1974) derived a relationship for tangent modulus E_t and the stresses in the form of:

$$E_t = \left[1 - \frac{R_f \cdot (1 - \sin\varphi) \cdot (\sigma_1 - \sigma_3)}{2 \cdot c \cdot \cos\varphi + 2 \cdot \sigma_3 \cdot \sin\varphi}\right]^2 \cdot K \cdot p_a \cdot \left(\frac{\sigma_3}{p_a}\right)^n \tag{11}$$

Where p_a is the atmospheric pressure in the applied unit. The un-/reloading modulus is expressed as:

$$E_{ur} = K_{ur} \cdot p_a \cdot \left(\frac{\sigma_3}{p_a}\right)^n \tag{12}$$

The tangent poission's ratio v_t varies with confining pressure and is expressed as:

$$v_t = \frac{G - F \cdot log\left(\frac{\sigma_3}{p_a}\right)}{\left[1 - \frac{d \cdot (\sigma_1 - \sigma_3)}{K \cdot p_a \cdot \left(\frac{\sigma_3}{p_a}\right)^n \cdot 1 - \frac{R_f \cdot (1 - \sin\varphi) \cdot (\sigma_1 - \sigma_3)}{2 \cdot c \cdot \cos\varphi + 2 \cdot \sigma_3 \cdot \sin\varphi}}\right]^2} \qquad \text{(13)}$$

As stated in chapter: 6 Stress-Strain-Behavior of Rockfill, most rockfills show significant curved Mohr envelops. DC model allows for this property, calculating the actual value of φ by the formula:

$$\varphi = \varphi_0 - \Delta\varphi \cdot log\left(\frac{\sigma_3}{p_a}\right) \qquad \text{(14)}$$

6.3.2.1.1   Assets and Drawbacks of Duncan-Chan model

The advantages of Duncan-Chan model are stress dependent selection of the actual tangent modulus. It offers full control of stress dependent volumetric straining, does also allow for un-/reloading effects and furthermore allows for most soils typical curved Mohr envelops.

6.3.2.2   Hardening soil model - Schanz

The hardening soil (HS) model of Schanz et al. (1999) allows for stress dependent stiffness and un-/reloading effects as Duncan-Chan model does. Referring to Plaxis (2009), the HS model supersedes DC model by far. The HS model introduces a yield cap (i.e. a second yield function) enabling the model to reproduce plastic straining due to primary deviatoric loading as well as plastic straining due to primary compression. Fell et al. (2005) point out that oedometer tests (i.e. primary compression) do better display the embankments filling process whilst triaxial tests (i.e. primary deviatoric loading) better display the loading due to first filling. HS model requires 9 input parameters, cohesion c, friction angle φ, angle of dilatancy ψ, secant modulus obtained from triaxial tests E_{50}^{ref}, tangent modulus obtained from oedometer tests E_{oed}^{ref}, un-/reloading modulus E_{ur}^{ref}, modulus exponent m (controls stress level dependency of stiffness), reference stress for stiffness p^{ref} and failure ratio $R_f = \frac{q_f}{q_a}$. Figure 21 shows the hyperbolic stress-strain relation for primary deviatoric loading.
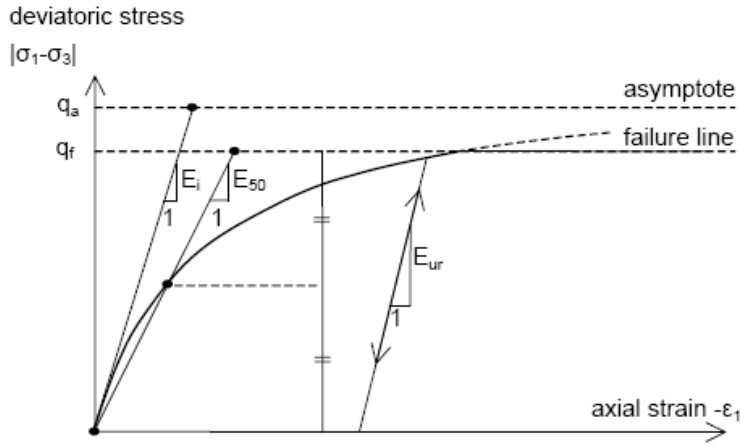
Figure 21 Hyperbolic stress-strain relation in primary deviatoric loading (Plaxis 2009, p. 5-3).

Triaxial test curves are approximated by hyperbolas. In HS model the axial strain rate is related to the deviatoric stress rate by:

$$-\varepsilon_1 = \frac{q}{E_i \cdot \left(1 - \frac{q}{q_a}\right)} \qquad if \; q < q_f \tag{15}$$

The initial stiffness E_i is related to the actual stiffness E_{50} by:

$$E_i = \frac{2 \cdot E_{50}}{2 - R_f} \tag{16}$$

The actual stiffness E_{50} is related to the input parameter E_{50}^{ref} by the equation:

$$E_{50} = E_{50}^{ref} \cdot \left(\frac{c \cdot \cos\varphi - \sigma_3' \cdot \sin\varphi}{c \cdot \cos\varphi + p^{ref} \cdot \sin\varphi}\right)^m \tag{17}$$

The failure line represented by the ultimate deviatoric stress is defined as:

$$q_f = (c \cdot \cot\varphi - \sigma_3') \cdot \frac{2 \cdot \sin\varphi}{1 - \sin\varphi} \tag{18}$$

The actual un-/reloading stiffness E_{ur}^{ref} is expressed by:

$$E_{ur} = E_{ur}^{ref} \cdot \left(\frac{c \cdot \cos\varphi - \sigma_3' \cdot \sin\varphi}{c \cdot \cos\varphi + p^{ref} \cdot \sin\varphi}\right)^m \tag{19}$$

Figure 22 shows the stress-strain relation for primary compression. The actual stiffness E_{oed} is defined by the equation:

$$E_{oed} = E_{oed}^{ref} \cdot \left(\frac{c \cdot \cos \varphi - \frac{\sigma_3'}{K_0^{NC}} \cdot \sin \varphi}{c \cdot \cos \varphi + p^{ref} \cdot \sin \varphi} \right)^m \qquad (20)$$

Where K_0^{NC} is the normal consolidated value K_0, which is set to 1-sin φ by default.
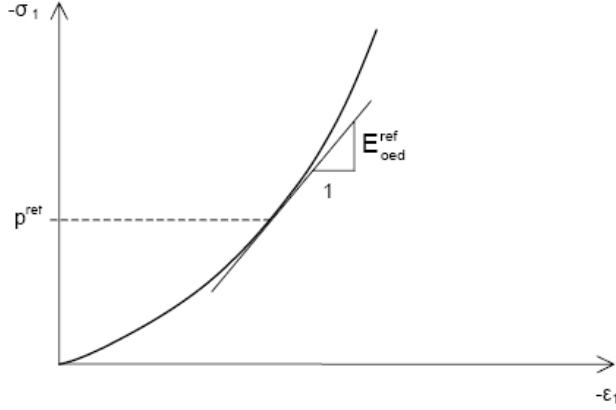
Figure 22 Stress – strain relation for primary compression (Plaxis 2009, p. 5-9).

Plastic straining is controlled by applying two yield functions (Figure 23). A detailed description of this yield functions and their interaction would go beyond the scope of this thesis. For further information, the reader is referred to Schanz et al. (1999).
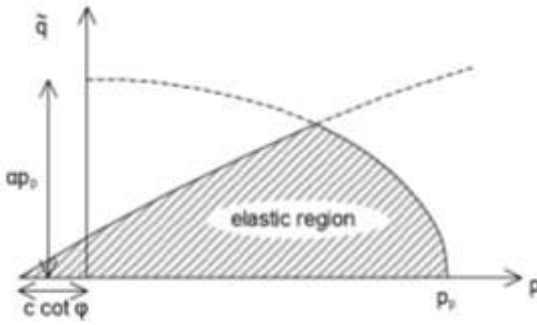
Figure 23 Yield surfaces of hardening soil model in p – q plane (Plaxis 2009, p. 5-13).

6.3.2.2.1   Assets and Drawbacks of HS Model

In contrast to Duncan-Chan model, the biggest advantage of HS model for dam engineers is the independent stress-strain relation for primary deviatoric and primary compressive stress states. This approach enables the user to make a differentiation for the material's stiffness during construction and the stiffness during impoundment. However, the above mentioned HS model does not allow for the curved nature of Mohr envelops. A single φ- value has to be applied for the whole embankment. Thus, making it difficult to represent the real behavior of:

- Points in the middle of the embankment, that might reach plasticity due to the smaller friction angle at high stress levels.

- Compared to points in shallow depths of the embankment, that will never reach plasticity due to the high initial friction angles for low stress levels.

Softening effects cannot be modeled in HS model. However, one has to decide, if the fill material shows significant softening effects (within the estimated range of stresses) a model should be applied allowing for that behavior. This will further be discussed in chapter: 10 Stress-Deformation Analysis of Sarigüzel Dam. HS model does not allow for full control of volumetric straining, which is discussed later in chapter: 10.5 Applied Material Parameters.

7   Principle Stress-Strain and Deformation Behavior of CFRDs and CFSGDs

This chapter summarizes historical records of CFRDs and CFSGDs, to gain a better understanding about expectable ranges of some point's deformation magnitude.

Most deformation analysis in practice do not allow for different stress-strain paths for primary vertical or primary deviatoric loading nor allow for time dependent behaviour or collapse settlements due to rupturing. This is due to the lack of detailed information, the time consuming nature of differentiated analysis or simply due to the restricted abilities of constitutive models if finite element method is used. Hunter and Fell (2002) evaluated the behaviour of 36 well documented dams, the paper is very helpful for practical issues.

7.1   End of Construction

One factor mainly dominating the dam's general behaviour at end of construction, first filling and for long term behaviour is the valley shape. If deriving appropriate material parameters from historical records (i.e. observed deformations), one always should bear in mind if arching was likely to occur.

Factors influencing the modulus at end of construction (E_{rc}) are discussed in chapter: 6 Stress-Strain-Behavior of Rockfill. Figure 24 shows the embankment's general behavior at end of construction and after first filling.

7.2   First Filling

7.2.1   Face slab deformation
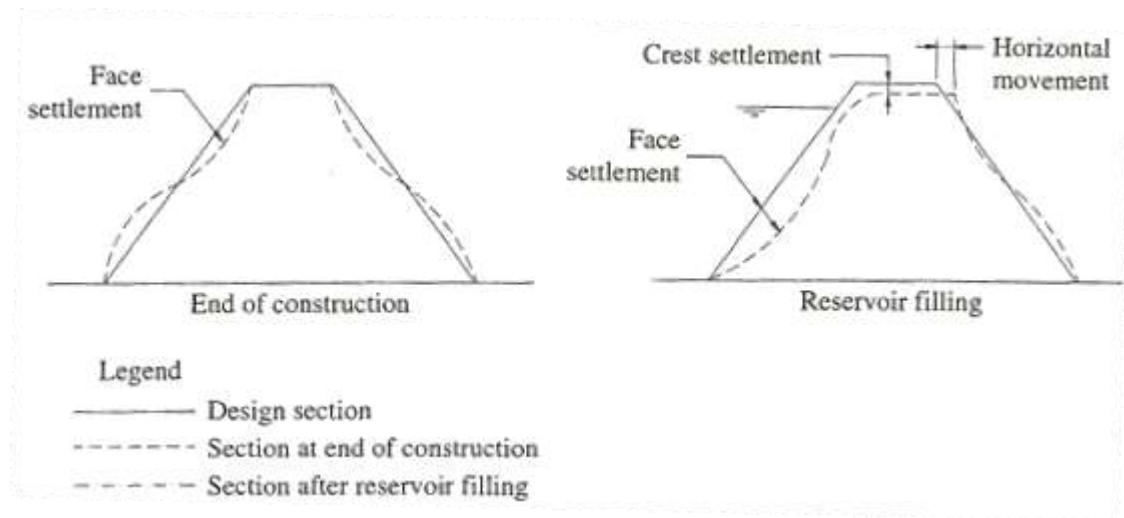
Figure 24 Settlements and deformation at end of construction stage and after impounding (Fell et al. 2005, p. 636).

Depending on whether the construction of the slab starts before or after the dam body reached its final elevation, the face slabs are abandoned to the embankment's settlement during construction. Reservoir impoundment consequently results in the slab's deflection. Due to first filling, the crest undergoes horizontal displacements and settlements. Fell et al. (2005) indicate that these plane normal slab deflections cause shear and tensile movements at the perimetric joint. Furthermore they lead to horizontal tensile stresses close to the abutments and horizontal compressive stresses in the central part of the facing. The stress distribution and general movement directions are shown in Figure 25. During first filling, maximum slab deflection is normally observed at the middle of the dam's height, reaching values from 2.8cm up to 131.7cm. The former was observed at Murchison dam, a 94m high dam consisting of rhyolite rockfill, compacted by a SDVR in 1m lifts. The latter was observed at Salt Spring dam, a 100m high dam consisting of granite rockfill, dumped and poorly sluiced in lifts of up to 52m. Slab deflections of this magnitude will harm the sealing and consequently results in high leakage rates. The factors highly influencing the deflections magnitude are compaction work (number of passes), layer thickness and used material (intact rock strength, grain shape).
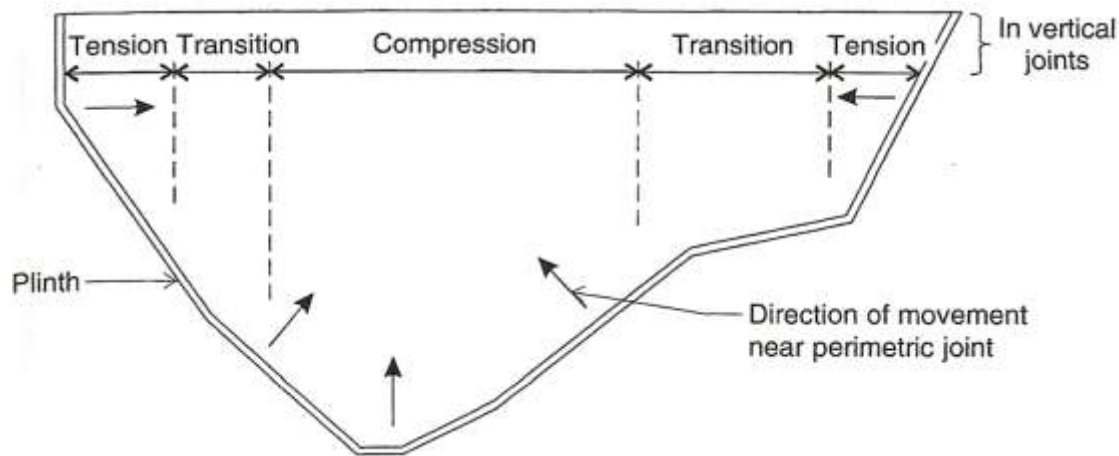
Figure 25 General movement directions and stress zones in face slabs after impounding (Fell at al., 2005, p. 637).

7.2.1.1 Crack Types in Face Slabs

Mori (1999) classified three typical crack types in concrete face slabs:

- Shrinkage: Typically of small width (tenth of a millimeter) and horizontal. They accumulate in slabs poured between already casted ones, however they tend to "self healing" by fine silts or calcification. Shrinkage cracks cannot be avoided, but the amount and width can be controlled by several measures, as proper design of concrete mixes, proper placement and curing of the concrete face.

- Cracks due to settlement of the underlying rockfill: They typically appear in the middle third of the dam's height and are caused by the ongoing bulging out-ward of the embankments surface after end of construction and prior to im-pounding (cp. Figure 24). Crack widths are in the range of a few tenth of a mil-limeter, evenly distributed in spaces of 0,5m to 1m. These cracks are consi-dered not to be a problem, they tend to close during impounding. This type of crack can be controlled by placing the steel bars closer to the upstream surface.

- Structural cracks due to differential movements within the embankment. Either due to strong varying stiffness of the embankment's zones or due to staged construction with an ahead running upstream shell. For example, a well known problem is cracks that appear in a range of 10m away from the perimetric joint, due to the varying stiffness of zone 2A in contrast to zone 2B. At Aquamilpa dam, a horizontal crack all over the dam's entire length occurred during first filling, resulting in high leakage values. The crack appeared due to the strong

varying stiffness of upstream alluvial gravel and downstream quarried ignim-brite.

For this type of cracks, the widths typically range from a few to several centi-meters, causing economically distressing leakage values. To avoid these cracks, a smooth alignment of the plinth (i.e. elimination of abrupt changes in rock to-pography) should be chosen or vertical expansion joints should be applied in this area.

Structural cracks may also be limited by adjusting the moduli of particular zones to those of adjacent zones.

During impounding the outer parts of the upstream shell undergo unloading. On the one hand principle stresses (σ_1,σ_3) turn slightly in direction of the water load, at-tended by slightly increasing major stresses (σ_1), but in general the minor stresses (σ_3) increase at larger extend, resulting in an overall reduction of the deviatoric stress (σ_1-σ_3) level. Zeping (2000).

Massive face slab cracking of some CFRDs ranging from 150 to 200m in height shocked the dam society in recent years. Herein, a brief introduction of these three dams is presented. A generally excepted reason is not found so far. Several aspects and con-struction methods are stilll in suspicion: The overall low modulus of quarried basaltic rockfill, the extruded curb method, joint arrangement and the embankment's zoning.

Mohale Dam

145m high; crest length: 540m; multipurpose scheme; rockfill type: quarried basaltic rock, upstream and central zone compacted in layers of 1m, downstream zone com-pacted in layers of 2m; steel rebars cross the concrete face's joints; extruded curb method used; At the end of a short first filling period, cracks occurred resulting in a peak leakage of 600l/sec. Figure 26 shows Mohale dam's zoning. Figure 27 shows the cracks occurred in Mohale's concrete facing.
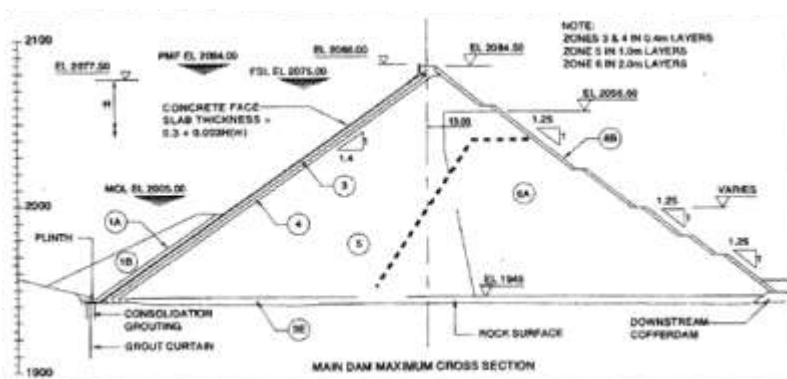
Figure 26 Mohale dam maximum section (Palmi and Sixtus, 2007 p. 16).
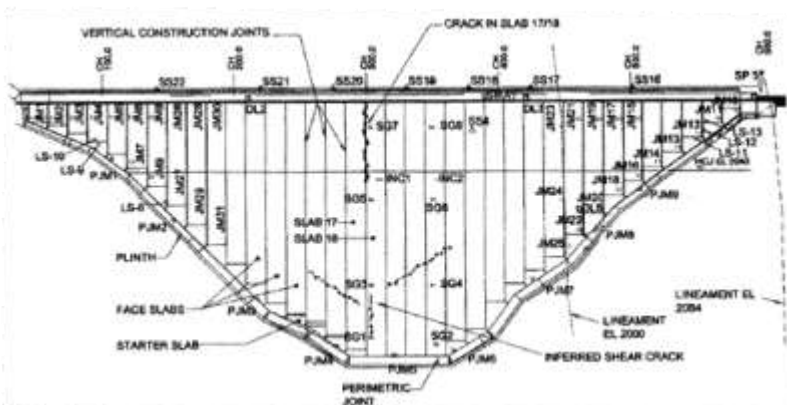
Figure 27 Mohale dam cracks (Palmi and Sixtus, 2007 p. 16).

Campos Novos

202m high; crest length: 590m; upstream slope: 1,3; downstream slope: 1,4; rockfill type: quarried basaltic rock, upstream and central zone compacted with additional water in layers of 1m, downstream zone compacted without water in layers of 1,6m; extrudet curb method used; plastic sheets were placed over the extruded curbs intended to reduce friction. 16m wide slabs, casted in two steps; During impounding a peak leakage of 1400l/sec was observed. Figure 28 shows the cracks in Campos Novos' facing. After impounding, the slab's maximum deflection was observed at the lower third and amounted to 86cm. The crest's horizontal deformation amounted to 33cm.
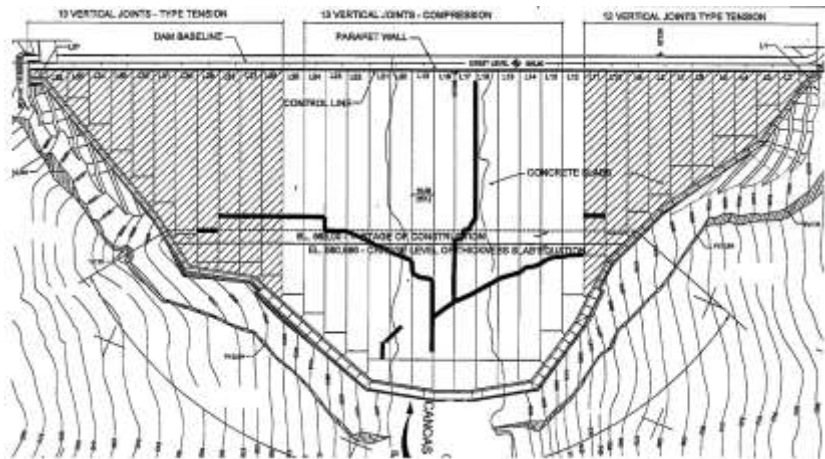
Figure 28 Cracks in Campos Novos concrete facing (IWP&DC, 2008).

Barra Grande

187m high; crest length: 665m; 708 MW; slab thickness: 0,3+0,002H>0,005H; upstream slope: 1,3; downstream slope: 1,4; rock fill type: quarried basaltic rock; extruded curb method used; plastic sheets were placed over the extruded. During impounding extensive rupturing of the concrete slab was observed, resulting in a peak leakage of 1280l/sec.

7.2.2 Leakage

Referring to ICOLD (2005, p.1-8):

> Many CFRDs have performed extremely well with respect to leakage rates…High leakage rates, … , are embarrassing to the engineer, the constructor and the owner and are to be avoided to the maximum extent possible…Avoiding this causes by means of selection of a appropriate filter and rockfill materials, upstream and downstream shell placement in thinner layers along with generous use of water during compaction, elimination of rock protrusions downstream of the perimetric joint, and avoiding inappropriate shell construction sequences, will lead to smaller deformations and a reduction in face slab cracking.

Reported leakage values from monitoring after first filling are generally in the range of 0 to 1800 l/sec (excluding dumped rockfill embankments, which showed significantly higher seepage in some cases (up to 4000 l/sec). Regarding this high values, a differentiation between seepage trough the face slab and seepage through failures in the grout curtain has to be made. However in most cases it is impossible to determine the seepages exact origin.

7.2.3 Crest settlements due to first filling

If deformations are compared to historical records, one always has to bear in mind the dam's history of loading.

For example: Aquamilpa dam withstood partial impoundment due to flooding during construction period. As mentioned in chapter: 6 Stress-Strain-Behavior of Rockfill, the deformation modulus is much higher during un-/reloading than on initial (virgin) loading. Thus the measured slab deformation in the affected area on "first" filling (i.e. the controlled impoundment) is smaller as it would have been without this partial flooding.

Figure 29 shows crest settlement due to first filling, whereas time dependent settlements prior t first filling are excluded. Hunter and Fell (2002) highlight factors affecting the crest settlement during first filling:

- Settlement increases with increasing filling time.
- Settlement increases with increasing dam height.
- Settlement increases with decreasing intact rockfill strength for quarried rockfills. However, gravels show similar settlements as very high strength rockfills.
- Settlement increases with increasing time between end of construction and first filling.
- Settlement decreases with decreasing compaction effort.
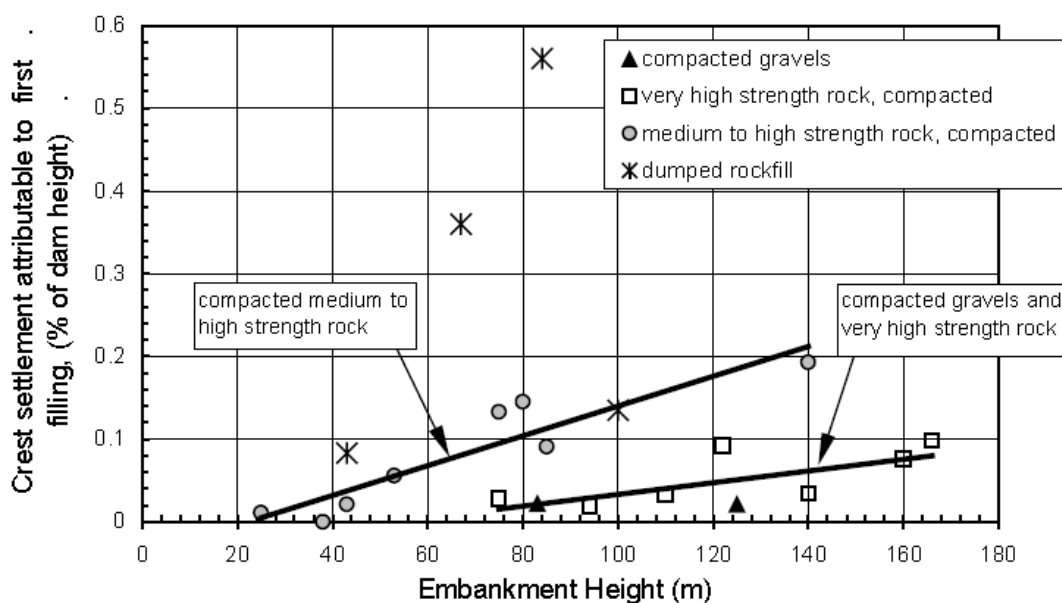
Figure 29 Crest settlement due to first filling, excluding time dependent settlements prior first filling (Hunter and Fell 2002, p.46).

The crest settlement during initial impounding can be used for estimating the long term behavior of the dam body. Initial crest settlement amounts to at least 50% of the long term settlements (Fell et al. 2005). Table 8 gives an overview on the general behavior of some CFSGD's, where monitoring data was published. The average E-moduli at end of construction were corrected for arching and do all fit to a vertical stress occurring in the embankment's center or lower half (Fell et al. 2005). Sarigüzel dam's embankment is provided to be of 82 m height. Assuming a specific weight of 21,5 kN/m^3, the E- modulus of Sarigüzel dam has to be adjusted to a vertical stress of 880 kN/m^2.

A correction to the applied deformation modulus for the range of the expected vertical stress levels is suggested. Unfortunately, there is not enough data for accurate proposals for the correction of sand-gravel fill. However, in general, the modulus increases with decreasing vertical stresses. (Fell et al. 2005)

Table 8 Overview on general deformation parameters of CFSGD (adapted from Hunter and Fell 2002, appendix pp. 3-10).

	Aquamilpa zone 3A	Salvajina	Wuluwati	Crotty	Golillas
Height [m]	186	148	138	83	125
Arcing likely?	No	Yes	Yes	Yes, a little	Yes
Average E-modulus end of construction [MN/m^2]	305 (250 - 330)	205 (175-260)	235 - 350	375 (113-636)	115 (145-165)
Corrected E-modulus end of construction [MN/m^2]	305	130	-	360	107
Corr. modulus refers to a vertical stress of [kN/m^2]	2000	1600	-	900	1350
Maximum settlement at end of construction [% of dam height]	-	-	0,27	-	-
Lateral crest displacement due to impounding [% of dam height]	-	-	-	0,0108 (9mm)	0,0056 (7mm)
Vertical crest settlement due to impounding [% of dam height]	0,119 (222mm)	0,00608 (>90mm)	-	0,00193 (16 mm)	0,0016 (20mm)
Maximum face slab deformation perpendicular to face slab [% of dam height]	0,172 (320mm) including long-term deformation	0,0372 (55mm)	-	0,0554 (46mm)	0,128 (160mm)

Compaction effort [passes of a ? to SDVR]	4 p. 10 to SDVR	4 p. 10 to SDVR	unknown p. 16-20 to SDVR	8-12 p. 6-10 to SDVR	4 p. 10 to SDVR
Layer thickness [m]	0,6	0,6	1	0,6	0,6
Water added? [%]	No, but in moist condition	Yes	No	Yes, a little	Yes
d_{80} [mm]	124	80	-	60	185
% finer 19 mm	34	32	-	48	40
% finer 0,075 mm	2	0-13	-	3,5	6
Material / grain shape	dredged gravels / rounded	alluvial gravels / rounded	alluvial sandy gravels / rounded	gravels / rounded	gravels / rounded
Clean / dirty	clean to dirty	dirty	dirty	dirty	dirty
Behavior / leakage	large horizontal crack in upper part of slabs, due to the strong varying modulus of up-stream and down-stream rockfill / 200 l/sec at first filling, no leakage till crack occurred	74 l/sec, 60l/sec trough face slab and 14 l/sec trough foundation	-	No cracks or joint rupturing observed during im-pounding, 45 l/sec	excessive leakage through the foundation during im-pounding, 1080 l/sec

7.3   Post Construction Crest Settlement

Table 9 shows the scatter rang of total post construction crest settlements, observed for CFRDs of different kinds of rockfill source. Herein, post construction settlements include settlements due to first impoundment as well as creeping and collapse settlements. In contrast to quarried rockfill, gravel fill shows minor post construction deformation. Weak quarried rockfill shows creep rates that are up to 10 times higher than that observed for sound, very high strength rockfill. (Fell et al. 2005).

Table 9 Post construction total crest settlement and long-term creep rate (Hunter and Fell, 2002)

Rockfill classification	Total post construction settlement (% of dam height)		Long-term creep rate (%/log cycle)
	10 years	30 years	
Dumped Rockfill	0.6 to 1.0%	1.0 to 1.5%	0.3 to 1.5
Well compacted rockfills			
– Medium to high strength	0.15 to 0.4	–	0.05 to 0.25
– Very high strength, quarried	0.06 to 0.2	–	0.02 to 0.10
– Gravel Rockfills	0.2 to <0.05	–	<0.10

Notes: (1) Rock substance unconfined compressive strength medium 6–20 MPa, high 20–70 MPa, very high 70–240 MPa.

Hunter and Fell (2002) highlight factors affecting the total post construction crest settlement:

- Settlement increases with increasing dam height.

- Settlement decreases with decreasing compaction effort.

- Settlement increases with decreasing intact rockfill strength for quarried rockfill.

- Well compacted gravels show significantly lower settlements in contrast to well compacted very high strength rockfill.

They furthermore highlight factors that are supposed to have some influence:

- Settlement increases with increasing d_{80}.

- Settlement increases with increasing size of downstream zone, containing weak or less compacted rockfill.

- Settlement increases with increasing amount of fluctuation in reservoir level.

- Settlement increases with increasing amount of average rainfall.

8   Sarigüzel Dam

8.1   General Layout

Sarigüzel HEPP project is an 100 MW scheme impounding the river Ceyhan. The dam is located in the province K. Maraş in the mediterranean area of Turkey (Figure 30). Owner and operator is the EnerjiSA Group, a consortium of the Turkish Sabanci Group and the Austrian Verbund AG.
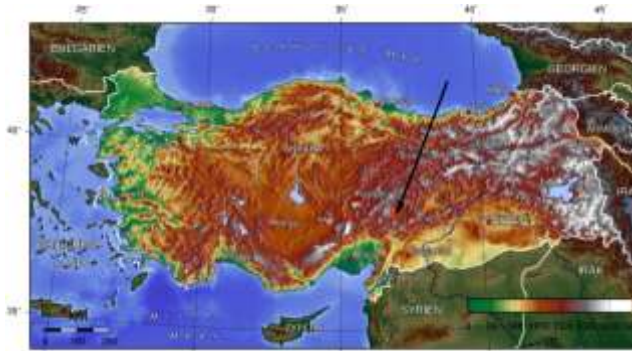
Figure 30 Map of Turkey and location of Sarigüzel HEPP.

8.2   Dam Design

Sarigüzel dam is provided as an 82m high Concrete Faced Sand Gravel Fill Dam, constructed on 30m deep alluvial disposals. The general layout is shown in Figure 31 . Project start is scheduled for June 15th, 2010.
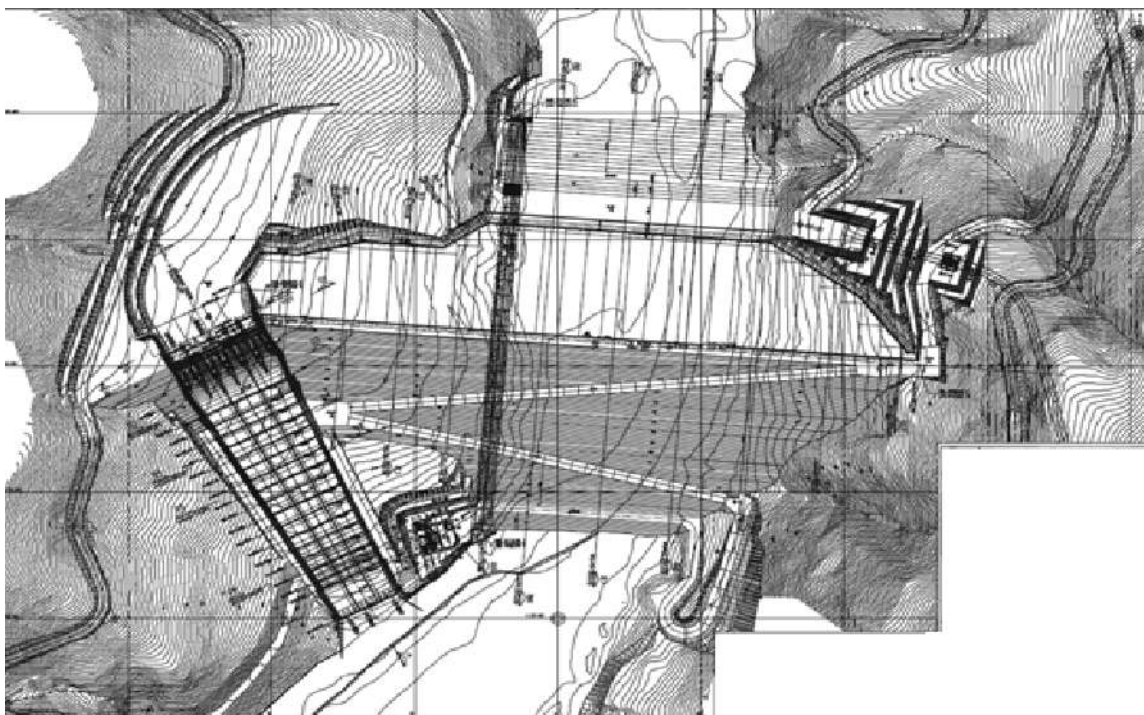
Figure 31 General preliminary layout of Sarigüzel HEPP (reproduced with permission of EnerjiSA).

Preliminary design includes a crest length of 460m, a concrete face area amounting to 38000m². The during construction period, the river diversion is done by in situ casted concrete outlets, each having a diameter of 4.5m. The outlets are arranged on top of the alluvial deposits, crossing the dam's body at section 5-5. After construction works, one of these is intended to provide residual flow, the other one shall act as bottom outlet. Residual flow is used for energy production too, powering an 8 MW Francis turbine. The upstream coffer dam is provided to be part of the dam's embankment. The 14m high coffer dam mainly consists of sandy gravel with an upstream clay sealing protected by a rip rap and an underlying filter.

Applied seepage control measures are:

- Chimney- and underdrain.
- Concrete sealing.
- Cut off wall (two-phase) providing "water tight" cut off in alluvial deposits.
- Grout curtain at the plinth to rock contact.

Due to borehole water pressure tests, the alluvial disposals are considered to be permeable to very permeable, whilst the underlying bedrock is found to be impermeable. Therefore, a cut off wall is constructed starting from the coffer dam's crest. The cut off wall (1m thick and 42m deep) is connected to the later casted plinth structure. Figure 35 shows the plinth structure in detail.

The design of the concrete sealing, panels, starter slabs and joint arrangement is shown in Figure 33. The panels are planed to be of 15m width, having a constant thickness of 40cm along the slab's entire length.

8.2.1 Fill Materials and Zoning

Figure 32 shows Sarigüzel dam's maximum section. As previously stated the dam reaches a maximum high of 82m from elevation 790 (top of alluvial disposal) up to elevation 872m (top of crest wall). It is planned to spray additional water during compaction of all zones.

Main embankment fill will consist of alluvial sandy gravels, containing an unspecified amount of boulders. Main fill material is applied to both, upstream and downstream shoulder. Figure 34 shows pictures of the material, provided to be used in zone 3A.

Figure 36 shows the materials estimated lower and upper grading boundaries. Upstream and downstream material is placed in 80cm lifts and compacted by a minimum of 6 passes of a 10 to vibratory roller.

It is intended to use the extruded curb method in Sarigüzel dam project.

The cushion zone underneath the concrete curbs will consist of processed (by sieving and washing) alluvial deposits having a minimum horizontal width of 2m. Grading is restricted to the gradation limits suggested in ICOLD (2005, Table 7). Cushion material is placed in layers of 40cm thickness and compacted by a minimum of 6 passes of a 10 to vibratory roller. The material shall meet filter and internal stability criteria.

The transitions zone is intended to have a horizontal width of 3m, consisting of unprocessed alluvial sandy gravel. It is assumed, that the transition material meets filter and internal stability criteria without additional processing.

Zone 2A material is limited to a gradation as suggested by ICOLD (2005, Table 5). The material shall be protected by 30mm of shotcrete on upstream side, as there is no extruded curb provided in this area. The material shall meet filter and internal stability criteria.

Drainage zone 2E is restricted to a "well graded" material with a minimum grain size of 10mm and a maximum grain size of 20mm. The material is compacted in layers of 80cm thickness and a minimum of 6 passes of a 10 to vibratory roller.

Downstream protection material 3D consists of processed rock or river cobbles.

Zones 1A and 1B shall be compacted in lifts of 20 cm by 2 passes of a 10 to vibratory roller.

Grout curtain layout consists of three rows of 3m spaced grouted holes and two further rows of consolidation holes, 1m up- and downstream of the curtain's axis.
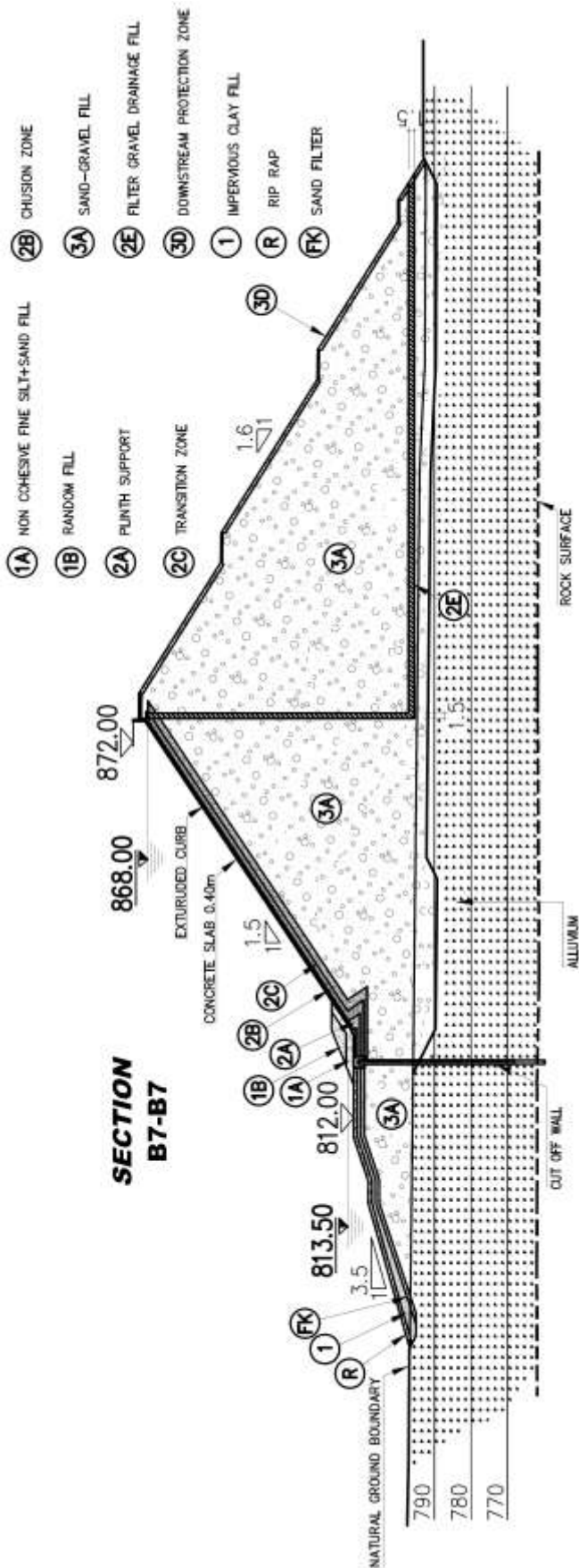
Figure 32 Main section of Sarigüzel Dam (reproduced with permission of EnerjiSA).
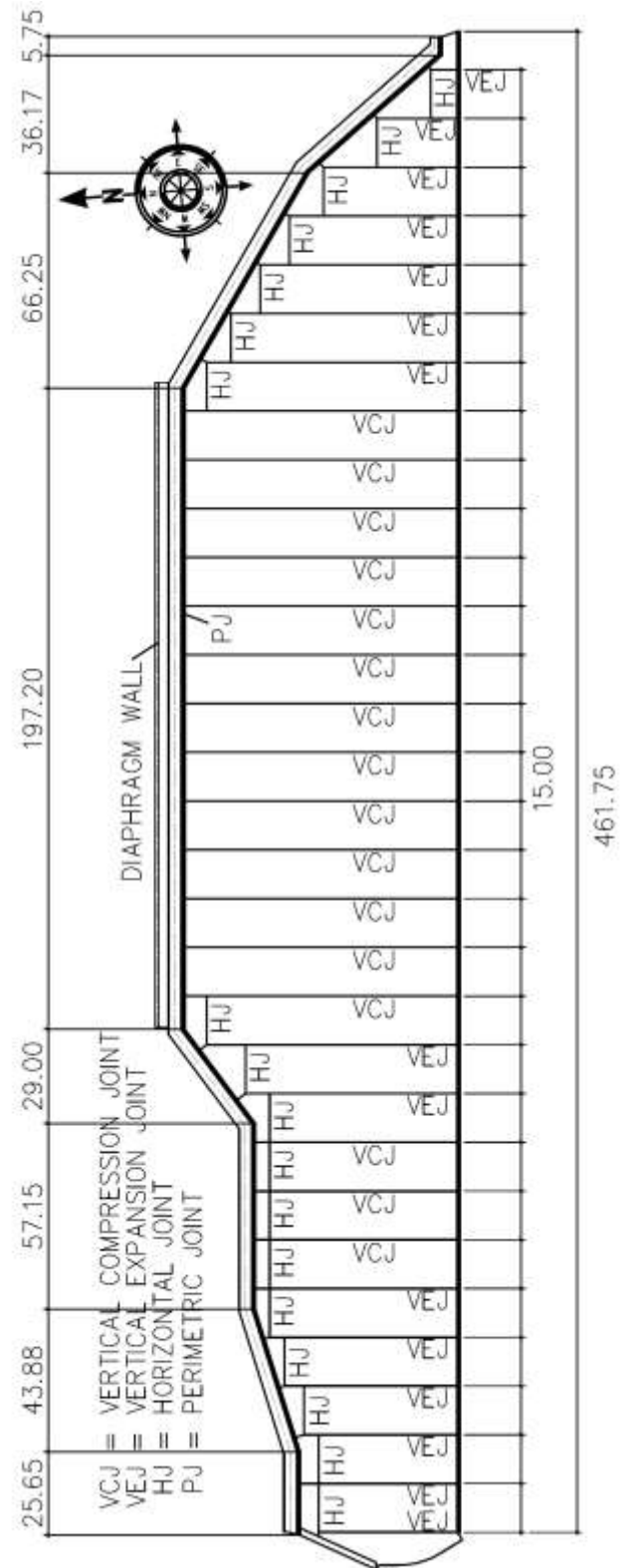
Figure 33 Design of concrete facing (reproduced with permission of EnerjiSA).
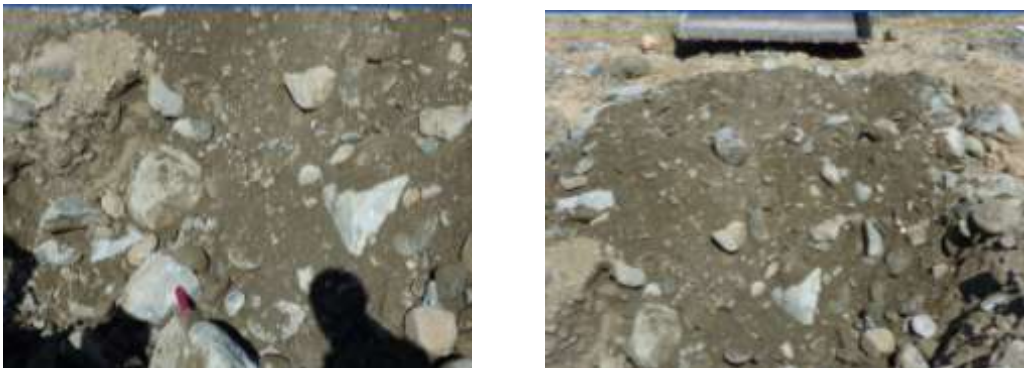
Figure 34 Pictures of Sarigüzel's main embankment material (reproduced with permission of EnerjiSA).
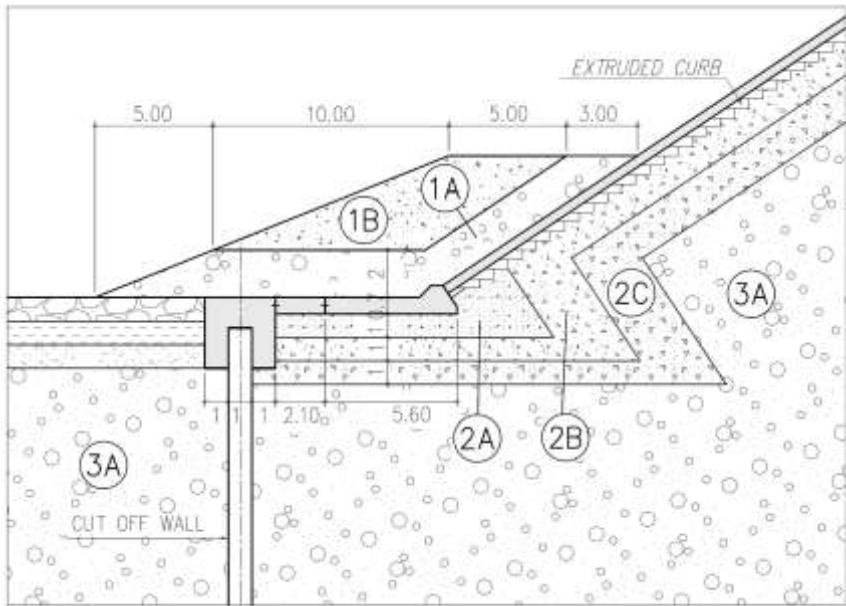
Figure 35 Plinth structure on coffer dam crest (reproduced with permission of EnerjiSA).
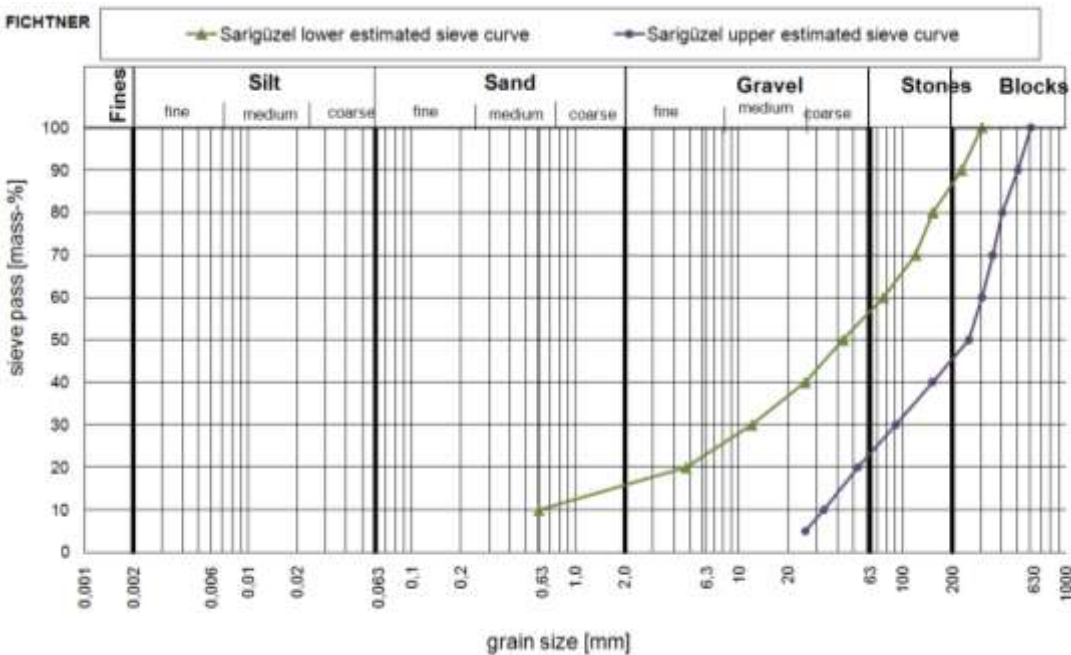
Figure 36 Estimated range of Sarigüzel main fill's grain size distribution.

8.2.2 Joint Details

Vertical compression joints are provided for all slabs that are connected to the cut off wall. Vertical expansion joints are applied close to the abutments and at abrupt changes in plinth alignment (Figure 33).

Figure 37 shows the applied materials and appurtenant numbers for Sarigüzel dam joint design.

① HYPALON BAND	④ TIMBER FILLER	⑦ STYROFOAM FILLER	⑩ DOWEL (M12) L=20cm WITH 30cm. SPACING
② GEOTEXTILE	⑤ COPPER WATERSTOP	⑧ PVC BAND	⑪ ANGLE IRON PROFILE (L 75.75.6)
③ MASTIC FILLER	⑥ NEOPRENE CYLINDER	⑨ SAND—ASPHALT MIXTURE	⑫ NEOPRENE BAND 4mm

Figure 37 Applied materials for Sarigüzel Dam (reproduced with permission of EnerjiSA).

Vertical compression joints (Figure 38 a) provide one watertight barrier, consisting of a "W" type copper water stop (Figure 43).

The horizontal joint, connecting the main and the starter slab (horizontal contraction joint, Figure 38 b), consists of one "defense" line too. A copper water stop lying on a neoprene band. The joint's gap is either filled with timber or asphalt.
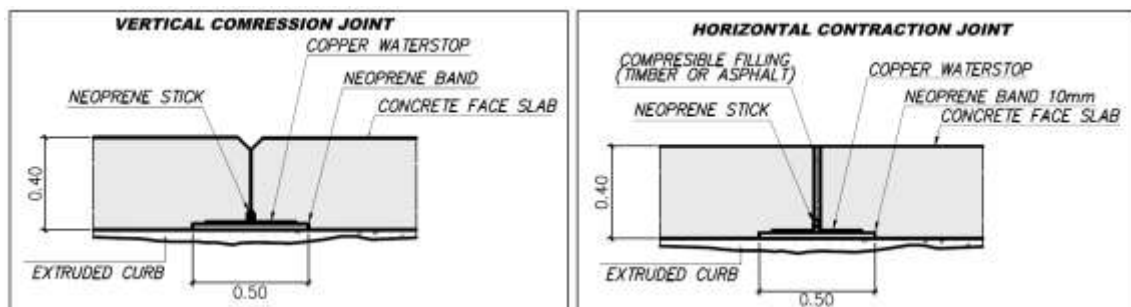
Figure 38 a) Vertical compression joint and b) horizontal contraction joint (reproduced with permission of Enerji-SA).

The vertical expansion joints (Figure 39) consist of two watertight barriers. On upstream side (detail "A", Figure 40) a hypalon band with geo textile covering mastic filler. The hypalon band is held in place and protected by angled steel bars. A copper water stop lying on a neoprene band is provided as downstream barrier. The neoprene band itself is directly placed on the extruded curb's surface.
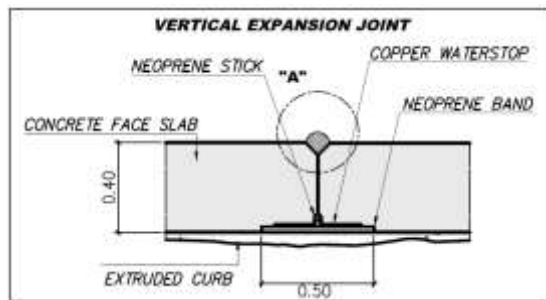
Figure 39 Vertical expansion joint (reproduced with permission of EnerjiSA).
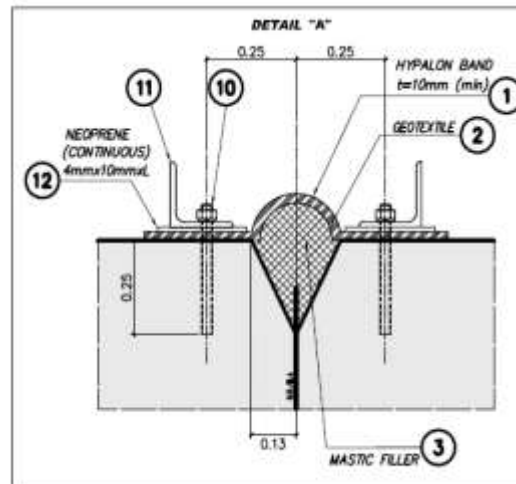
Figure 40 Detail "A" (reproduced with permission of EnerjiSA).

The design of the perimetric joint is illustrated in Figure 41. The perimetric joint is covered by material 1A, with zone 2A acting as filter to that material. Thus, providing a "self healing" character in case of joint rupturing. The joint itself, consists of two further sealing lines. On upstream side a hypalon band, covering geo textile and mastic filler. On downstream side a "W"-type copper water stop placed on a sand asphalt pad. The perimetric joint is filled with compressible wood.
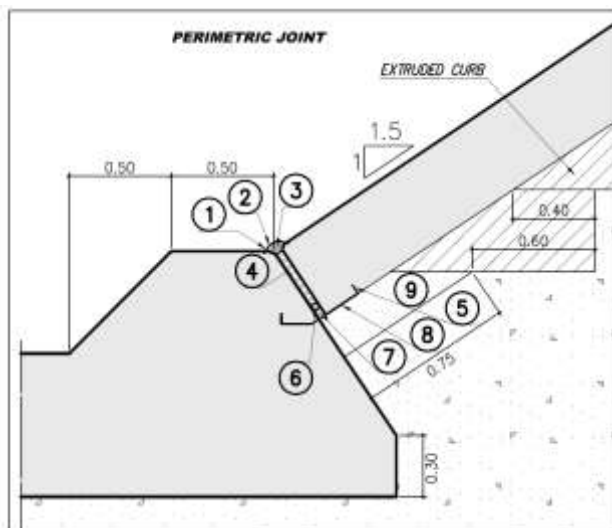
Figure 41 Perimetric joint detail (reproduced with permission of EnerjiSA).

The crest wall's connection joint is pictured in Figure 42 b. The joint consists of three defense lines. A hypalon band, geo textile and mastic filler, covering the timber filled joint on upstream side. Second defense line arranged in the slab's axis is a PVC water stop with central bulb. Third line on downstream side is a "W"-type copper water stop

with a sand asphalt pad underneath.

The joint connecting the plinth to the cut off wall (Figure 42 a) consists of three water tight barriers. From upstream to downstream side: hypalon band plus geo textile covering a mastic filler. A PVC water stop with central bulb, and a "W"- type copper water stop over head a sand asphalt pad. The joint is filled with timber. Two joints of this type are provided to connect the plinth to the cut off wall. One plinth to plinth joint and one plinth to cut off wall joint.
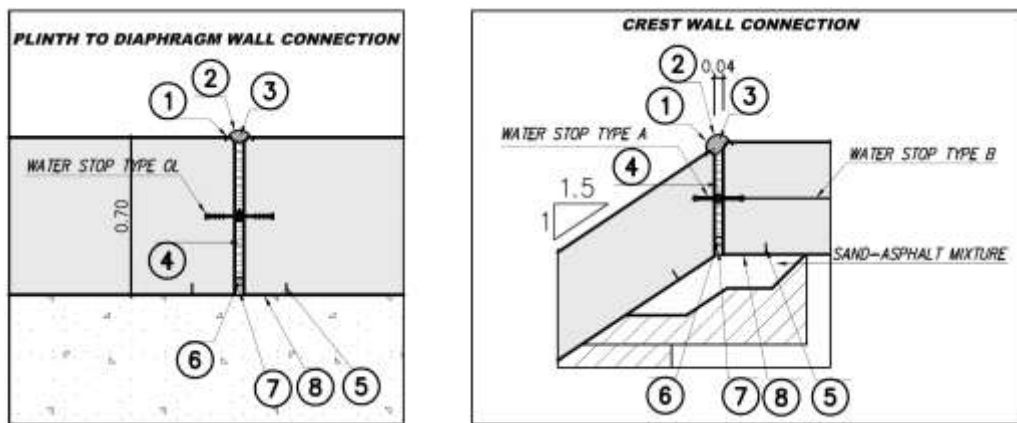
Figure 42 Details: a) Plinth to cut off wall connection and b) Crest wall connection (reproduced with permission of EnerjiSA).

Figure 43, Figure 44 and Figure 45 show water stop details, applied to Sarigüzel dam.
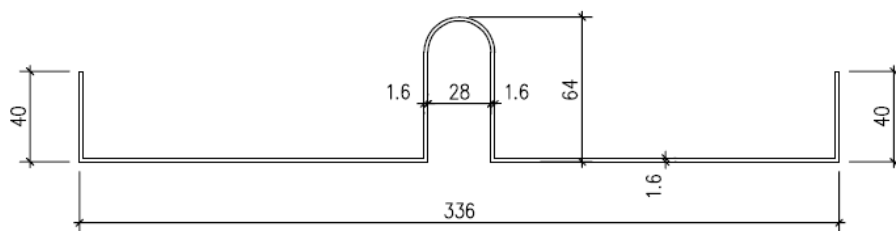
Figure 43 Copper water stop detail applied to Sarigüzel dam [mm] (reproduced with permission of EnerjiSA).
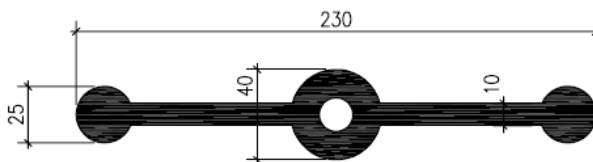
Figure 44 PVC water stop detail type "A" applied to Sarigüzel dam [mm] (reproduced with permission of EnerjiSA).
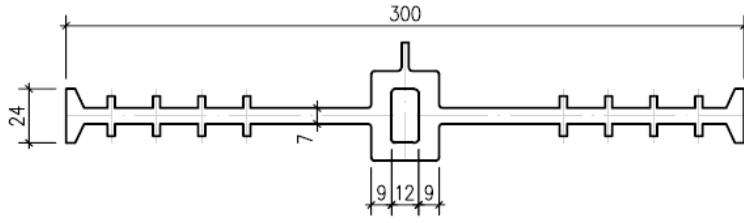
Figure 45 PVC water stop detail type "OL" applied to Sarigüzel dam [mm] (reproduced with permission of Enerji-SA).

8.3 Applied Material Parameters

This chapter summarizes material parameters, chosen for and applied to different calculations by the Sargüzel dam design engineer. In general the chosen values are estimated and are not based on direct laboratory tests (e.g. oedometer or triaxial tests). All data presented in this chapter refers to the unpublished design report.

8.3.1 Load Cases

The following load cases were considered:

- Downstream slope stability after construction with and without pseudo static earthquake loads (MDE = 0,2g, MCE = 0,18g, OBE = 0,1g)
- Downstream slope stability after impounding (up to normal water table) with and without pseudo static earthquake loads (MDE = 0,2g, MCE = 0,18g, OBE = 0,1g)

8.3.2 Liquefaction

SPT tests displayed the dense structure of the alluvial sediments (lowest value obtained was actually 33). "As far as the dense structure and the coarse cobble-boulder gravelly gradation of the zone are taken into account, it is possible to state that there is no liquefaction risk."

8.3.3 Stability Analysis

Shear strength of zone 3A and underlying alluvium was calculated by applying a curved Mohr envelope, modeling the material's non-linear and stress dependent behavior.

$$\tau = c + a \cdot (\sigma_n)^b$$

Where τ is shear strength (kN/m^2), c cohesion (kN/m^2), and a, b are coefficients (no unit). Table 10 shows the material parameters applied in stability analysis.

Mohr Coulomb failure criterion was applied to the underlying bedrock in the calculation. The concrete face does not contribute to the dam's slip resistance. Stability analyses were undertaken for the downstream slope, making the assumption that the downstream shell remains unsaturated above the tail water level in all cases.

Table 10 Material parameters applied in stability analysis (reproduced with permission of EnerjiSA).

Number	Material Type	γ_n (kN/m³)	γ_{sat} (kN/m³)	c' (kN/m²)	ϕ' (degrees)	Force Model Parameter a	Force Model Parameter b
1	Alluvium	17.5	19.0	3	-	1.4	0.89
2	3B	19.0	20.0	5	-	2.8	0.78
3	Bedrock	23.0	23.0	250	35		
4	Concrete	24.0	24.0	-	-		

No extra calculation was undertaken for maximum water level, due to the fact that an additional water load of 1.74m does not affect the stability of an 80m high dam. Table 11 shows safety factors, obtained by the stability analysis.

Table 11 Safety factors obtained from stability analysis (reproduced with permission of EnerjiSA).

Loading Number	Type of Analysis	Factor of Safety
1	Downstream face, end of construction, static condition	1.536
2	Downstream face, end of construction, earthquake condition (0.10 g)	1.255
3	Downstream face, end of construction, earthquake condition (0.18 g)	1.083
4	Downstream face, end of construction, earthquake condition (0.20 g)	1.046
5	Downstream face, reservoir full case, static condition	1.552
6	Downstream face, end of construction, earthquake condition (0.10 g)	1.245
7	Downstream face, end of construction, earthquake condition (0.18 g)	1.061
8	Downstream face, reservoir full case, earthquake condition (0.20 g)	1.021

8.3.4 Seepage Analysis

No seepage analysis was undertaken, since the main fill material is assumed to be highly permeable. The concrete face is considered to be impermeable, in case of face slab cracking or rupturing, a chimney drain linked to an underdrain is applied.

8.3.5 Deformation Analysis

Settlements and deformations were calculated using PHASE 2 software. In general, Mohr-Coulomb material model was applied to all zones. Whereas linear behavior was assumed for the concrete face and linear elastic-perfectly-plastic behavior was assumed for the other materials. Table 12 shows the material parameters applied for deformation analysis.

Table 12 Material parameters applied in deformation analysis (reproduced with permission of EnerjiSA).

Number	Material Type	γ_n (kN/m³)	γ_{sat} (kN/m³)	c' (kN/m²)	ϕ'_{peak} (degrees)	ϕ'_{res} (degrees)	E (kN/m²)	Poisson Ratio (ν)
1	Alluvium	17.5	19.0	3	34	32	90000	0.25
2	3B	19.0	20.0	5	36	33	210000	0.22
3	Bedrock	23.0	23.0	250	35	35	2000000	0.20
4	Concrete	24.0	24.0	-	-	-	28500000	0.20

The embankment's raising was modeled by 25 phases whereas concrete casting was the 25th phase. First filling was modeled in 3 phases. It was assumed, that the embankment remains unsaturated during construction and impounding. The analyses were restricted to static deformations.

After end of construction, the maximum deformation for Sarigüzel dam resulted in 54,1cm at 795,5m elevation and 8,73m downstream of the dam axis, which is 0,68% of the dam's height.

After impounding, the maximum deformation (measured orthogonal to slab surface) resulted in 24,3cm at 812m elevation (excluding construction deformation).

9   CFSGDs - Case Studies taken from Literature

In the subsequent descriptions of CFRDs of similar design, the emphasis is put on:

- Main fill material.
- Filter design.
- Joint details.
- Behavior during construction and impounding.
- Alluvial deposits.

If more specific information is needed, the reader will find references for every described dam in the particular chapter.

9.1 Aquamilpa Dam, Mexico

Aquamilpa dam is a 187m high CFRD situated in central Mexico. The dam is part of a multipurpose project including irrigation, flood control and electricity generation with an installed capacity of 960 MW. At the time of construction, Aquamilpa dam was the highest CFRD in the world and alluvial deposits were used in the upstream embankment as filling material. The dam's volume amounts to approximately 13 Mio. m^3. Figure 46 shows Aquamilpa dam's main section. The applied slope angles are: 1:1.5 for upstream and 1:1.4 for downstream slope. The lower part of the concrete facing is covered with silty sand and random fill (Figure 46).
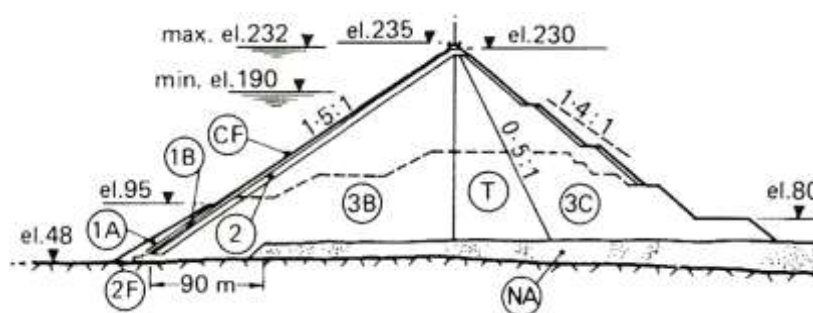
Figure 46 Main section of Aquamilpa Dam (Montanez-Cartaxo, 1992).

- NA… Natural alluvium
- 1A… Random fill
- 1B… Silty sand
- 2F… Alluvial gravel and silty sand mixture
- 2…. Sieved, crushed alluvial gravel sand mixture
- 3B… Dredged alluvium
- 3C… Quarried rockfill
- T….. Quarried rockfill
- CF… Concrete facing

Zone 3C consists of quarried rockfill, compacted in 120cm thick layers. Zone T is composed of the same material as zone 3B, but is compacted in thinner layers (60cm) to achieve a higher deformation modulus. Zone T acts as a transition between 3B material's high and 3C material's low deformation modulus. (Montanez-Cartaxo, 1992).

9.1.1 Main Fill Material

Zone 3B consists of dredged alluvial gravels. This method ensured a very low content of fines. The material was compacted in 60cm lifts by 4 passes of a 10 ton smooth drum vibratory roller. Figure 60 shows the gradation of 3B material. Observed mea-

surements indicated, that Material 3B is 3 to 3.5 times stiffer than material 3C. Thus Zone T was applied. (Montanez-Cartaxo, 1992).

9.1.2 Chimney Drain

Due to the high permeability and the low fines content of the main fill material, no special drainage zones were applied.

9.1.3 Alluvial Deposit

Excepting a 90m wide zone behind the plinth structure, the natural alluvium was left in place. (Montanez-Cartaxo, 1992).

9.1.4 Joint Details

The arrangement and design of Aquamilpa dam's joints is shown in Figure 47.
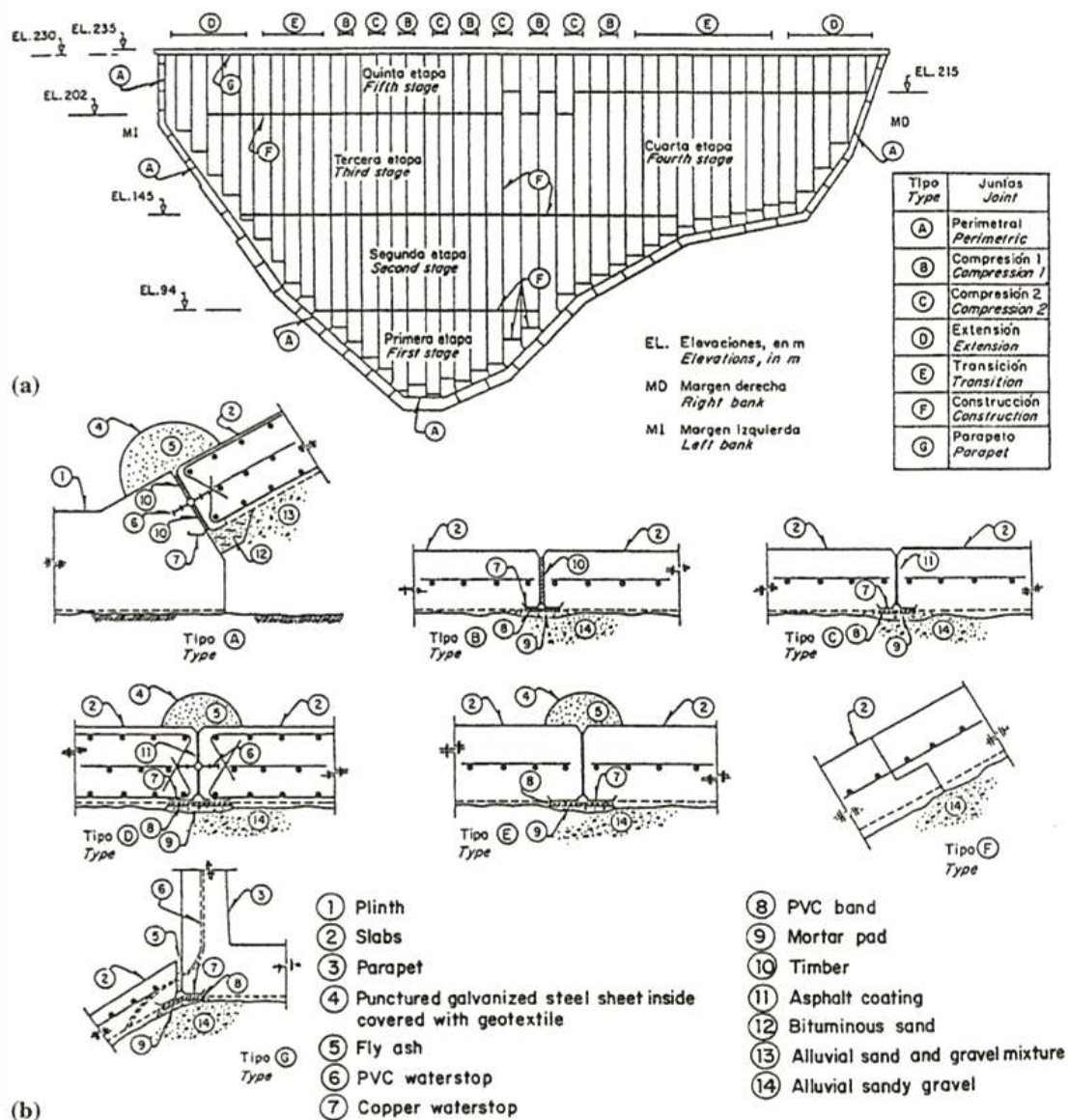
Figure 47 Joint arrangement (a) and joint design (b) of Aquamilpa Dam (Valencia and Sandoval, 1997).

Due to the fact that Aquamilpa dam provided several new design approaches, the Mexican Federal Commission of Electricity started a research program to investigate the water stops' maximum tolerable movements. Subject to the tests were PVC water stops with central bulb, copper water stops and the effect of "self healing" materials on ruptured joints. The water stops were moved under increasing water pressure in longitudinal, tangential and vertical directions. The water load, affecting the water stops at Aquamilpa dam is up to 2 MPa. Figure 48 shows the tested PVC and copper water stops, given values are fixed the others are varied in all tests.

key

(a) = PVC waterstop

(b) = copper waterstop

c = 38 mm

d = 25·4 mm

Ø, t = (see tables I and II)
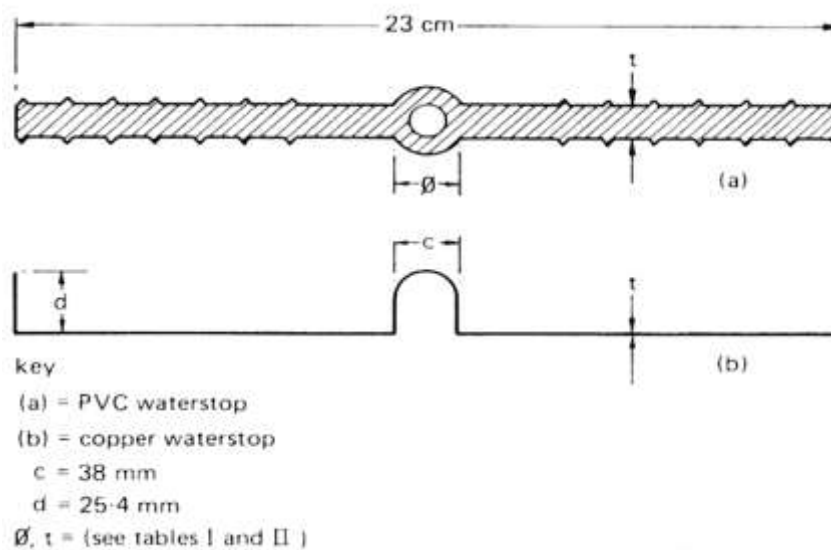
Figure 48 Tested PVC and copper water stops (Montanez-Cartaxo, 1992).

Table 13 shows test results of the PVC water stop and its conditions at failure. The Vynilex product (number 5 in Table 13) was the only one resisting a water load of 2MPa and the below mentioned movements. Table 14 shows the results of all tested copper water stops. (Montanez-Cartaxo, 1992)

Table 13 PVC water stop test, results and conditions at failure (Montanez-Cartaxo, 1992).

Test no	Dimensions (mm) LWS ø	t	RWS ø	t	σh at failure, in MPS LWS	RWS	LWS deformations at failure (mm) Δ	Ω	τ	Failure in LWS	RWS
1	18	3	36	5	1	0.7	15.6	7.5	8.2	X	
1*					0	±1.1	Not measured				X
2	18	3	36	5	0	1	Not measured				X
3	36	5	36	5	1	1	25	2	19.5		X
3*					≈0.8	0	—	30	—	X	
4ᵃ	38	12	38	12	1.6	1.1	41.6	13.4	24.2	X	
5ᵇ	38	12	38	12	2	1.4	34.1	13.8	13.5	None	
5*					0	2	—	±20	—	None	

LWS = left waterstop; RWS = right waterstop; σh = internal hydraulic pressure; Δ = settlement; Ω = opening; τ = shear; ø = bulb diameter; t = waterstop thickness; * = test of the second waterstop after the failure of the first one; a = Mexican band specifically fabricated for the tests-first sample; and, b = North American Vynilex band similar to the one used on Salvajina dam.

Table 14 Copper water stop test, results and conditions at failure (Montanez-Cartaxo, 1992).

Table II — Tests with copper waterstops: conditions at failure

Test No.	t (mm)	σh at failure (MPa) LWS	RWS	LWS deformations at failure (mm) Δ	Ω	τ	Type of failure
1	1.3	1.2	1.2	5	−2.7	−0.9	TCB
2	0.9	1.6	1.6	0	2.2	2	TCB
2*	0.9	1.1	1.1	19.7	−5.2	3.7	W
3	0.4	1.5	1.5	−0.1	−2.6	0.7	None
3*	0.4	1.4	1.1	20.2	23.2	19.1	Adh

LWS, RWS, σh, Δ, Ω and τ are defined in Table I.
t = Thickness of both waterstops
TCB = Tension failure of the concrete blocks
W = Welding failure after sealing with fly-ash most of the concrete fissures that appeared in the first stage of this test.
Adh = Lack of adherence concrete-copper
* = Second stage of test.

The test results highlight that even small movements may cause rupturing, especially if simultaneously occurring in all three directions.

Montanez-Cartaxo (1992) suggests the use of fly ash as third defense line instead of mastic fill. Figure 49 shows the third defense line of Aquamilpa's upper joints (from el. 95 upwards). Fly ash develops significant cohesion when dried up, but it disappears immediately when wetted. The test demonstrated, that fly ash significantly decreased leakage and furthermore, reduced the pore pressures to 25% of the affecting hydraulic head within the crack depth!
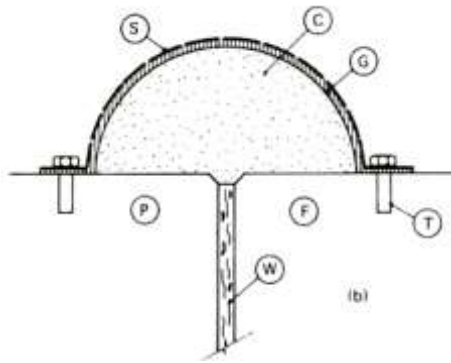
Figure 49 Third defense line of Aquamilpa Dam (Montanez-Cartaxo, 1992).

- S... perforated, galvanized steel cover

- G... geotextile

- C... fly ash

- F... concrete face

- P... plinth

- W... timber

- T... bolts
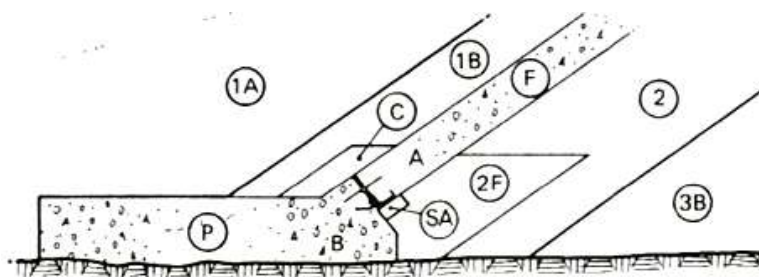
Figure 50 Plinth design of Aquamilpa Dam (Montanez-Cartaxo, 1992).

SA... sand asphalt

A... PVC water stop

9.2   Salvajina Dam, Colombia

Salvajina dam is a 145m high CFRD, situated in Columbia. Slope angles are 1:1.5 on upstream slope and 1:1.3-1.4 on downstream slope. Further information can be found in Thomas, M. (1988).
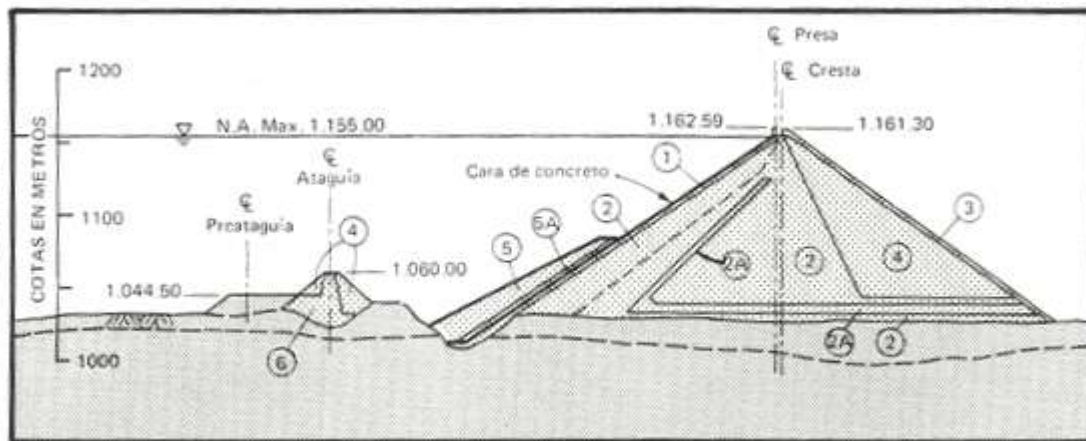
Figure 51 Maximum section of Salvajina Dam (Thomas 1988, p. 378).

9.2.1   Main Fill Material

Main embankment consists of dredger tailings, obtained from alluvial deposits downstream from site. The material may be qualified as very well graded, rounded, cobble gravel, having a maximum grain size of 30 cm. Figure 52 shows the grain size distribution of zone 2. The material was compacted in 50cm layers, by 4 passes of a 10 ton vibratory roller. (Thomas, 1988)

Sieve size (mm)	Dam, year (% passing) Salvijina, 1984
300	100
150	65–100 (98)
75	35–100 (80)
25	10–80 (40)
4.76	0–30 (8)
1.18	0–25 (6)
0.075	0–12 (3)

Figure 52 Grading of Salvajina gravels (Fell et al 2005, p.600).

9.2.2   Chimney Drain

 Due to segregation during placement and the low vertical permeability of the compacted fill, a chimney drain with inclined slot was applied. Zone 2A is obtained from processed dredger tailings. Due to the lack of fines and a maximum grain size of 40cm,

problems during placement and compaction occurred. The drainage zones were compacted by 4 passes of a 10 to SDVR. A gradation restricted to a much smaller maximum grain size of would have been better. (Thomas, 1988)

According to Gouhou dam failure, where rupturing of the crest wall to slab joint caused the catastrophe, the inclined chimney drain of Salvajina dam should have been raised up to the crest wall. Especially if regarding the low permeability of Salvajina dam's zone 4 (zone 4 is obtained from excavated silt- and sandstone resulting in up to 80% passing the 2,5cm sieve).

9.2.3   Alluvial Deposit

The river channels alluvial deposits were found to be at least as competent as the embankment fill itself and consequently were left in place. The material is shown in Figure 51 underneath zone 2A and zone 2. The alluvial deposits consist of dense boulders, gravels and silty sand.

9.2.4   Joint Details

Figure 53 shows the general joint arrangement of Salvajina dam's concrete facing. The contraction joint, applied to the outer slabs is shown in Figure 55. Three defense lines are provided. On downstream side a copper water stop, an axially arranged PVC water stop and a hypalon band covering mastic fill on upstream side. Figure 54 shows the compression joints, applied to the inner slabs. The only "defense" line provided in compression joint design is a copper water stop.
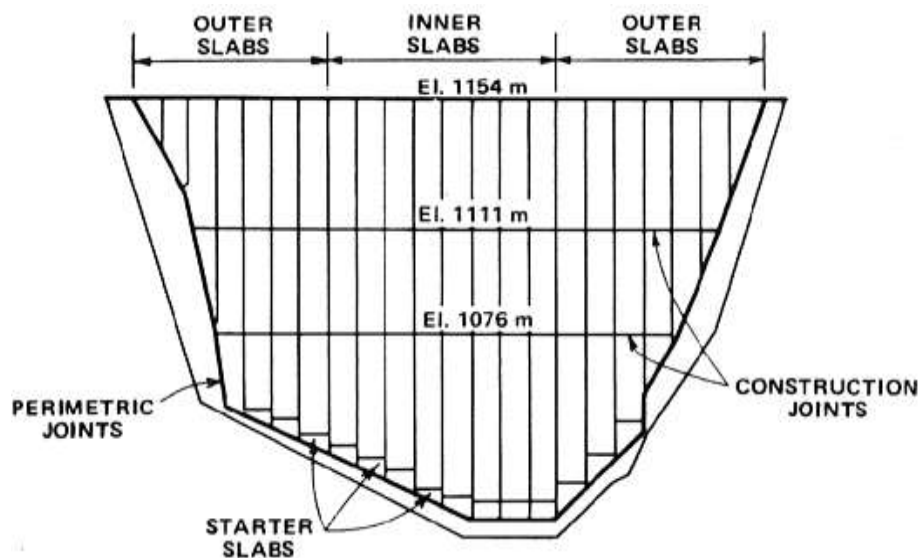
Figure 53 Design of concrete facing and joint arrangement (Thomas 1988, p. 379).
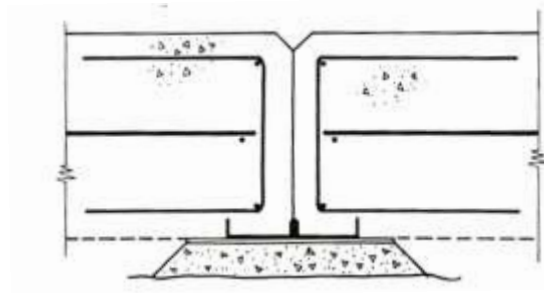
Figure 54 Compression joint (Thomas 1988, p. 379).   **Figure 55 Contraction joint (Thomas 1988, p. 379).**
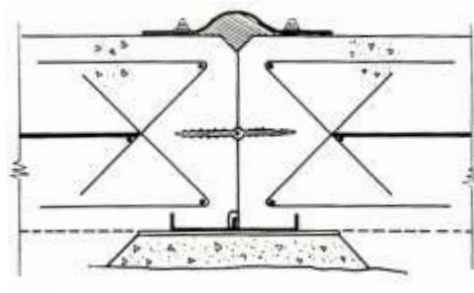
A detail of the perimetric joint is shown in Figure 56. Apart of the additional wood filler, the perimetric joint's design is similar to the contraction joints' design, providing a copper water stop bedded on sand asphalt, a PVC water stop and a hypalon band with mastic filler. The mastic filler should be squeezed into the gap by water pressure, if the joint opens.

According to Cooke and Sherard (1987) a hypalon band provides the advantage of proven resistance even under exposed weather conditions. The mastic filler is stopped by the other water stops. However, if these stops are ruptured, the mastic is stopped by the mortar pad and then sealed by the reservoir's fines content. They go on pointing out, that in most cases, the ongoing joint opening stop and remain constant after a period of 10-20 years.
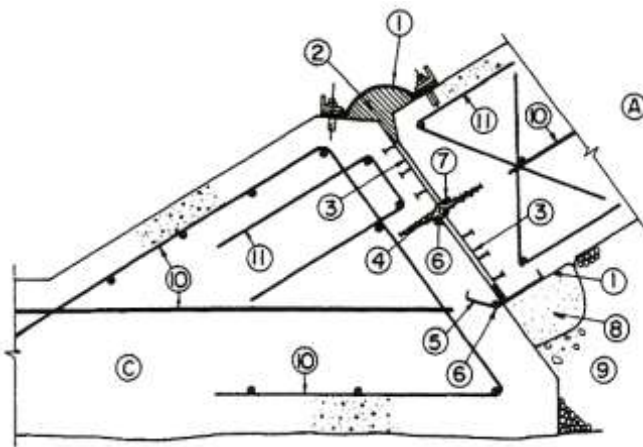
Figure 56 Perimetric joint detail (ICOLD 1989a).

    (1) Hypalon Band.
    (2) Mastic Filler.
    (3) Compressible Wood Filler.
    (4) PVC Water Stop.
    (5) Copper Water Stop.
    (6) Neoprene Cylinder.
    (7) Styrofoam Filler.

(8) Sand Asphaltic Mixture.

(9) Zone 2.

(10)   Steel Reinforcement.

(11)   Steel Reinforcement.

Pinkerton et al. (1985) named tolerable shear displacements:

- 7.5mm for copper or stainless steel.

- 50mm for a 230mm central bulb water stop.

- 10mm for PVC water stop.

In general, tolerable shear displacements depend on the projects special joint design, the herein presented values shall only give a feeling.

9.3   Santa Juana Dam, Chile

Santa Junta dam is a 103m high CFRD, impounding the river Huasco for irrigation purpose, located in northern Chile. The dam is situated in a steep valley, has a crest length of 400m and its volume is in the order of 2.7 Mio. m^3. Design and zoning is shown in Figure 57. Slope angles are 1:1.5 on upstream and 1:1.6 on downstream slope. (Astete et al 1992).
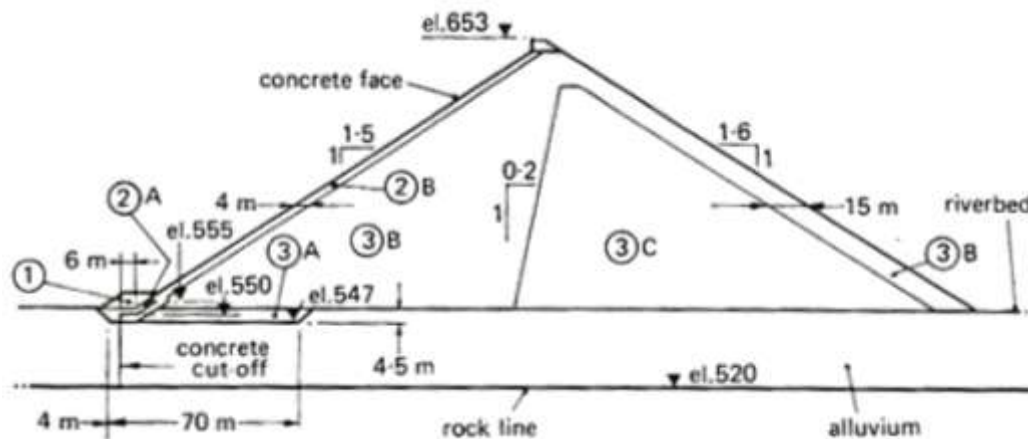
Figure 57 Design and zoning of Santa Juana Dam (Astete et al 1992).

9.3.1   Alluvial Deposit

Santa Juana dam is completely constructed on 30m deep alluvial disposals and provided a new approach: A cut off wall that is flexibly connected to the plinth structure. The plinth itself is bedded on top of the alluvial deposits. Main fill material consists of clean (low fines content) alluvial gravel, available in abundance upstream of the dam site. (Astete et al, 1992)

9.3.2 Main Fill Material

Zone 3B consists of gravels < 600mm, compacted in layers of 80cm thickness. The high quality of alluvial gravel allowed for winning and compaction without processing the material. Zone 3C consists of alternating gravel und quarried rock fill layers, compacted in 1.2m lifts. The quarried rock fill was obtained from necessary excavations as spillway construction and tunneling. (Astete et al, 1992)

9.3.3 Chimney Drain

Due to the high permeability of the main fill, no special drainage zone was applied.

9.3.4 Joint Details (Perimetric Joint)

Figure 58 shows the flexible plinth structure, connecting the concrete slab to the cut off wall.
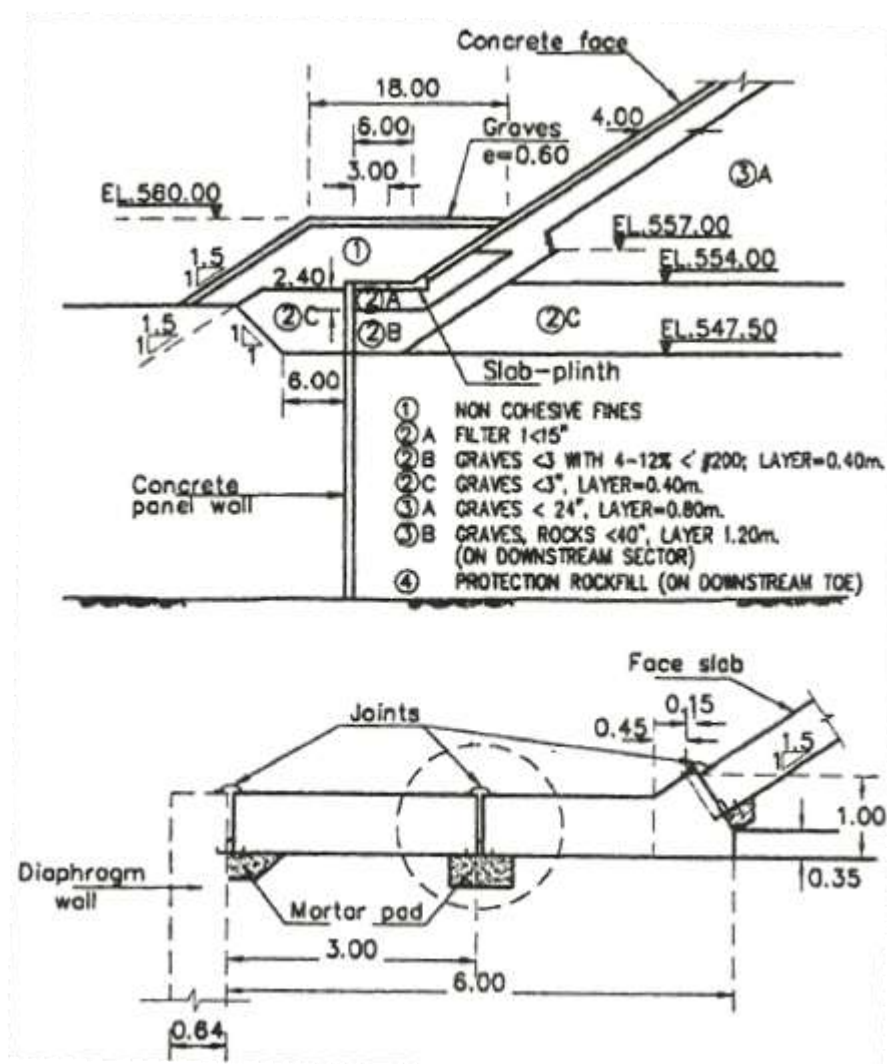
Figure 58 Foundation treatment and plinth design Santa Juana Dam (Marulanda and Pinto, 2000).

9.4   Puclaro Dam, Chile

Puclaro dam is an 83m high CFRD, impounding the river Elqui for irrigation purpose. The dam's crest length is 640m and its total volume amounts to 4.63 Mio. m^3. Slope angles are 1:1.5 on upstream and 1:1.6 on downstream slope. (Noguera et al 1999).
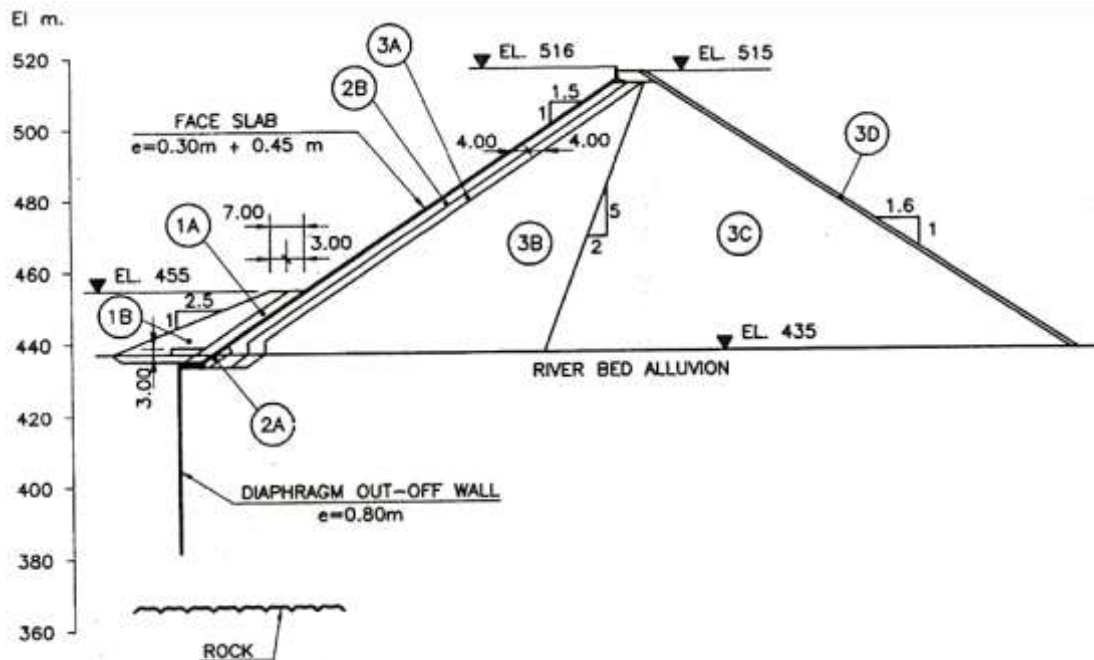
Figure 59 Design and zoning of Puclaro Dam (Noguera et al 1999).

9.4.1   Main Fill Material

Main embankment fill is obtained from river bed alluvium, downstream of the dam site. The gradation is shown in Figure 60. Zone 3B is compacted in lifts of 60cm providing a maximum grain size of 60cm. Zone 3C is compacted in 90cm layers and includes grains up to 90cm. (Noguera et al 1999).

9.4.2   Chimney Drain

Due to the high permeability of the main fill, no special drainage zones were applied.

9.4.3   Alluvial Deposit

The alluvial deposits at site are very deep, up to 113m. A vertical cut off wall in the order of 58m maximum depth is applied to decrease the amount of losses. Conductivity tests resulted in a permeability of 10^{-3} m/s for the upper 60m and 10^{-5} m/s for the lower 60 to 113m. Figure 60 shows the grain size distribution of Puclaro dam gravel compared to Santa Juana, Salvajina and Aquamilpa dam. Due to geotechnical exploration, the alluvium is found to be highly incompressible. (Noguera et al 1999).
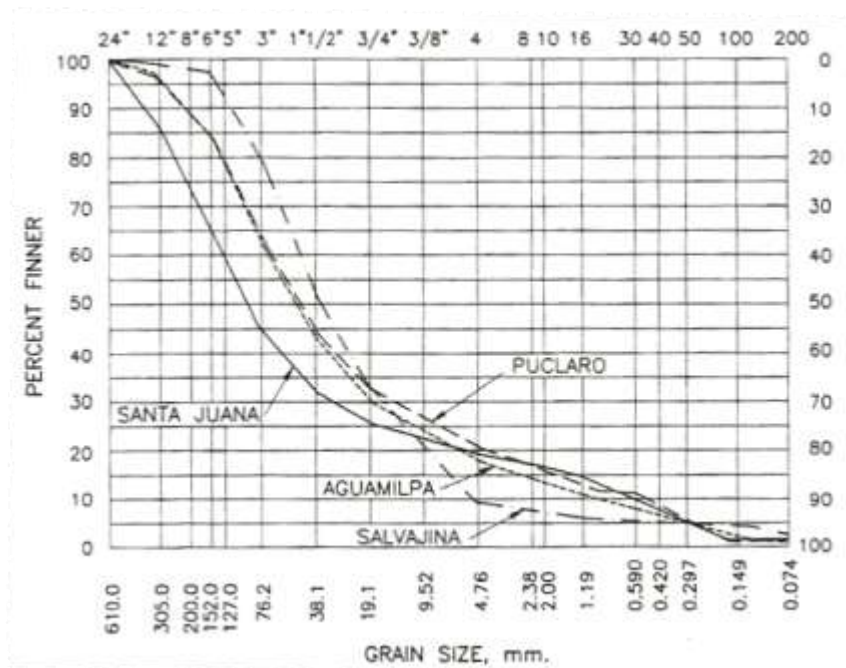
Figure 60 Main fill grain size distributions of Puclaro, Santa Juana, Aquamilpa and Salvajina Dam (Noguera et al 1999).

9.4.4 Joint Details (Perimetric Joint)

The Puclaro dam's plinth structure and its connection to the vertical cut off wall are very similar to the design of Santa Juana dam. Two defense lines are applied, a copper water stop and a hypalon band with mastic filler.
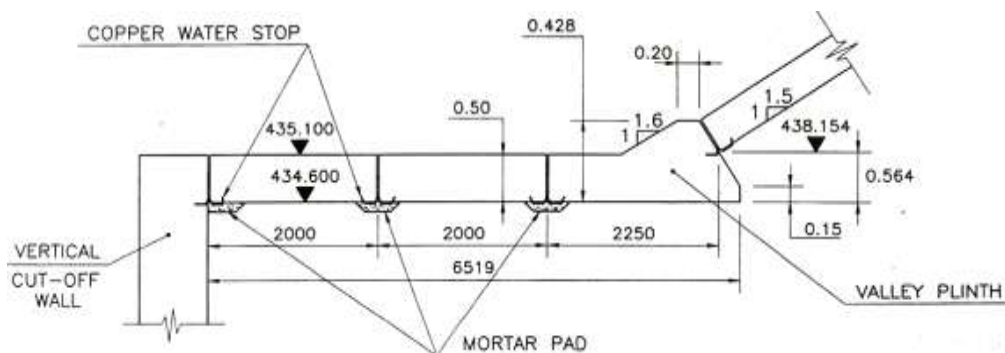
Figure 61 Plinth structure and perimetric joint detail of Puclaro Dam (Noguera et al 1999).

9.5 Siping Dam, China

Siping dam is a multipurpose scheme located at the river Fenqing in China. Main purpose is electricity generation with an installed capacity of 60 MW. Siping dam is a 90.5m height CFSGD resting on 10 to 15 m deep alluvial deposits, while the plinth structure is constructed on sound rock. Figure 62 shows the main section of Siping dam. Natural alluvial gravels are used as upstream main filling material, whilst the downstream rockfill is quarried shale / sandy shale.
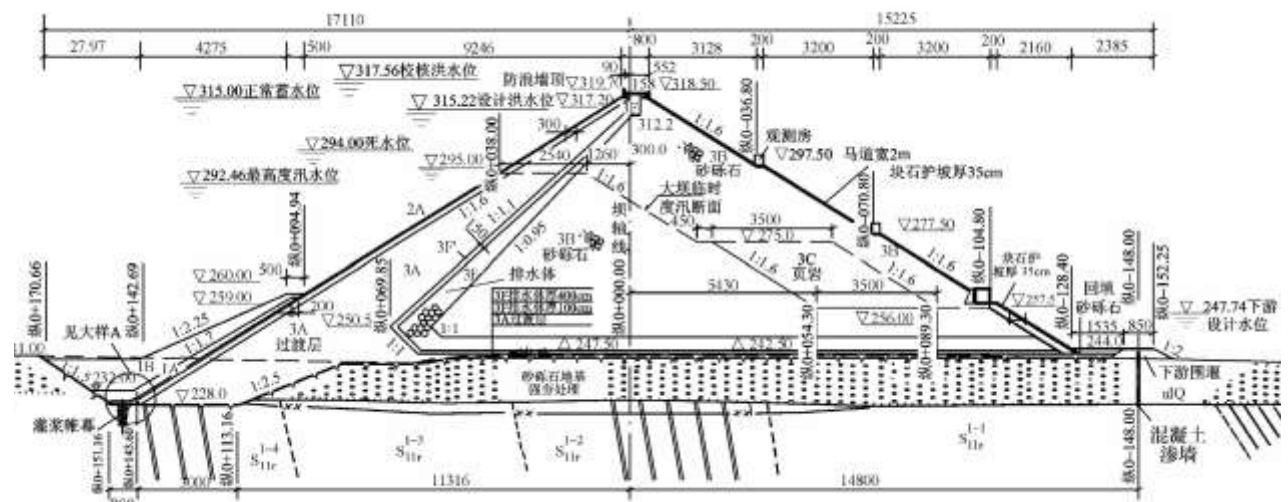
Figure 62 Design and zoning of Siping dam (Feng and Fu, 2009).

9.5.1 Main Fill Material

Maximum grain size of the natural gravel resulted in 500 mm. Siping dam's gravels tend to internal instability. Consequently, piping is a potential failure mechanism. Hence several actions have been taken to make use of the material in spite of its unfavorable properties. The upstream gravel fill was compacted in 80cm lifts by 6 to 8 passes of a 16 to 18 to SDVR including spraying of additional water in the order of 15% but without any preprocessing.

Gravel used for cushion and transition zone was artificially regraded to guaranty internal stability and to ensure that the zones withstand the high gradients occurring in case of local joint failure.

9.5.2 Chimney Drain

A chimney drain linked to a high conductive horizontal underdrain is provided to lower the seepage line on downstream side. The chimney drain is of 2.7 to 12m thickness and is protected from clocking by a 1.5m thick filter to ensure internal stability be-

tween the drainage and the gravel fill zone. Both, the small particle filter and the drainage zone were compacted in 80cm lifts by 6-8 passes of an 18 to 25 to SDVR.

9.5.3 Alluvial Deposit

The horizontal under drain is protected from particles potentially washed out of the remaining alluvial soil by an intermediate filter.

Additionally, the remaining alluvial deposits were dynamically compacted by falling weights, due to the unsuitable physical properties of the covering gravel layer.

10 Stress-Deformation Analysis of Sarigüzel Dam

10.1 General

10.1.1 2D-3D Analysis

To come to the decision which kind of analysis has to be done, for deformations analysis of sufficient accuracy, three methods were found in literature:

Pinto and Marques Filho (1998) defined a "valley shape factor" from historical records. $SF=A/H^2$. Where H is the embankment height and A the concrete face slab area [m, m^2]. They point out that the shape of the valley can be classified in narrow and wide valleys, whereas wide valleys show a shape factor greater than 4 and narrow valleys show a shape factor less than 3.5. If a valley is classified as wide, the valley's effect on deformations is negligible. To calculate Sarigüzel dam's valley shape factor, the project's abnormalities have to be considered. Sarigüzel dam's concrete face starts from top of a coffer dam, which itself is resting on 34m deep alluvial deposits. By this reason, the maximum height considered in calculation is 110m and the face slab area would be in the order of approximately 48500 m^2 if the plinth was constructed on sound rock. Assuming the above mentioned, the valley shape factor turns out to be slightly higher than 4, indicating a wide valley. This value indicates that a two dimensional plane strain analysis is sufficient in this case. Hence, potentially occurring arcing effects may be excluded.

Guidici et al (2000) undertook 3D analysis of an idealized CFRD with varying river bed width and abutment slopes to investigate their influence on deformation behavior (Figure 63). Sarigüzel's river bed shows a width of 130m. According to results B in Figure 63 and assuming abutment slopes of 1H to 1V, which is in fact much steeper than

in reality, the crest length to height ratio turns out to be 3,7 indicating that 2D analysis should provide sufficient accuracy. The steepest part of Sarigüzel's abutment is 1,2H to 1V. Assuming this slope on both abutments, creates a virtual crest length of 317m, resulting in a ratio of 4.1. It should be noted, that the analysis, undertaken by Guidici et al (2000) assume embankment rising in only one stage. Referring to Hunter and Fell (2002) this leads to an under estimation of the embankment's stresses.
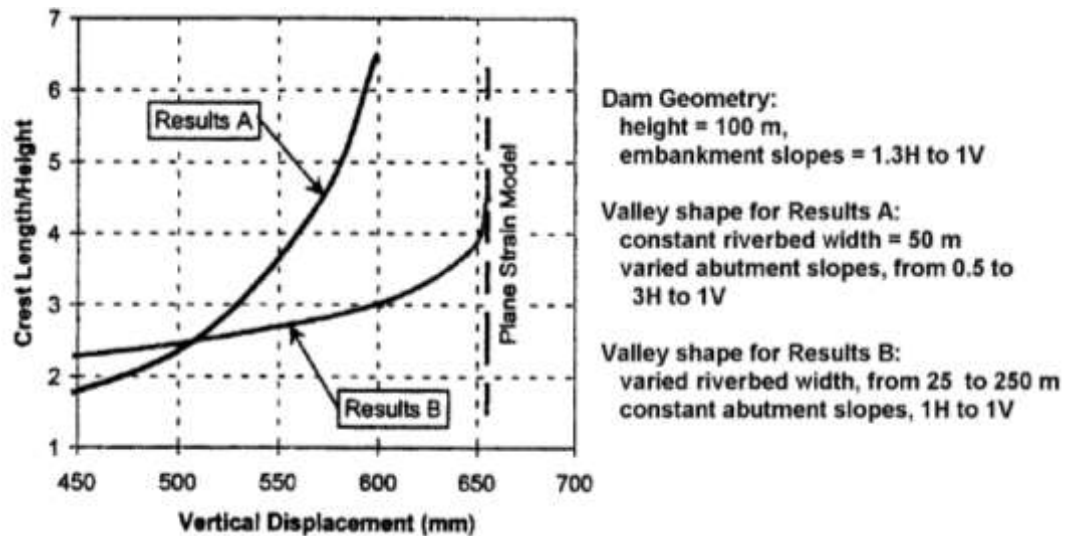
Figure 63 Effect of valley shape on vertical displacement (Guidici et al, 2000).

Hunter and Fell (2002 p.26) investigated the effect of valley shape with two dimensional layered finite difference analysis for an idealized embankment of 100m height. They conclude, that:

- Cross-valley arching is only significant (greater than 20% reduction in vertical stress) for narrow valleys (river width less than 30 to 40% of the dam height) with steep abutment slopes (greater than about 50 degrees, but also dependent on river width), and then only in the lower third to half of the embankment.

- Where the river width is approximately equal to half the embankment height, cross valley arching has some effect (10 to 20% reduction in vertical stress) for abutment slopes steeper than about 45 degrees, and then only in the lower third to half of the embankment.

- Negligible arching is observed for river widths equal to about the embankment height regardless of the abutment slope.

Considering the above mentioned, 2D analysis will provide sufficient accuracy for Sarigüzel dam's deformation analysis.

10.2 Finite Element Analyses

Fell et al. (2005, p.479) wrote a good introduction for this chapter, it shall be recited inhere:

The author's view is that the overwhelming problem in too many cases is that those doing the analysis have neither the proper understanding of the mechanics of the problem and what are reasonable properties, nor a good, detailed understanding of the computer programs. The result is an unfortunate waste of time and money.

They go on, pointing out a general problem of deformation analysis: "The ability to numerically model generally is greater than the ability to provide accurate material properties.

10.2.1 Layered construction

In contrast to, stress calculation, where one staged and layered construction lead to similar results for 2 dimensional analyses, layered construction is of essential interest in deformation analysis (ATV–DVWK-M502, 2002).

In analysis, where the embankment is "filled" in one stage, the crest and upper third will show maximum settlements, which is contrary to measured deformations in every dam. In reality, due to the embankments layered construction, the initial settlement of every new layer (i.e. by reason of its own weight) is compensated by fill material of the next layer. That is to say, in reality initial settlements are cleared, whilst settlements due to further embankment rising "add up". Layered construction provides the opportunity to clear these initial settlements and allows for the summing up of all following deformations. Holzmann (2008).

Layered construction is of special interest if 3D analyses are undertaken. One staged construction will result in overestimation of cross valley arcing effects Fell et al. (2005). The number of layers in staged construction (i.e. multi layer construction) has significant influence on calculation time and the effort on "building" the finite element model. Kulhawy (1969) gives extensive information on selecting the correct minimum number of layers. He also discusses factors influencing the minimum number (e.g. constitutive models). However, due to fast developments in computation power, calculation time decreased in recent years and emphasis is put on selecting an appropriate number of layers instead of selecting the minimum.

Duncan et al. (1980) point out that in case of 2 dimensional finite element analyses, the embankment should at least be constructed of 8 layers to calculate deformations of sufficient accuracy. This value is in general agreement with the results presented by Kulhawy (1969) for both, linear elastic and stress dependent hardening soil models.

10.2.2 Anisotropic behavior of embankments

Due to the particles' segregation during spreading and grain breakage during compaction, the layer's upper region shows a significantly higher oedometer modulus (up to 3 times) than observed in the layer's lower region. Cook (1984) and Kovacevic (1994) demonstrate, that considering the above mentioned in deformation analysis will only have negligible effects on the face slab deformation and therefore does not have to be considered in finite element analysis.

10.2.3 Boundary effects / size of modeled FE-detail

The surrounding rock mass, considered for in the FE-detail, has a significant influence on calculated results, if boundaries / fixities are too close to the dam's general dimensions.

In case of embankments constructed on compressible foundations, Duncan et al. (1980) advise to extend the vertical boundary's distance to the dam's toe to at least three times the foundation's thickness. If the foundation is considered to show a rigid behavior, it might be ignored.

Referring to Meißner (1991), the boundaries have to be extended, till stresses or deformations in points of interest vary less than a few percent.

Holzmann (2008) suggests extending the boundaries, till the calculated stress distributions close to the vertical boundaries vary less than 2%. Whereas, initial stresses and stresses due the embankment's one staged construction are compared.

10.2.4 Mesh properties

Meißner (1991) points out that the size of particular finite elements has to be adapted to the results (stresses, deformation) gradients, i.e. elements close to e.g. single loads have to be finer than in regions with e.g. constant bedding. In general, the mesh has to be refined till stresses or deformations in points of interest vary less than a few percent. Triangular elements should not exceed a ratio of 5 regarding circumscribed radius to inscribed radius. Quadrangular elements should not exceed a height to width ratio of 5 and should not draw an angle smaller than 45°.

10.2.5 Zoning

Again calculation time and effort increases with increasing complexity of the FE-model. By this reason, one has to decide which zones are to be modeled. The FE-model should include all zones that are assumed to have significant influence on points of interest. If one is not sure about the effects of special zones, comparative calculations will shed light on it.

10.3 Applied FEM-Model

All deformation analysis were conducted utilizing the software Plaxis 2D. The results of MC analysis calculated by Plaxis 2D, where controlled by utilizing the software package GeoStudio2007. In general, the results were in good agreement.

All analysis display section 7-7. It is provided to embed observation measurements to section 7-7. Referring to Meißner (1991) and Holzmann (2008), the models vertical boundaries are extended to 1720m (i.e. ~ 16 times the dam's height). The lower horizontal boundary is set to -150m (including 31m alluvial deposits). Figure 64 shows the finite element model applied in all Plaxis 2D deformation analysis.
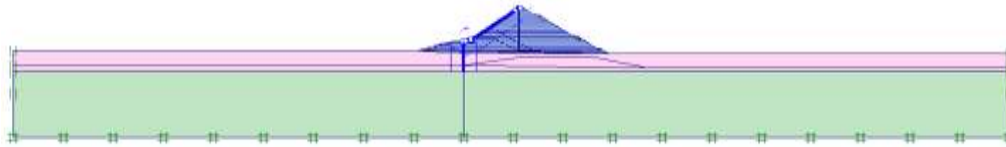
Figure 64 Finite element model of Sarigüzel dam.

The model's horizontal expansion amounts to 11.5 times the model's vertical expansion. This is due to the alluviums' low stiffness, compared to the stiffness of the foundation rock. Especially when regarding the alluvium's low stiffness for low confining pressures, occurring in the deposit's upper part, close to the vertical boundaries. According to the applied fixities, horizontal deformations are constrained for vertical boundaries, whilst horizontal and vertical deformations are constrained for the lower horizontal boundary. Coordinates origin is the coffer dam's upstream toe.

The dam's construction and impounding is simulated in 59 phases. The foundation's initial stresses are calculated by gravity loading and the resulting initial deformations are set to zero in the following phase. The water table for all phases prior to first filling is set to top of the alluvium, representing the natural elevation of river Ceyhan. The phases 2 to 6 display the filling of the later incorporated upstream coffer dam up to elevation 11,3m (Figure 65). Phases 7 to 16 display first stage backfilling of the coffer dam and the embankment's rising up to an elevation of 25.3m (Figure 66). Phases 17 to 29 simulate the 2nd stage backfilling and embankment raising up to an elevation of 33,3m (Figure 67). Phases 30 to 53 simulate 3rd stage backfilling and embankment rising up to an elevation of 71.5m (i.e. bottom of crest wall, Figure 68). The cut off wall is "built" in phase 31. The plinth construction is modeled in phase 53. The concrete slab is "casted" in one stage in phase 54 (as obvious from schedule). The crest wall is "constructed" in phase 55. Embankment rising up to the final level of 75.8m and filling of the upstream self healing and protection material is modeled in phase 56 which furthermore indicates the end of construction works (Figure 69).
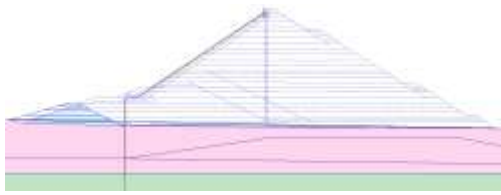
Figure 65 Phase 2 to 6, coffer dam.
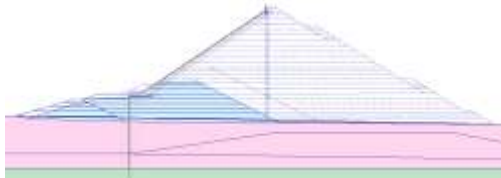
Figure 66 Phase 7 to 16, first stage backfilling.
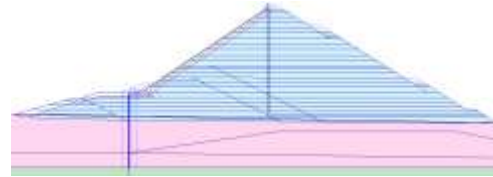
Figure 68 Phase 30 to 53, 3rd stage backfilling and plinth construction.
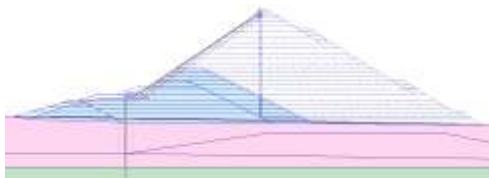
Figure 67 Phase 17 to 29, 2nd stage backfilling.
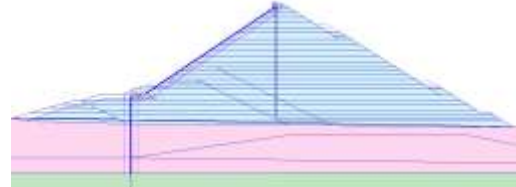
Figure 69 Phase 56, end of construction works.

The embankment is "filled" in 23 layers which is, indeed much more than suggested by Duncan et al (1980) but shall guaranty academic accuracy. Maximum layer thickness is 4.10m. Phase 57 simulates the reservoir's first filling (Figure 70). In phase 57, it is assumed, that tail water rises to its maximum level during impounding. No cracks are assumed to occur in during first filling, consequently the whole embankment downstream the cut off wall, plinth and concrete slab remain dry (excluding the alluvial deposits, wetted by tail water impoundment). Figure 71 shows the pore water pressures for first filling. Phase 58 simulates a draw down to dead water level and phase 59 simulates the reservoir's 2nd filling. All phases and construction stages are in agreement with the preliminary design's provided time schedule.
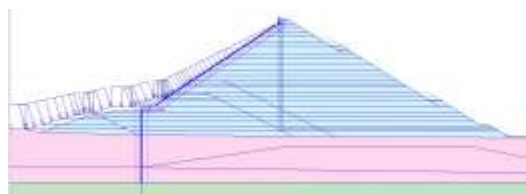
Figure 70 Phase 57, first filling of the reservoir.
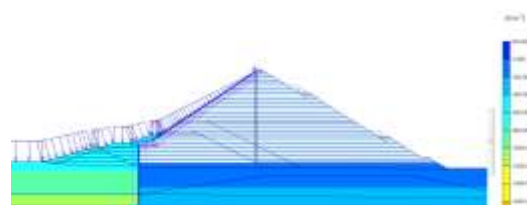
Figure 71 Pore water pressures during first filling.

The zones/materials incorporated in deformation analysis are: alluvial deposits, upstream and downstream main fill, plinth support, cushion and transition, upstream self

healing and protection, drainage and a material simulating the coffer dam's protection, clay sealing and filter all in one. Furthermore the model includes the plates/beams: cut off wall, plinth, concrete slab and crest wall.

10.4 Finite Element Mesh

Figure 72 gives an overview of the finite element net applied to Sarigüzel dam's deformation analysis. A detailed view is shown in Figure 73. The applied mesh fulfills all requirements mentioned in chapter: 10.2.4 Mesh properties.
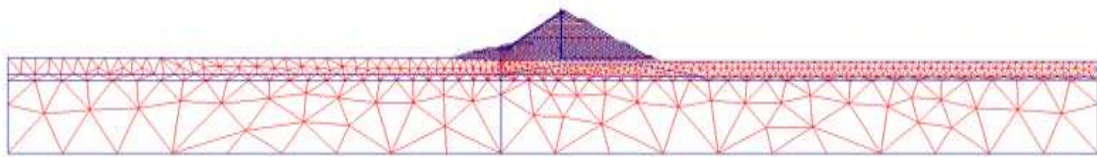
Figure 72 Finite element mesh.
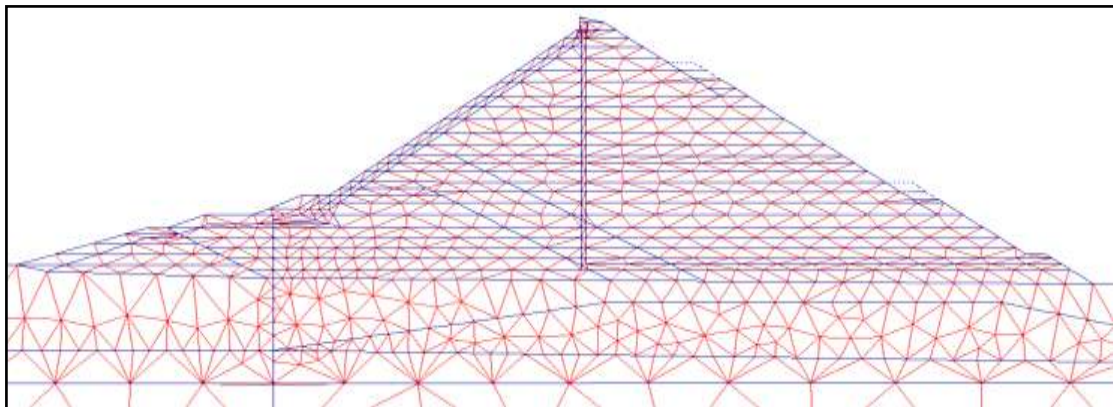
Figure 73 Detailed view on the dam structure's finite element mesh.

10.5 Applied Material Parameters

Scope of this thesis is to compare the results of two constitutive models for two different kinds of material. The applied main fill materials are on the one hand a very height strength rockfill (herein sand gravel fill) and on the other hand weak rockfill.

Therefore, the following calculations are conducted:

- Sand gravel, HS analysis
- Sand gravel, MC analysis
- Weak rockfill, HS analysis
- Weak rockfill, MC analysis

The applied parameters were estimated by studying and comparing observed deformations of dams in operation as well as considering results of large scale triaxial tests. Materials that are assumed to show rigid behavior (concrete structures) are modeled linear elastic in MC and HS analysis (Table 15). Foundation rock and coffer dam clay/filter/protection are modeled linear elastic-ideally plastic in MC and HS analysis (Table 18).

Table 15 Parameters applied to plates and beams.

	Normal stiffness	Flexural rigidity	Ideal thickness	Poisons ratio	Weight
	EA	EI	d	ν	γ
Name of plate/beam	[kN/m]	[kN/m^3]	[m]	[-]	[kN/m/m]
Plinth	23100000	943300	0,7	0,2	17,5
Concrete Slab	13200000	176000	0,4	0,2	10
Crest wall	16500000	343800	0,5	0,2	12,5
Cut off wall 30 day	28000	2333,33	1	0,33	24
Cut off wall 100 day	75000	6250	1	0,3	24
Cut off wall 200 day	86000	7167	1	0,27	24

When simulating the natural behavior of a cut off wall, the stiffness has to increase with time. This was simulated by introducing 3 different moduli (i.e. 30, 100 and 200 day = final stiffness, updated in phase 31, 39 and 46). Figure 74 shows the time dependent compressive strength and the associated modulus of two cut off wall mixtures.
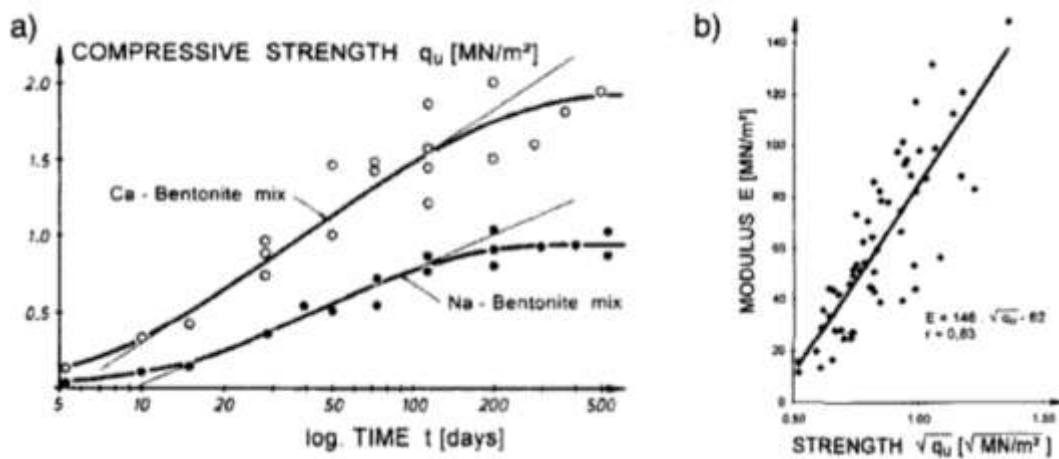
Figure 74   a) compressive strength of 2 different cut off wall mixtures (Brandl, 1996). b) Modulus versus strength of cut off wall mixtures (Brandl, 1996).

To calculate the cut off wall's stresses more accurately, the time dependent behavior should be modeled by introducing more than 3 moduli. The cut off's behavior was calculated assuming a calcium bentonit mixture. However, its real technical properties are not specified to date. Due to the uncertainties in schedule and mixtures, it was decided to pass on a more accurate calculation.

Interface elements are provided for all plates and fill materials. Plaxis uses the formula:

$$\tan \varphi_{interface} = R_{inter} \cdot \tan \varphi_{soil} \quad and \quad c_{inter} = R_{inter} \cdot c_{soil} \quad \quad (21)$$

Where R_{inter} is a factor that relates the friction and cohesion of the interface material to the friction and cohesion of the adjacent soil. Table 16 summarizes all factors applied for MC and HS analysis.

Table 16 Strength reduction factor R_{inter} applied to interface elements in MC and HS analysis.

Adjacent soil	Name of plate/beam			
	Plinth	Concrete Slab	Crest wall	Cut off wall
Alluvium	-	-	-	0,5
Main fill sand gravel	-	-	0,7	0,5
Main fill weak rockfill	-	-	-	-
Cushion	-	0,95	0,7	0,5
Transition	-	0,9	0,7	0,5
Plinth support	0,8	-	-	0,8
Drainage	-	-	0,7	-
Self healing	0,7	0,7	-	-
coffer dam clay/filter/protection	-	-	-	0,2

10.5.1 Hardening – Soil model

Table 17 shows the parameters applied for hardening soil analysis.

Table 17 Parameters applied for HS analysis.

Material name	unsaturated specific weight γ [kN/m³]	saturated specific weight γ_{sat} [kN/m³]	cohesion c [kN/m²]	internal friction angle φ [°]	dilatation ψ [°]	deformation modulus E_{oed}^{ref} [kN/m²]	un-/reloading modulus E_{ur}^{ref} [kN/m²]	modulus E_{50}^{ref} [kN/m²]	power m [-]	failure ratio R_f [-]	reference pressure p_{ref} [kN/m²]
Cushion	22,2	23,8	3	49	11	68000	165000	80700	0,42	0,87	100
Transition	21,7	23,4	0,2	50	8	65000	160000	78500	0,47	0,8	100
Plinth support	22,3	23,8	4	39	9	60000	156000	78000	0,5	0,9	100
main fill US+DS sand gravel	21,5	23,3	0,2	45	9	55000	151000	73000	0,35	0,85	100
main fill US+DS weak rockfill (shale)	20,5	22,0	0,2	39	16	16000	60000	20000	0,01	0,9	100
Alluvium	21,7	23,2	0,2	47	10	50500	112000	56000	0,4	0,86	100
Drainage	20	22	0,2	46	3	40000	98000	49000	0,35	0,85	100
Selfhealing material	15,5	18	0,2	24	0	6000	24000	8000	1	0,9	100
Selfhealing protection	18	21	0,2	54	0	24000	93000	31000	0,5	0,9	100

Figure 76 shows the behavior of wetted Pancrudo gravel (cp. Figure 17) approximated by the hardening soil model. It is obvious that hyperbolas cannot accurately approximate real soil behavior, especially in case of weak rockfills. Regarding Pancrudo's stress strain relation, the tested material shows a significant decrease of stiffness if particular stress states are exceeded. This effect cannot be displayed by the HS model and consequently axial strain is overestimated for deviatoric stresses below 500kN/m². In general, expectable deformations will be much higher in embankments constructed of weak rockfills. Therefore the constitutive model and its applied parameter set, has to display the materials behavior even at high strain states. This is in direct contrast to modeling stiff rockfill material, where the constitutive model has to display low axial strain states most accurately. Axial strains calculated by the weak rockfill analysis result in a maximum of 9.5% (cp.2.5% in sand gravel fill analysis). The parameter set dis-

playing the behavior of Pancrudo gravel (Figure 76, Table 17, Table 18), is applied to Sarigüzel dam as main fill to highlight the differences in modeling rockfills of stiff manner compared to weak rockfills, regardless the unfavorable effects of weak rockfill on the concrete slab. If modeling rockfills of soft rock source (unconfined strength < 30 MN/m^2), wetting and creeping effects have to be considered in deformation analysis to be consistent with the materials natural behavior. However, scope of this thesis is to highlight only general differences, because of that, wetting and creeping deformations are not part of the weak rockfill analysis.

The parameters E_{50}, m, γ and ψ applied to MC analysis were adapted to the data, tested with a confining pressure of $300kN/m^2$. Figure 76 shows the material behavior in MC analysis.

The parameters applied to drainage zones remain unmodified, making the assumption, that the compaction effort for both drainage zones is the same as for main fill material. Furthermore it is indirectly assumed that drainage material is again borrowed, washed and processed material obtained from alluvial deposits.

Figure 75 shows the stress strain behavior of particular materials in comparison to each other. These stress strain plots are obtained from numerical soil tests. All materials were isotropically consolidated up to a pressure of -200 kN/m^2 and thereafter axially loaded up to specimen's failure.
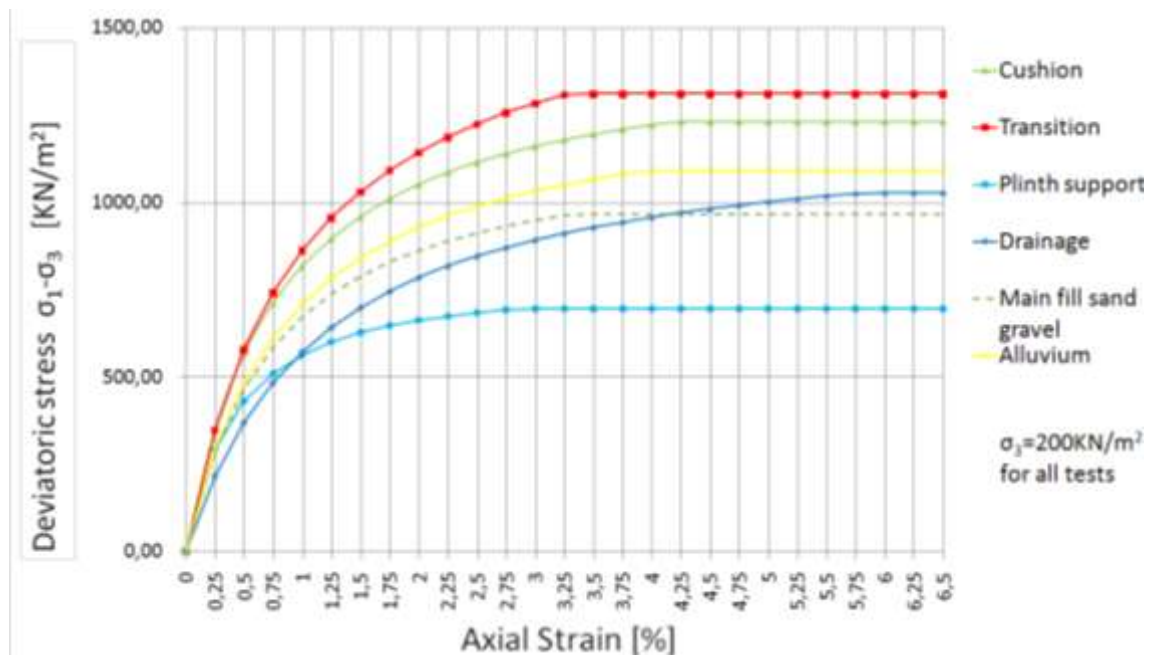
Figure 75 Stress strain behavior of Sarigüzel dam materials, tested under a confining pressure of 200kN/m².

Dashed lines = data obtained from triaxial tests on wetted Pancrudo gravel (shist) .
Solid lines = material behavior approximated by the HS model.
Dotted lines = material behavior approximated by the MC model.

Dashed lines = data obtained from triaxial tests on wetted Pancrudo gravel (shist) .
Solid lines = material behavior approximated by the HS model.
Dotted lines = material behavior approximated by the MC model.

Figure 76 Material behavior of Pancrudo gravel (shale) approximated by MC and HS model (cp. Figure 17).

Figure 77 shows the estimated stress strain behavior of Sarigüzel sand gravel fill at stress levels ranging from 100 to 400kN/m², which are assumed to occur in Sarigüzel embankment. Plaxis offers the opportunity for dilatancy cut off at large strain levels,

however axial strain rates are assumed to be smaller than 2.5% in Sarigüzel's embankment and in case of sand gravel fill, so it has been decided to pass on this option.
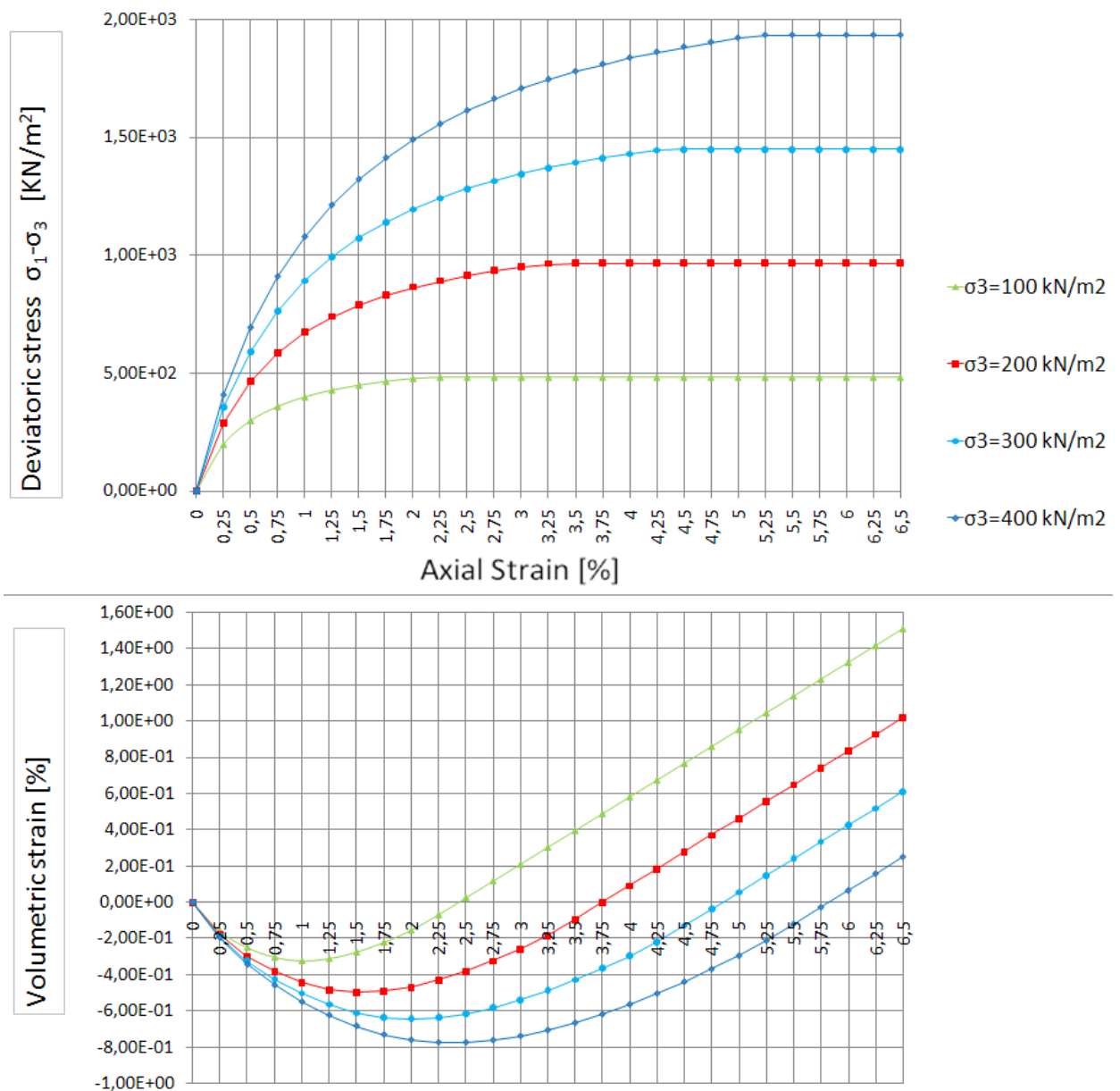
Figure 77 Stress strain behavior of sand gravel main fill tested for varying confining pressures in HS analysis.

10.5.2 Mohr – Coulomb model

All parameters applied in Mohr-Coulomb analysis are obtained from data sets used for hardening soil analysis, excluding the parameter set for weak rockfill. Stress-strain plots from HS materials, where adjusted to the average deviatoric stress state, assumed to occur in the particular material. For that reason, the MC modulus differs

from the HS-E_{50} modulus, as the HS-E_{50} value is related to a reference pressure of p_{ref}=100kN/m^2 . Remember, the HS model will adjust the stiffness to the present stress state automatically. The modulus applied to MC model is the secant modulus, intercepting at 50% of the ultimate deviatoric stress level. Table 18 shows all parameters applied for MC-analysis.

Table 18 Parameters applied for MC-analysis.

	Young's modulus	Poisons ratio	Unsaturated specific weight	Saturated specific weight	Cohesion	Internal friction angle	Dilatation	According to a average lateral stress state of:
	E	ν	γ	γ_{sat}	c	φ	Ψ	σ_3
Material name	[kN/m^2]	[-]	[kN/m^3]	[kN/m^3]	[kN/m^2]	[°]	[°]	[kN/m^2]
Cushion	88300	0,32	22,2	23,8	3	49	11	140
Transition	90800	0,32	21,7	23,4	0,2	50	8	140
Plinth support	88900	0,35	22,3	23,8	4	39	9	260
Main fill US+DS sand gravel	89100	0,30	21,5	23,3	0,2	45	9	200
main fill US+DS weak rockfill (shale)	23540	0,20	20,5	22,0	0,2	39	8	300
Alluvium	107000	0,29	21,7	23,2	0,2	47	10	500
Drainage	61300	0,3	20	22	0,2	46	3	200
Selfhealing material	14500	0,33	15,5	18	0,2	24	0	200
Selfhealing protection	45600	0,25	18	21	0,2	54	0	200
Coffer dam clay/filter/protection	20000	0,33	17	19	0,2	24	0	200
Foundation rock	2000000	0,20	23	23	250	35	32	1400

According to the applied modulus of sand gravel fill: The lowest modulus during construction (corrected for arching effects), found in literature, was shown by Gollilas dam. The Gollilas embankment consists of dirty gravels, compacted by 4 passes of a 10 to SDVR in lifts of 60cm (water added). Resulting in an average value of $107000kN/m^2$ (at a vertical stress of $1350kN/m^2$). At Sarigüzel dam it is provided to compact the upstream and downstream main fill material with a minimum of 6 passes of a 10 to SDVR in lifts of 80 cm with additional water. Most CFSGD's showed significantly higher moduli. For example, Crotty dam showed a modulus of $360000kN/m^2$ (dirty gravel, 60 cm lifts, 8-12 passes of a $6 – 10$ to SDVR, water added, at a vertical stress of $900kN/m^2$). Wuluwati dam was constructed in 1m lifts, compacted by an unpublished number of passes of a 16-20 to SDVR without additional water. The modulus varied from $235000 – 350000kN/m^2$ during construction (Yan, no date).

However, according to criteria suggested by Fell et al. (2005), arcing is likely in Sarigüzel embankment's lower third.

Once again, it shall be pointed out, that the main purpose of class A finite element analysis (i.e. analysis prior to construction) is to gain information about the materials lower boundaries instead of predicting the exact deformation. In a next step, when more accurate information on the material's properties and compaction tests or again in a later stage, monitoring data from smaller dam sections is available, further calculations might be conducted to predict the dam's deformation more accurately. By reason of poor information at this stage, deformation parameters where estimated conservatively.

Since the coffer dam is a part of the Sarigüzel's embankment, it is provided that the coffer dam's embankment has to reach the same specifications as the main fill material. Because of that, the material parameters applied for coffer dam fill and main fill are the same.

Figure 78 shows the stress strain behavior of sand gravel fill applied for MC analysis at the same stress states as obvious in Figure 77. According to the volumetric changes in Figure 75 and Figure 77 it is obvious, that the soil will behave totally different, even if the same parameters are applied in both analyses. This highlights that the user has to exercise caution, if applying commonly known soil parameters to new constitutive ma-

terial models (even, if the parameter is identically denominated and shows the same description in the user's manual).

In contrast to HS model, MC model requires the input parameter poission's ratio. As obvious from Figure 78 in MC model, the volumetric change is controlled and linearly approximated by two input parameters (poison's ratio and dilatancy angle), while HS model does not allow for the specified control of volumetric changes at small axial strain states.
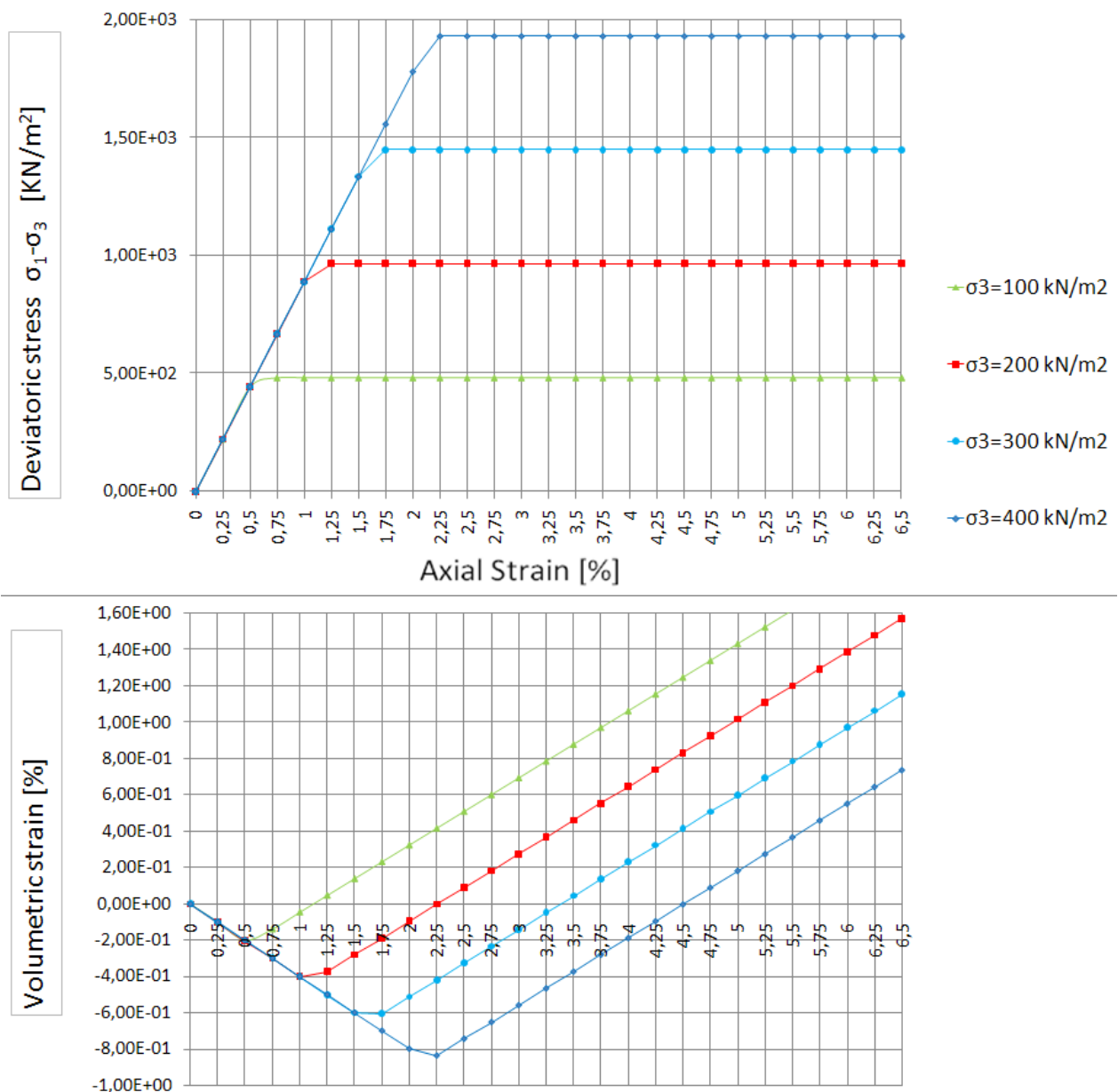

Figure 78 Stress strain behavior of sand gravel main fill tested for varying confining pressures in MC analysis.

10.6 Results

Deformation plots of Sarigüzel embankment are presented in this chapter. These plots were created using the software Surfer V09. Plaxis does not offer the opportunity to sum up the differential (phase) deformations. Therefore, all differential deformations have been copied into an additional Excel sheet. This sheet includes a macro that clears the initial deformations of all points that are activated for the first time.

10.6.1 Sand Gravel Fill

10.6.1.1 Stress-Strain-Behavior, HS-Analysis

10.6.1.1.1 End of Construction

Figure 79 shows the effective horizontal stresses at end of construction stage for HS analysis. Figure 80 shows the vertical effective stresses at end of construction. Maximum stresses occur in the alluvial deposits and are found to be -500kN/m^2 and -1800kN/m^2 (horizontal and vertical stress).

Figure 81 shows the embankment's deformation at end of construction. According to the applied material parameters, the maximum settlement at end of construction amounts to 50cm (or 0.45 % of dam height). Maximum settlement approximately occurs in the middle of the dam's height.

Figure 82 shows plastic points in Sarigüzel embankment at end of construction. Commonly, a plastic point is a point that reaches the Mohr Coulomb failure criterion (in HS analyses and in MC analyses too). According to Figure 82, a distinction is made in HS analyses, highlighting which kind of plastic straining occurs. Whether the point of interest shows pure hardening (i.e. axial compaction without increasing lateral pressure, strains are mainly controlled by E_{50}), is located on the yield cap (i.e. triaxial compaction, strains are mainly controlled by E_{oed}), shows both effects (cf. Figure 23) or meets the failure criterion. As obvious, the failure criterion is not reached in the embankment at the end of construction. For a better understanding the author wants to point out, that the plotted plastic points are due to differential stresses of a phases new load condition. The plotted phase herein is phase 56. Within this phase the selfhealing material and the material above the crest wall are placed. Figure 82 shows an area that is obviously unaffected by the new load condition, which does not mean that these points did never undergo hardening during construction. It does only show that these

points are not affected by the phases new load condition.
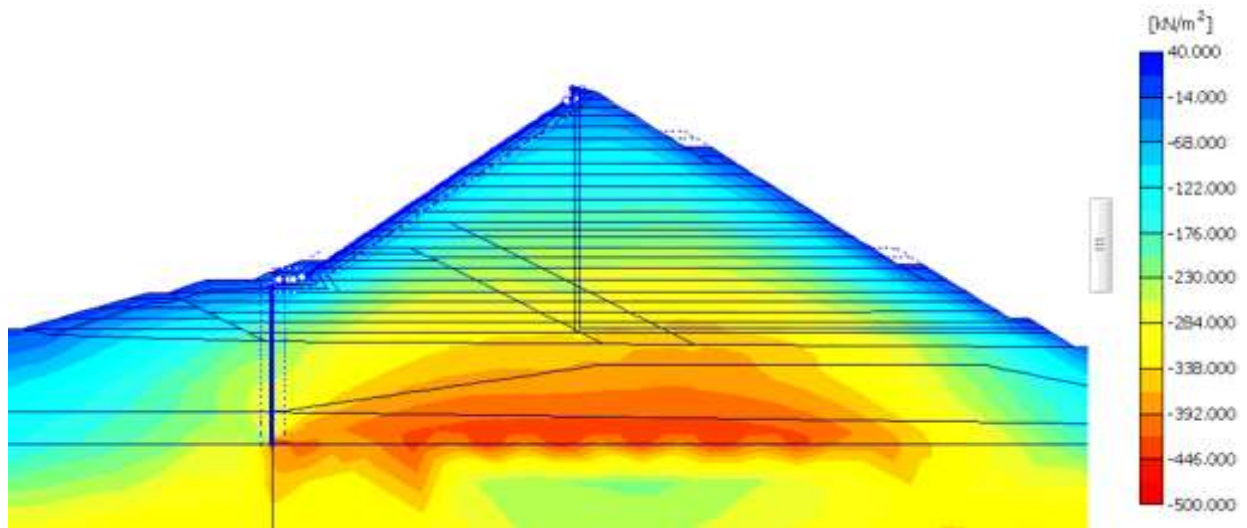
Figure 79 Horizontal effective stresses at end of construction (HS, sand gravel fill).
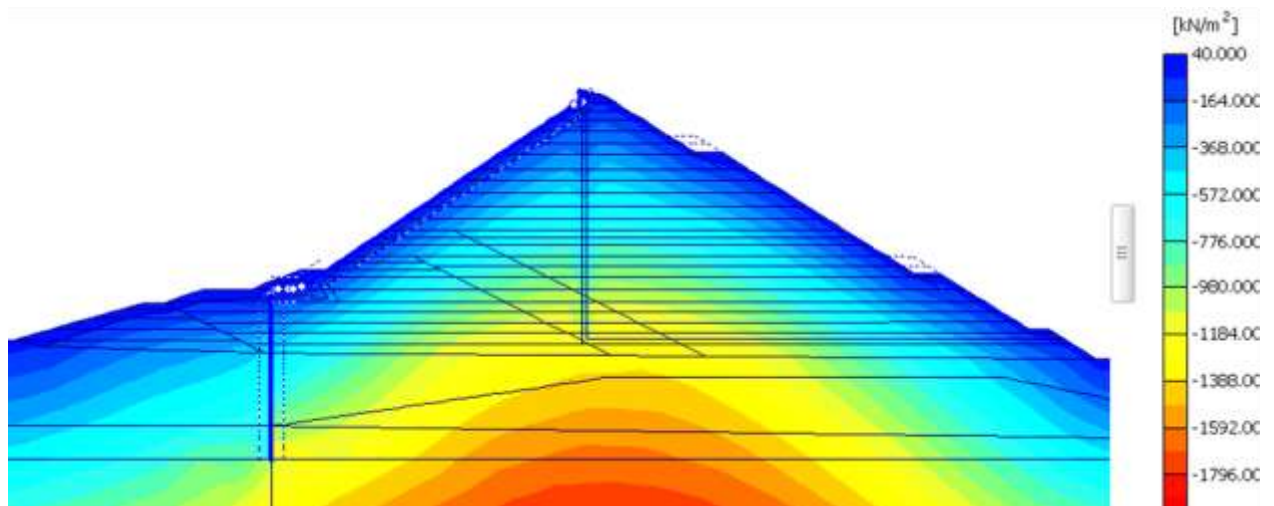
Figure 80 Vertical effective stresses at end of construction (HS, sand gravel fill).
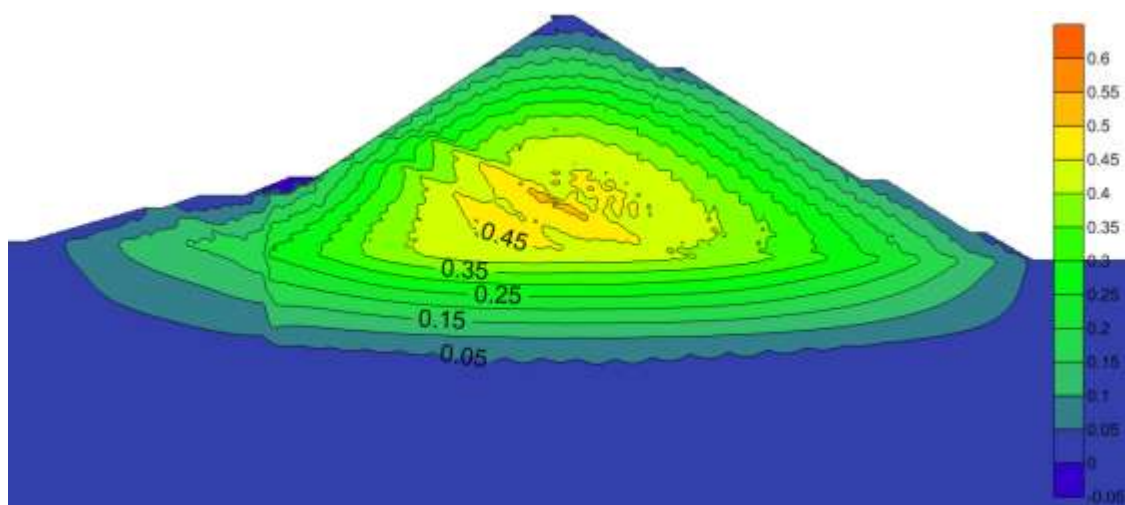
Figure 81 Total settlements at end of construction [m] (HS, sand gravel fill).
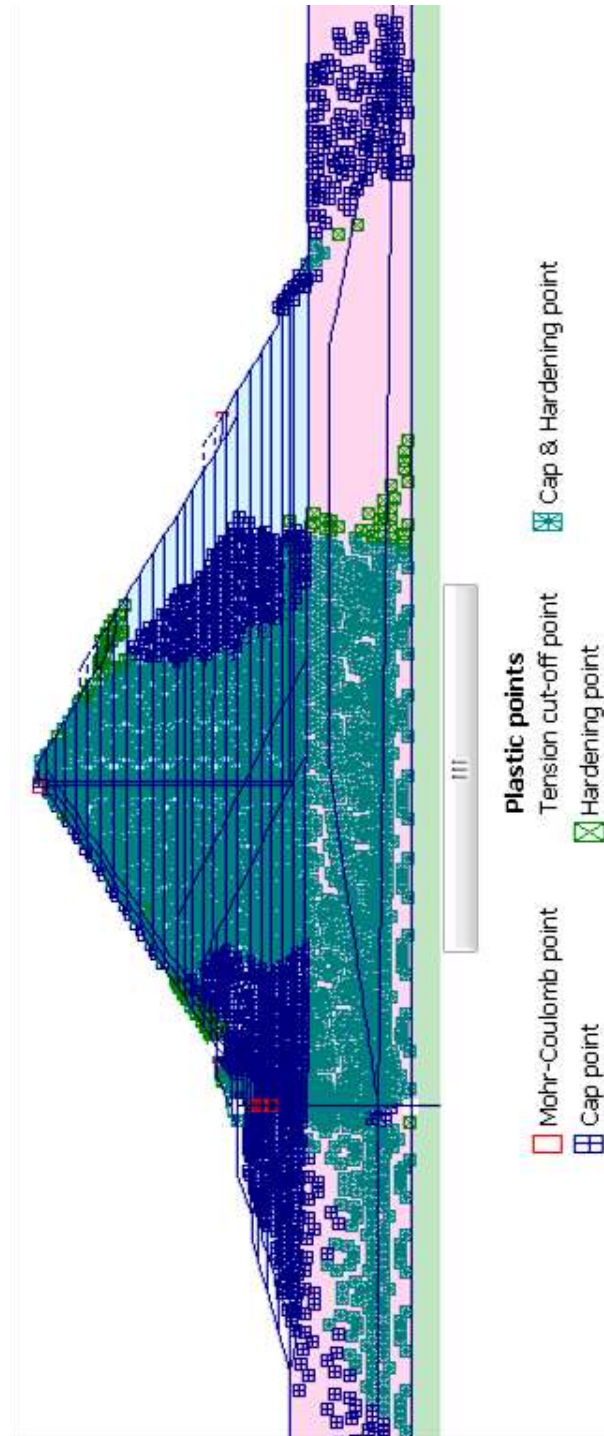
Figure 82 Plastic points in Sarigüzel embankment at end of construction (HS, sand gravel fill).

10.6.1.1.2 First Filling

Figure 86 shows the embankment's settlement after first filling. Maximum settlement results in 55cm (0.50 % of dam height). Of special interest are the differential settlements due to first filling. Figure 89 shows the phase displacements while Figure 87 and Figure 88 show the phase displacements split up in its horizontal and vertical compo-

nents. Figure 88 shows uplifting of the coffer dam during impounding. When the water level rises, the coffer dam's embankment is wetted (i.e. unloaded) resulting in an uplift of this area. With ongoing filling, the water load applied on the cut off wall increases. The cut off wall is deflected to downstream side, resulting in decreasing confining pressures in the coffer dam's embankment close to the cut off wall. Hence the coffer dam's upper part settles significantly. The results show a maximum crest settlement of 4.5 cm and a maximum horizontal crest deformation amounting to 11cm. Compared to dams in operation, the crest settlements during first filling period seem to be underestimated, but in contrast to Sarigüzel embankment, all case studies contain weaker rockfill material in their downstream shoulders and some show arching effects. In preliminary design of Sarigüzel dam it is provided to apply sand gravel in upstream and downstream shoulder, in both cases compacted in 80cm lifts by the same number of passes of the SDVR. Hence, in contrast to other dams, the crest settlement of Sarigüzel dam has to be smaller.

The Long term crest settlement is estimated utilizing the method of Hunter and Fell (2002). In case of well compacted alluvial gravels, they suggest a long term crest settlement rate of 0.05%/log circle of time (i.e. years). This value is taken from monitoring data of Gollilas and Crotty dam.

Both dams show arching effects. The author's point of view is to reduce this value. If arching occurs, the stresses concentrate and increase, consequently creeping deformations are significantly larger than they would occur without arching (cf. Figure 15). Hence, to estimate Sarigüzel dam's long term crest settlement, a rate of 0.03%/log circle is applied: The crest settles 3,3cm within the first year after first filling, plus 3.3cm from 1 to 10 years after first filling and again 3.3cm from 10 to 100 years after first filling.

The crest's lateral displacement seems to be overestimated by the HS model. Crotty and Golillas dam have shown lateral displacements less than 1cm. However, arching is likely in both cases.

Figure 83 Horizontal effective stresses after first filling (HS, sand gravel fill).

Figure 84 Vertical effective stresses after first filling (HS, sand gravel fill).
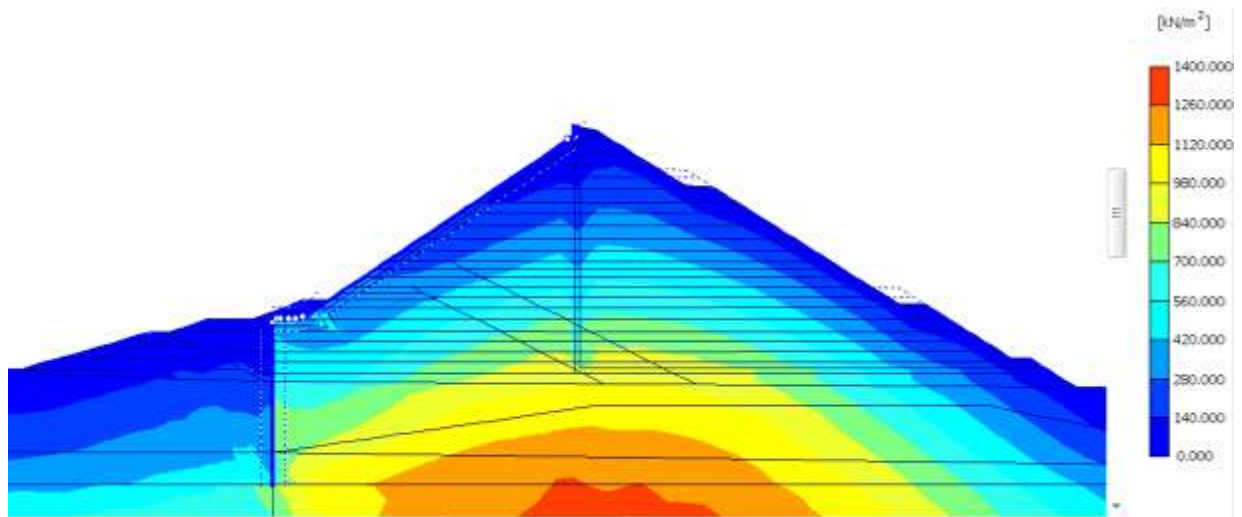
Figure 85 Total deviatoric stresses after first filling (HS, sand gravel fill).
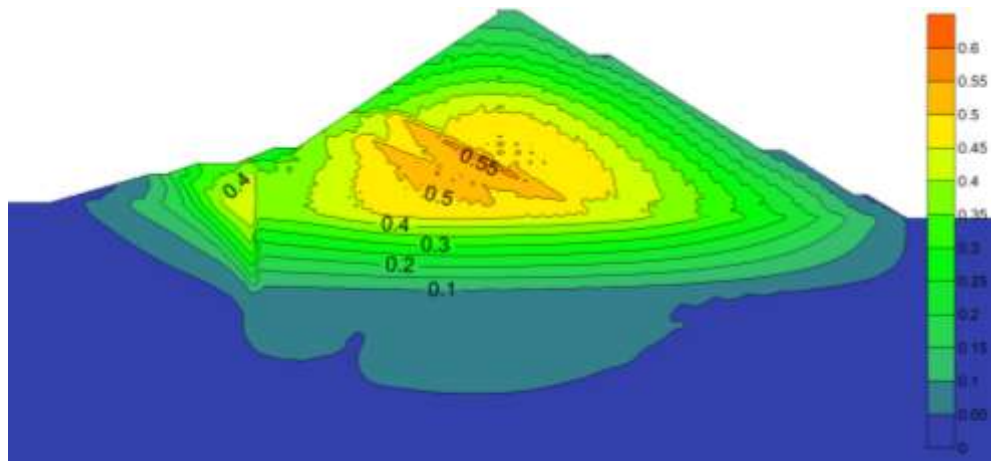
Figure 86 Total settlements after first filling [m] (HS, sand gravel fill).
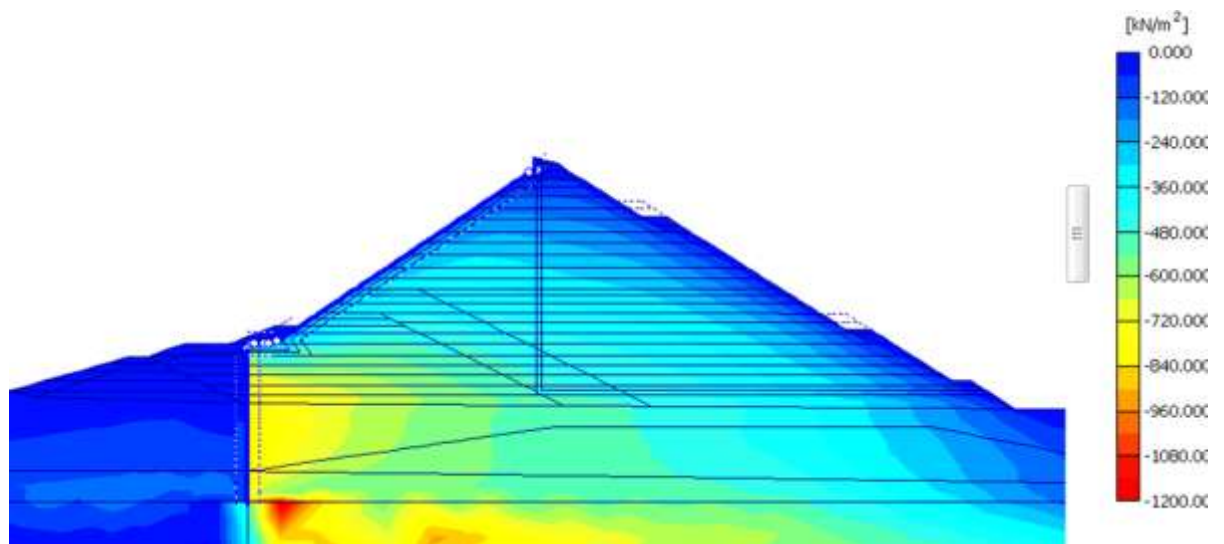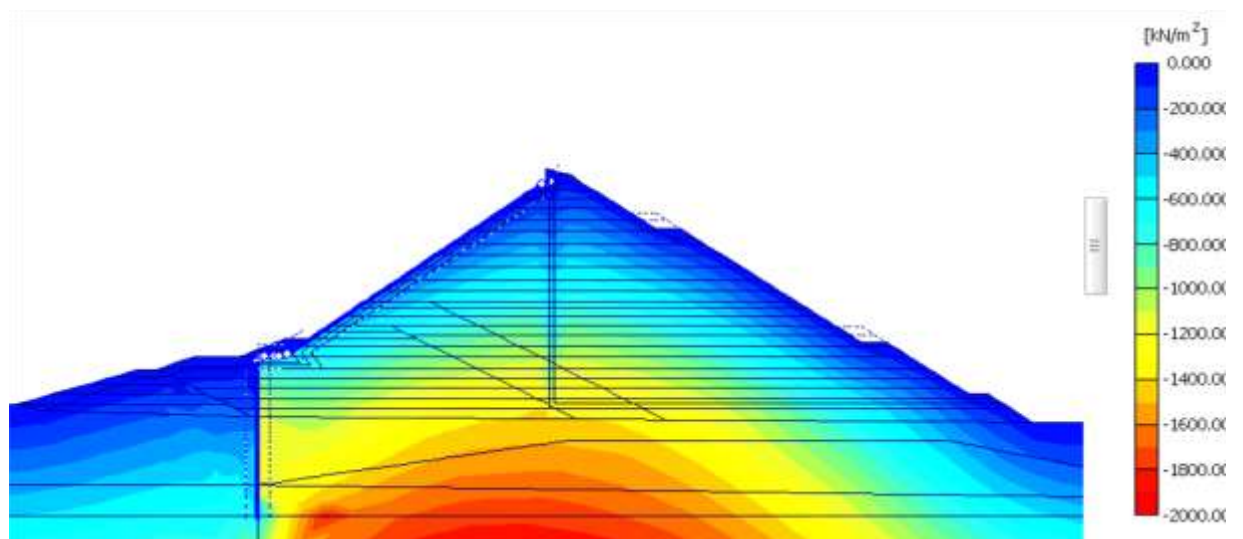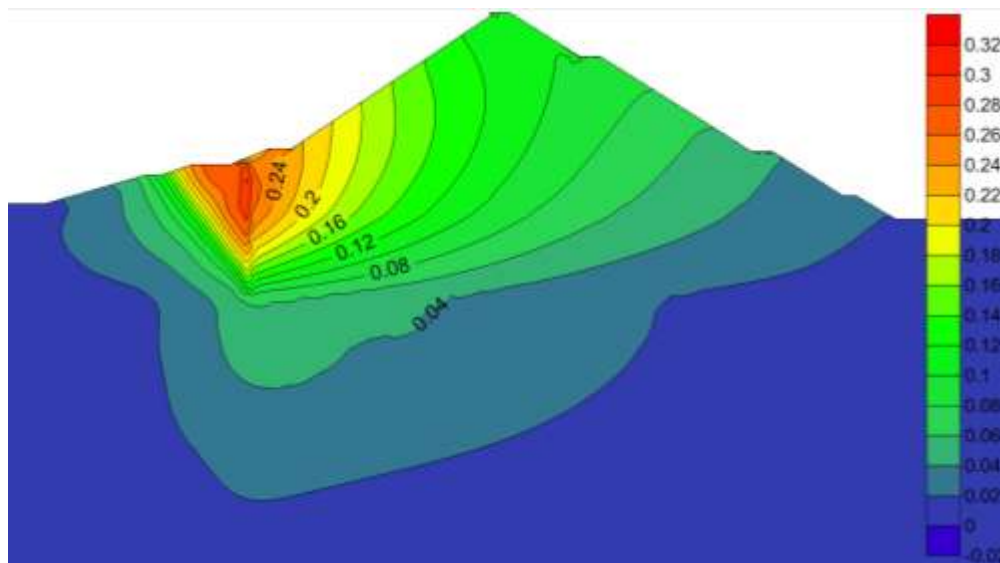

Figure 87 Horizontal phase displacements due to first filling [m] (HS, sand gravel fill).
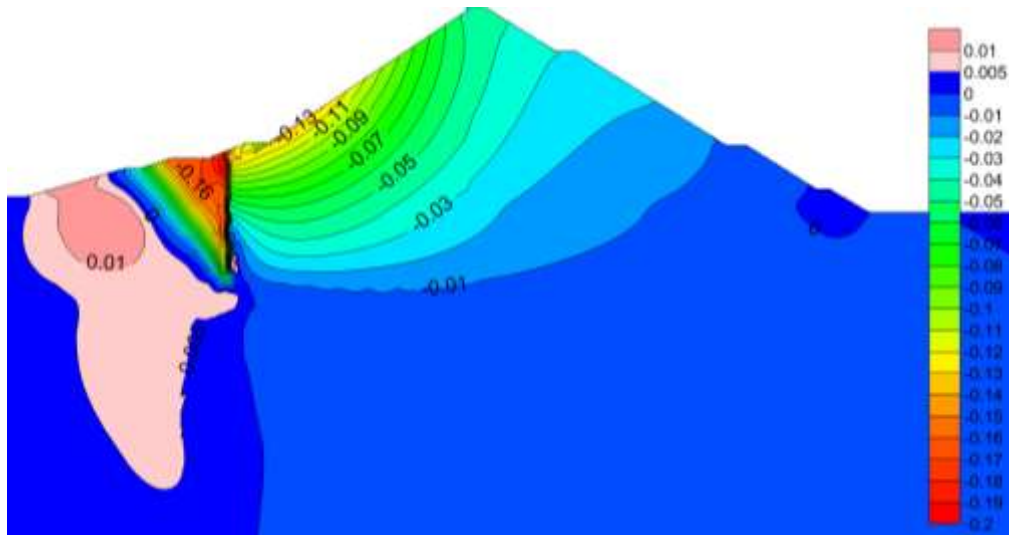
Figure 88 Vertical phase displacements due to first filling [m] (HS, sand gravel fill).
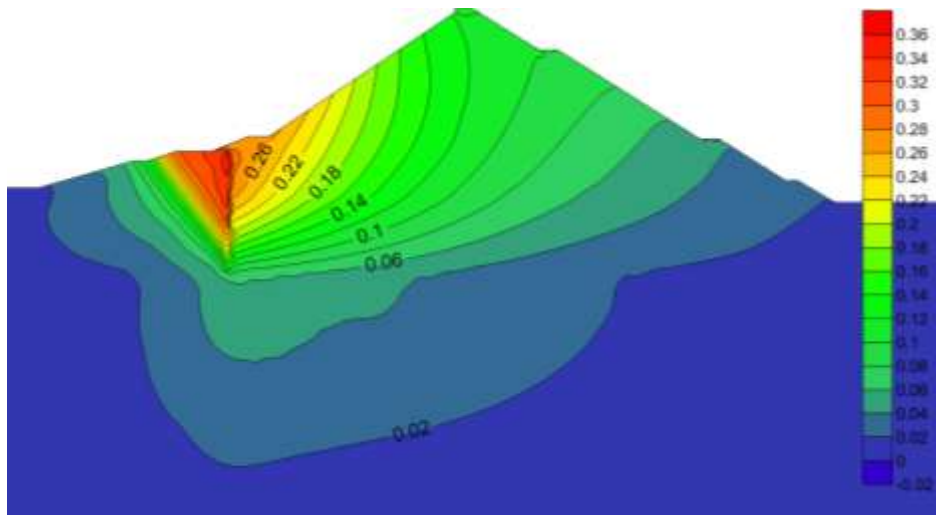
Figure 89 Phase displacements due to first filling [m] (HS, sand gravel fill).

10.6.1.2 Slab / Plinth / Cut off Wall Displacements, HS-Analysis

Since the plinth and concrete slab are casted afterwards the majority (98%) of the embankment is filled, only the differential displacements due to first filling and selfhealing material's placement are of special interest.

10.6.1.2.1 Plinth

A detailed view on the plinth structure is shown in Figure 35. The plinth is the impermeable connecting link between cut off wall and concrete slab. Two joint details are provided in plinth design (Figure 42). These two joints are simulated by hinges. Unfortunately, Plaxis does not offer advanced options for hinges to allow for bending and to restrict the transmission of tension and shear forces at the same time. Beyond that, it is impossible to introduce "joint material" of small thickness, to approximate the

joint's behavior. Due to the researched problem's general dimensions, the finite element's average diameter is in the order of 2m, too coarse for simulating joints of 2cm thickness. However, this drawback does not have a significant effect on the plinth's displacement. As long as joint failures and cracks do not occur during impounding, the whole cut off – plinth – slab structure is forced towards downstream side. This behavior forms a significant contrast to the behavior of plinth structures directly casted on sound rock, were the plinth is fixed to the rock surface and the concrete slab is forced towards downstream. However, as mentioned above, if pore water pressures on the cut off's downstream side are similar or equal to the upstream water pressures, the cut off wall is not forced towards downstream anymore. Consequently the plinth's connection joints will open.

According to the applied material data and considering the above mentioned, the maximum plinth displacement during impounding amounts to 22cm in horizontal and -16cm in vertical at the cut off connection and 22cm in horizontal respectively -15cm in vertical at the concrete slab connection. Figure 90 shows the total plinth displacement during impounding. The Maximum displacement due to the selfhealing material's placement results in -0.2cm in horizontal (towards upstream) and -2.3cm in vertical direction (i.e. downwards). Figure 91 shows the plinth displacement after selfhealing material's placement.
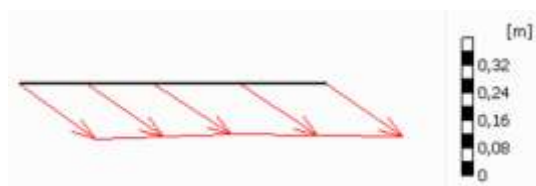

Figure 90 Plinth displacement during first filling.

Figure 91 Plinth displacement due to selfhealing material's placement.

10.6.1.2.2 Concrete Slab

As obvious in Figure 89, maximum displacements occur at the slab to plinth contact point and result in 22cm in horizontal and -15cm in vertical direction. Maximum total displacement at this point therefore amounts to 27cm. Displacements at top of the concrete slab result in 12cm in horizontal and -3cm in vertical direction.

According to cracks, due to tensile stresses in axial direction, the calculation shows that tensile stresses do only occur during placement of the self healing material amounting to:

Axial force: +40kN/m

Shear force: 19kN/m

Bending moment: +67kNm/m

This is thought to be partly realistic and partly due to the lack of advanced hinges in Plaxis, as discussed in chapter: 6.3.2.2.1 Assets and Drawbacks of HS Model. For example: During the selfhealing material's placement, the perimetric joint opens in reality. The joint's opening is restricted in Plaxis model and therefore leads to an overestimation of the slabs tensile stresses during placement. Assuming, that the concrete's average resistance to tensile stresses is 2.2MN/m^2 (EN-1992-1-1, 2004, C20/25, p. 29), the above mentioned stress resultants will cause cracks due to bending on downstream side.

During impounding the tensile stresses turn to compressive stresses. Maximum axial stress results in -11.2MN/m^2 (already increased by a security factor of 1.35 for static loading). 28 day strength normally varies from 20 to 24MN/m^2 (ICOLD 1989). Hence, the compressive stresses are found to be unproblematic, according to most parts of the concrete slab (11.2MN/m^2 < 13.3MN/m^2, which is the C20/25 strength, 20MN/m^2 decreased by a security factor of 1.5).

However, the slab's maximum bending moment is found to be 231.6kNm/m occurring in combination with an axial compressive force of -1990kN/m and a shearing force of –47.2kN/m close to the slab to plinth connection. These stress resultants are found, not to be a local singularity, as the finite element mesh in this area is relatively fine and additional interface elements were applied between the slab and the cushion. This load (not increased by a safety factor) will at least lead to tension cracks on upstream side, reducing the effective concrete section to a maximum of 20cm (if the steel bars

are located in the middle of the 40cm thick concrete slab). Assuming an axial reinforcement of 0,3% (12 cm^2/m) in axial direction, located at the slabs axis and no shear reinforcement applied, the concrete slabs resistance is found to be too weak in this case. Therefore, either two layers of reinforcement (i.e. 0,15% = 6cm^2/m on upstream and downstream side) have to be applied or a higher deformation modulus for the main fill material has to be reached on site. Remember, the calculation of the slab's resistance in case of a two layered reinforcement layout includes appropriate safety factors.

There is no doubt about which of the two above mentioned possibilities results in lower construction costs, beyond that, a two layered reinforcement layout provides further advantages. If bending cracks occur, two layers of reinforcement provide a significantly bigger compressed concrete zone, thus resulting in smaller hydraulic gradients and hence, a better seepage control.

10.6.1.2.3 Upper vertical and horizontal Joints

Many CFRDs have shown rupturing of vertical joints at crest elevation. Figure 25 shows the general behavior of all concrete panels due to impounding. A rough estimation of the vertical joints opening is made herein. The maximum horizontal and vertical displacement at top of the concrete slab is thought to be 12.263cm and 3.215cm. The maximum total displacement in this case is 12.68cm, which is 0.1167% of the dam's height in section 7-7 (were dam height in this case, is the crest to foundation rock length at the dams axis, according to the geological drawings). Figure 92 shows the estimated displacements of all concrete panels along the entire width of the valley. The displacements are calculated by assuming a deformation of 0.1167% of the dam's height in the respective section.
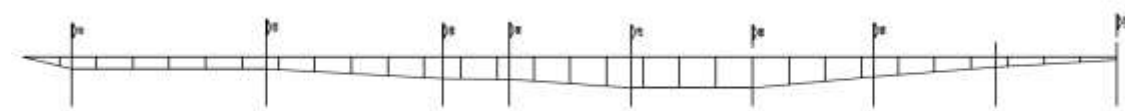
Figure 92 Estimated displacements of concrete slabs at crest elevation.

The average strain along the crest is 0.03‰ (1.3cm elongation along the entire crest length). The steepest part (i.e. the largest changes in displacement) is found to be between sections 1 and the spillway connection. In this area the slab is theoretically

stretched 0.61cm. This elongation has to be compensated by two adjacent vertical joints, resulting in settlements, opening and shear movements. The maximum water pressure affecting Sarigüzel dam's joints is 0.6MPa. Compared to the results of joints tested for Aquamilpa dam (Table 13 and Table 14), these deformations will not harm the water stops.

10.6.1.2.4 Lower vertical and perimetric joints

The maximum total displacement of the lowest point on the concrete slab is 26.92cm (section7-7). According to the geological drawings, the cutoff – rock intersection line is smooth, without any irregularities. For this reason, a parabolic deformation of the plinth structure is assumed. A maximum deflection of 26.92cm results in a strain of 0.005‰, harmless for all joints as well as for the cut off wall. Figure 93 shows the assumed displacements of all concrete panels at plinth elevation.
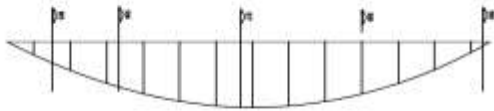
Figure 93 Estimated displacements of concrete slabs at plinth elevation.

10.6.1.2.5 Cut off Wall

The cut off is placed in phase 31. Starting from phase 31 to phase 56 (end of construction) the cut off wall is deflected towards upstream side. This is due to the ongoing embankment filling. Maximum deflection towards upstream prior to first filling is located on the cut off's top and amounts to -4cm in horizontal and -5.5cm (i.e. downwards) in vertical direction. Maximum differential displacement due to first filling results in 25cm in horizontal (towards downstream) and -16cm in vertical (downwards), again on the cut off's top. Here, the author wants to point out again, that information about the cut off wall's technical specification was limited. Anyway, the above mentioned values can give a feeling about the cut off's general behavior.

10.6.1.3 Stress-Strain-Behavior MC-Analysis

10.6.1.3.1 End of Construction

Compared to HS analysis, MC analysis result in higher horizontal stresses (-700 instead of -500kN/m^2 maximum, plus 40%, Figure 94), and at same time they are more concentrated in their horizontal extension. This is thought to be due to the fact that HS model counts for the stress dependency of volumetric straining, whilst MC model does not. Considering the fact, that maximum axial strain is smaller than 2,5% all over the entire embankment, MC model overestimates the axial strains. Effective vertical stresses are the same for HS and MC analysis (maximum of -1800kN/m^2, Figure 95). According to total settlements at end of construction, MC analyses result in smaller settlement (Figure 96). Maximum value amounts to 45cm (0.41% of dam height), which is 5cm less (minus 10%) than calculated in HS analysis. Maximum settlement appears at the same location as it does in HS analysis. Figure 97 shows plastic points in Sarigüzel embankment at end of construction. Plastic points occur in the selfhealing material due to the overburden of its protection material. No plastic points are observed in the concrete slab and plinth structure (at end of construction stage). Plastic points occur at the crest's downstream surface. During the embankment's raising the failure criterion is reached several times on upstream and downstream surface. This is to be due to the fact that lateral pressures amount to zero close to the surface. Further plastic points occur in interface elements close to the crest wall during the placement of this layer and in the cut off wall. As previously stated, the cut off is not part of the research work within this thesis. The failure criterion is not reached within the main embankment fill in MC HS analysis too.
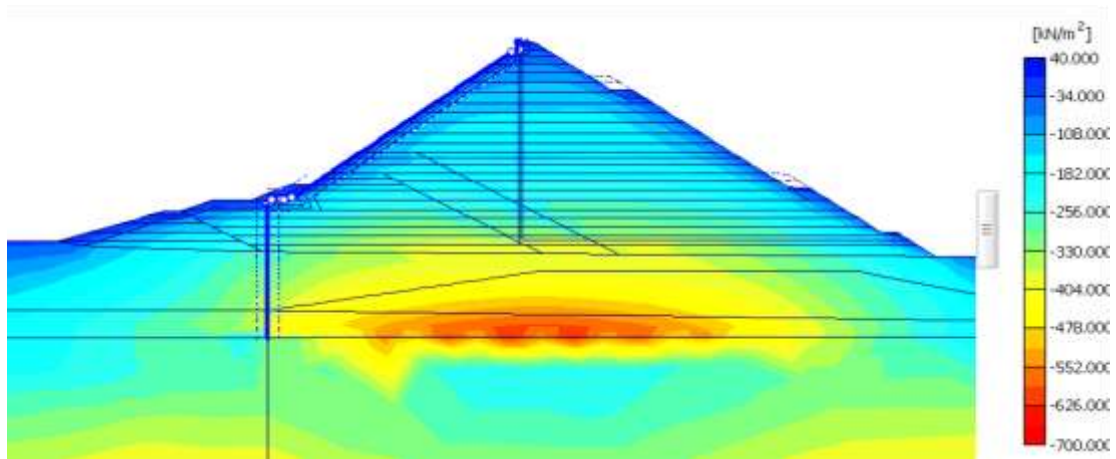
Figure 94 Horizontal effective stresses at end of construction (MC, sand gravel fill).
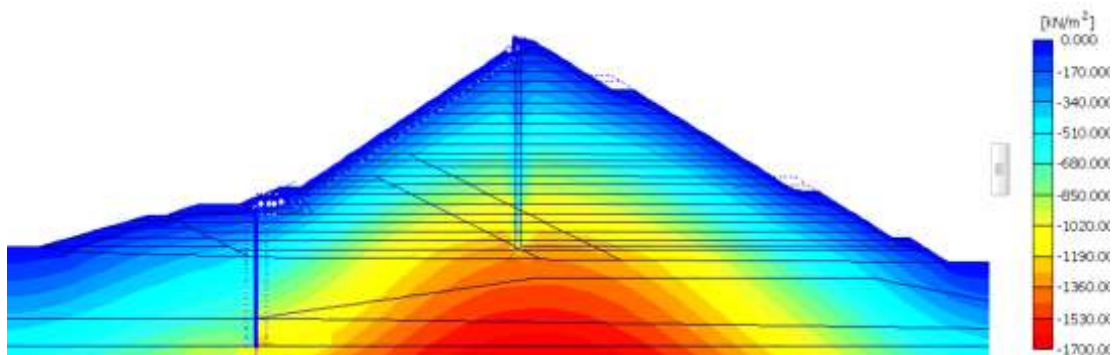

Figure 95 Vertical effective stresses at end of construction (MC, sand gravel fill).
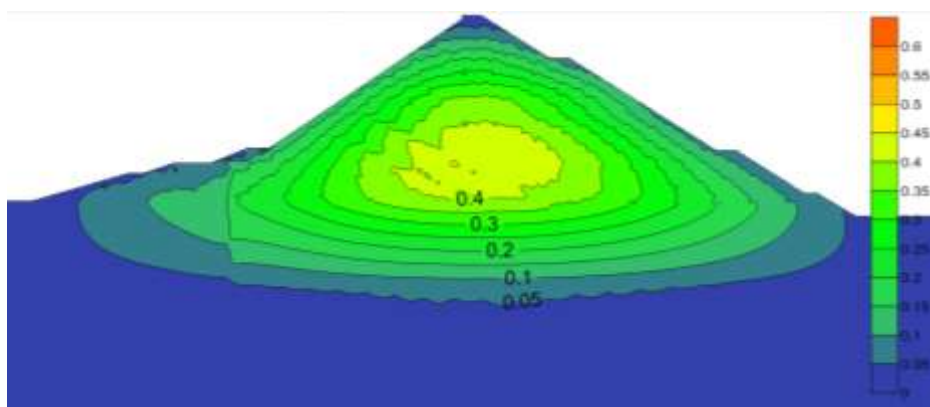
Figure 96 Total settlements at end of construction [m] (MC, sand gravel fill).
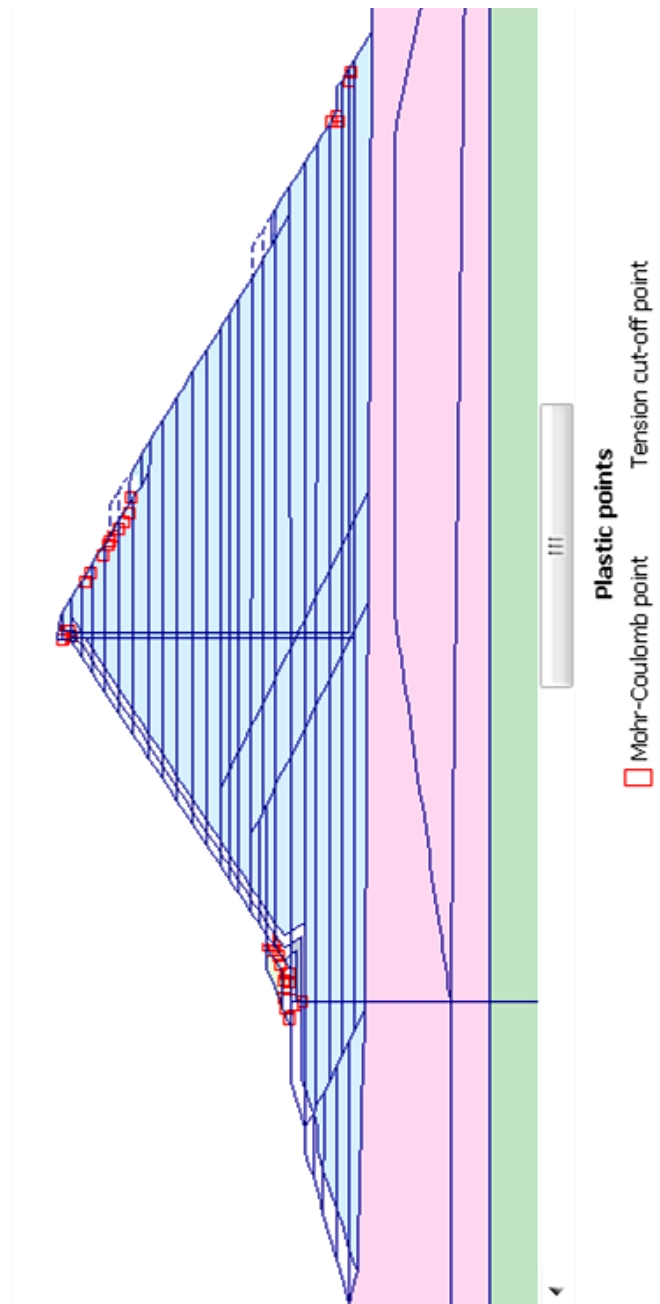
Figure 97 Plastic points in Sarigüzel embankment at end of construction (MC, sand gravel fill).

10.6.1.3.2 First Filling

Horizontal effective stresses as well as vertical effective stresses do not vary in large

extend in MC and HS analysis (Figure 98 and Figure 99). Regarding the deformation

due to first filling (Figure 101), the embankment's maximum settlement is found to be

45cm (0.41% of dam height), which is 10cm less (minus 18%) than calculated by the HS

model. The maximum settlement underneath the concrete slab is 40cm, 5cm more

than in HS analysis (plus 14%). This is due to the fact that MC model does not count for

the materials stiffer behavior on unloading (this is discussed in chapter: 7 Principle

Stress-Strain and Deformation Behavior of CFRDs and CFSGDs). Maximum horizontal

crest displacement results in 20cm, 9cm more (plus 81%) than in HS analysis (Figure 102). The crest settlement due to impounding is found to be zero, which is unrealistic and 5.5 cm less than in HS analysis.

Figure 103 furthermore shows unrealistic uplifting (maximum 1.5 cm) in the dam's upper downstream part. To verify these results, a simplified calculation was undertaken, returning the same, uplift in this area. It turned out that the uplift is due to two mechanisms:

- During impounding, the tail water level raises 4.40m. Thus, the recently wetted material is unloaded (the specific weight is reduced). Due to the fact that MC model does not allow for the stiffer behavior during unloading, the uplift is over estimated.

- While the upstream water level increases, the major principle stresses in this area increases too, however the minor principle stress does not increase, especially at shallow depths. According to Figure 78, the dilatancy leads to unrealistic volumetric expansion at very low confining pressures, thus resulting in unrealistic plastic straining (i.e. expansion in this case) and consequently results in an uplift in this region. Maximum total phase displacement (at the cut off`s downstream side) is 36cm, 10cm more (plus 38%) than in HS analysis.
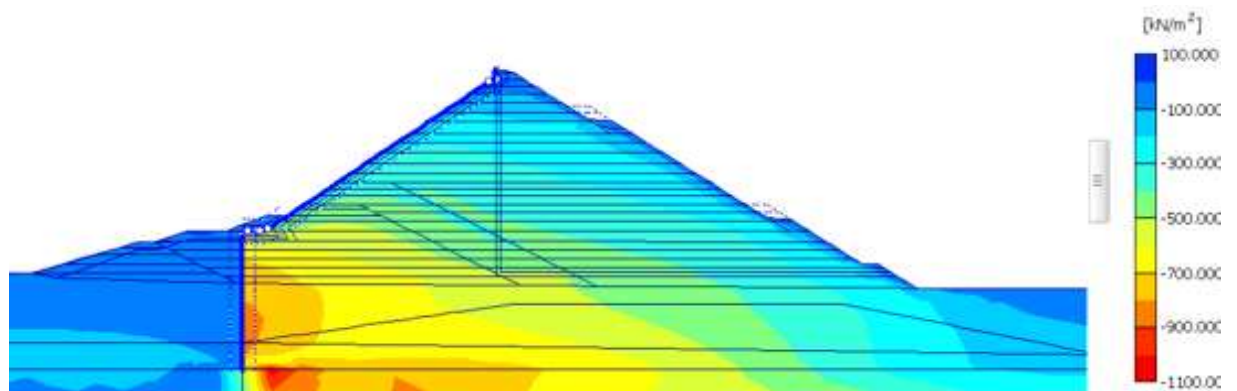
Figure 98 Horizontal effective stresses after first filling (MC, sand gravel fill).
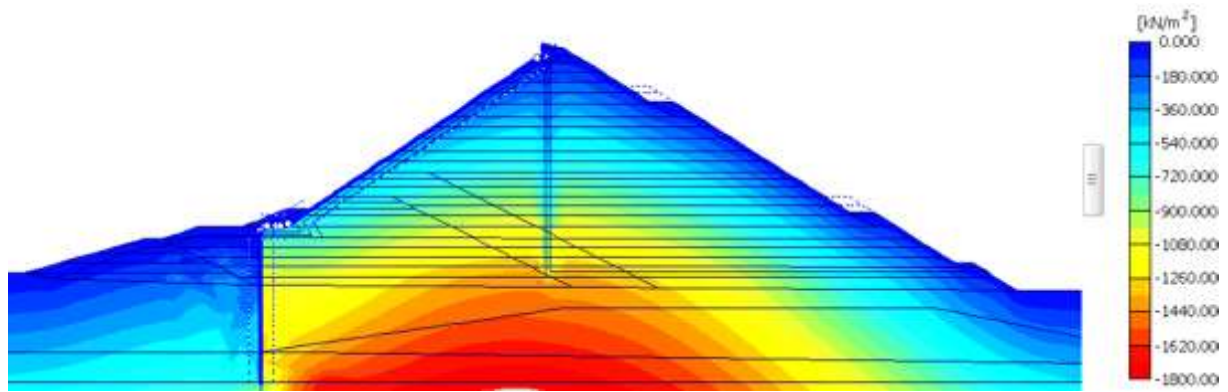
Figure 99 Vertical effective stresses after first filling (MC, sand gravel fill).
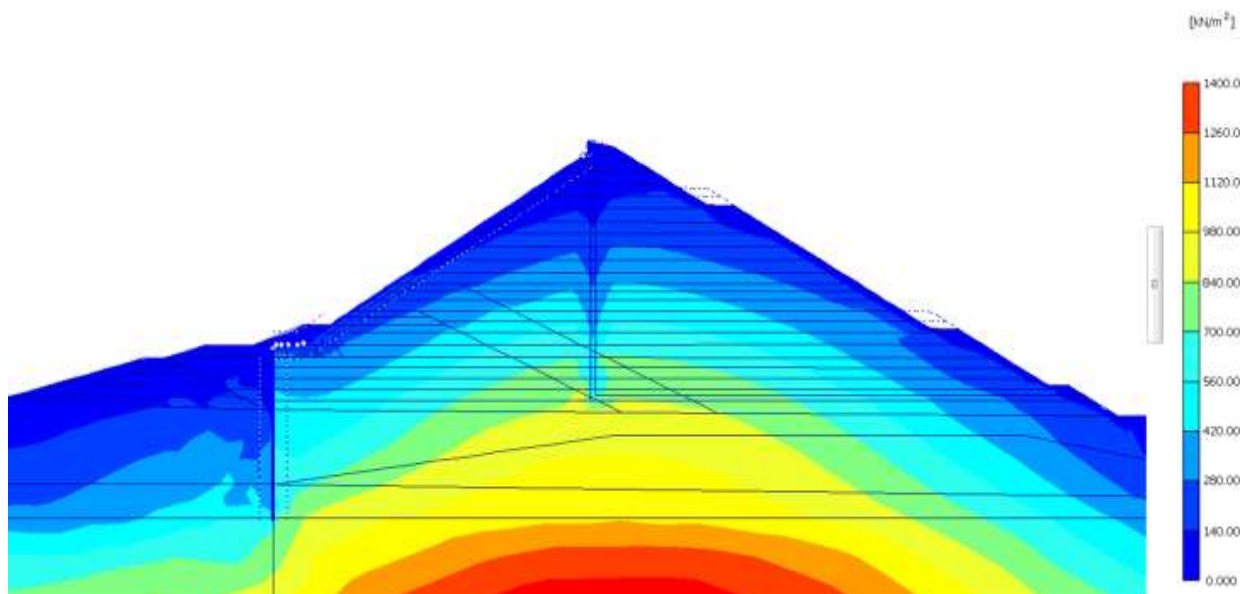
Figure 100 Total deviatoric stresses after first filling (MC, sand gravel fill).
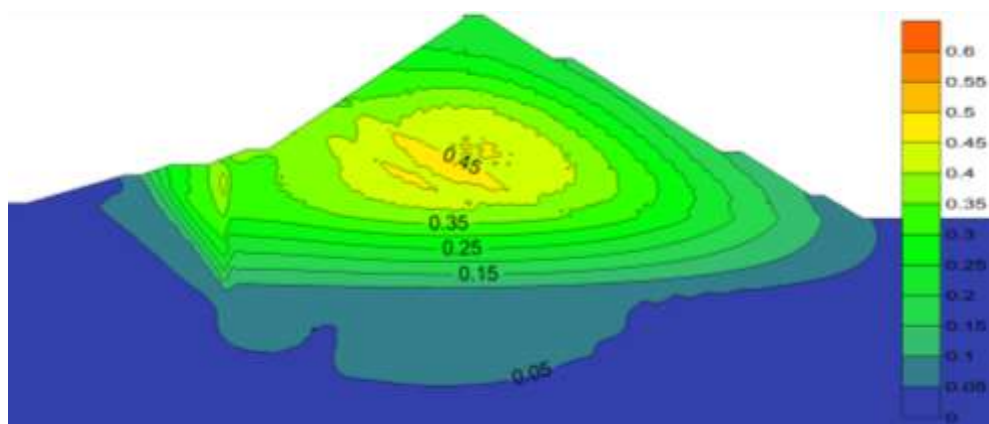
Figure 101 Total settlements after first filling [m] (MC, sand gravel fill).
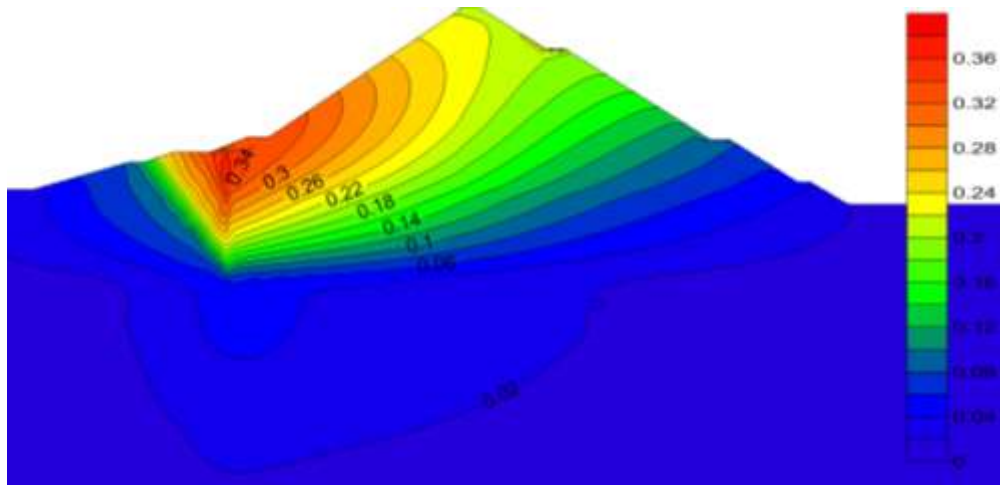
Figure 102 Horizontal phase displacements due to first filling [m] (MC, sand gravel fill).
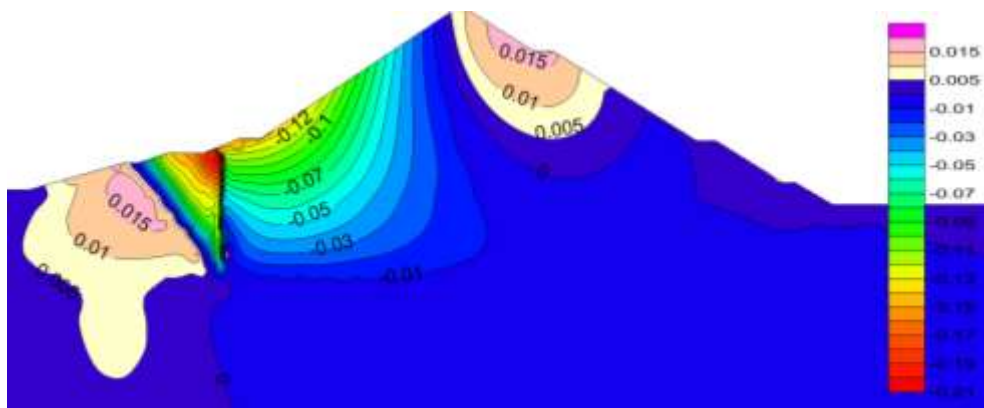
Figure 103 Vertical phase displacements due to first filling [m] (MC, sand gravel fill).

Figure 104 Total phase displacements due to first filling [m] (MC, sand gravel fill).

10.6.1.4 Slab / Plinth / Cut off Wall Displacements MC-Analysis

10.6.1.4.1 Plinth

The maximum plinth displacement during impounding amounts to 33cm in horizontal and -14.5cm in vertical direction at the cut off to plinth connection and 33cm in horizontal and -15cm in vertical direction at the slab to plinth connection. Compared to HS analysis, horizontal deformations are higher (plus 10cm or 45%) whilst vertical deformation remains the same.

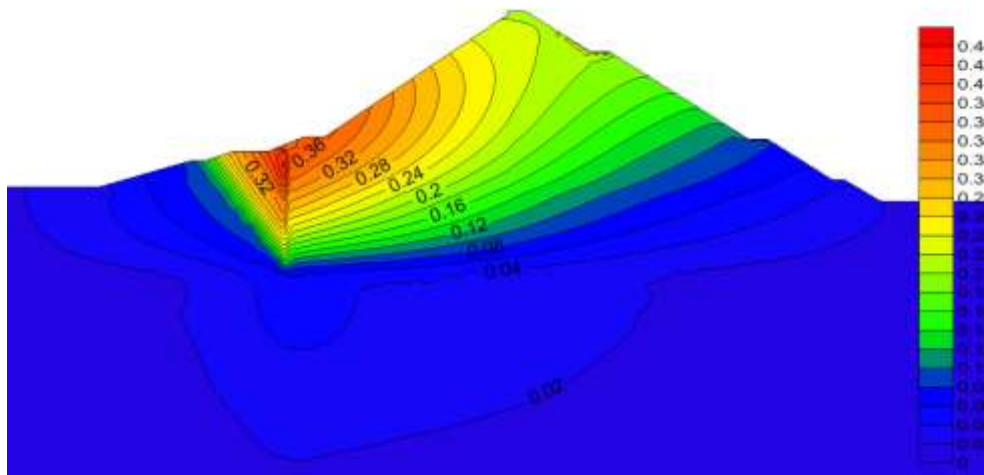The Maximum displacement due to placement of the selfhealing material is -0.1cm in horizontal (towards upstream) and -2.0cm in vertical direction (downwards).

10.6.1.4.2 Concrete Slab

As obvious in Figure 104, maximum displacements will occur at the plinth to slab contact point and amount to 33cm (plus 10cm or 45%) in horizontal and -15cm ($\pm$0cm) in vertical direction. Maximum total displacement at this point therefore results in 37cm, which is 10cm more (plus 37%) than obtained in HS analysis. Displacements at the concrete slab's top are 22cm (plus 10cm or plus 83%) in horizontal and 0.5cm in vertical direction (i.e. an uplift, this unrealistic behavior is discussed in chapter: 10.6.1.3.2 First Filling).

In common with HS analysis, the concrete slab shows tensile stresses during the self healing material's placement, which turn to compressive stresses during impounding. Maximum/minimum stress resultants occurring in the slab in MC analysis are:

Axial force: +148kN/m; -1500kN/m

Shear force: +7kN/m; -5kN/m

Bending moment: 38kN/m; -24kN/m

In contrast to HS analysis, the tensile force increases during the selfhealing material's placement, whilst compressive force and bending moment seem to decrease during impounding. Assuming, that the concrete's average resistance to tension stress is 2.2MN/m^2 (EN-1992-1-1, 2004, p. 29). These forces will not lead to bending cracks in the slab (forces not increased by safety factors). Assuming an axial reinforcement of 0.3% (12 cm^2/m) in axial direction, located at the slabs axis and no additional shear reinforcement applied, the concrete slab's resistance is found to be appropriate in this case.

10.6.1.4.3 Cut off Wall

Maximum deflection towards upstream prior to first filling is located on the cut off's top again in common with HS analysis and amounts to -6cm (plus 50%) in horizontal and -4cm (minus 27%) in vertical direction. Maximum differential displacement due to first filling results in 33cm (plus 8cm or 32%) in horizontal (towards downstream) and -14.5cm (minus 1.5cm or 9%) in vertical direction (downwards), again on the cut off's top.

10.6.2 Weak Rockfill

10.6.2.1 Stress-Strain-Behavior HS-Analysis

10.6.2.1.1 End of Construction

Maximum stresses at end of construction are -700kN/m^2 in horizontal and -3000kN/m^2 in vertical direction, located at the lowest part of the vertical drainage zone (Figure 105 and Figure 106). In contrast to HS analysis of sand gravel fill material (HS SG analysis), maximum stresses are generally higher (plus 40% in horizontal and plus 65% in vertical) and are concentrated to a very small area. This is to be due to the stiff behavior of the drainage zone. Compared to drainage material, the weak rockfill undergoes higher straining and hence, "hangs up" on the vertical drainage. The same effect is evident for cushion and transition zone too (Figure 105).

Maximum calculated deformation at end of construction (Figure 107) results in 1.5m, located in the middle of dam's main filling zone, 8m above the maximum calculated in HS SG analysis.

Figure 108 shows plastic points in Sarigüzel embankment at end of construction. Failure criterion is not reached in Sarigüzel's main embankment fill. According to the concentrated stresses at the drainage's lowest part, stress of this order results in significant straining. Hence, further measures as additional transition zones or drainage material obtained from weaker rock have to be taken.
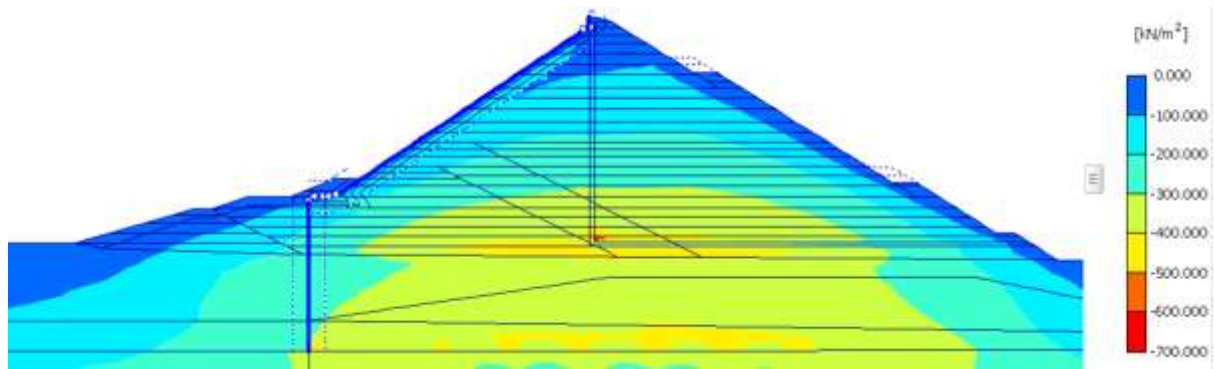
Figure 105 Horizontal effective stresses at end of construction (HS, weak rockfill).
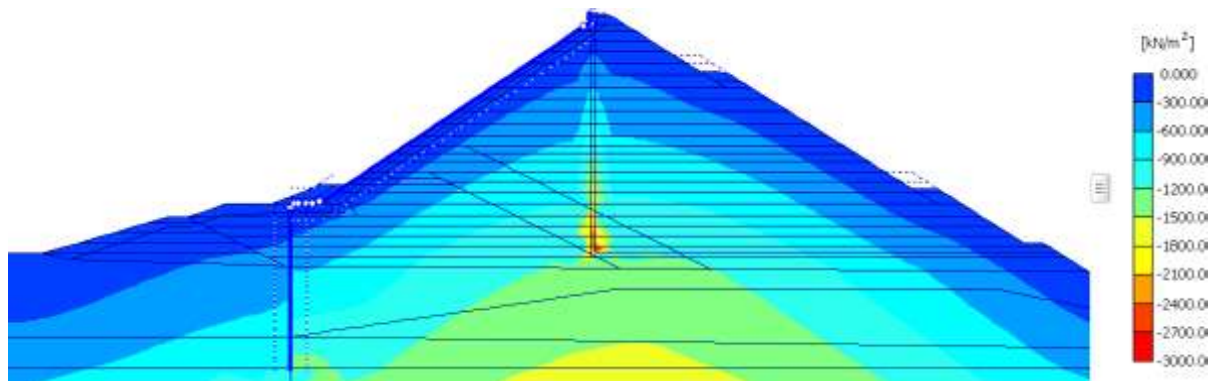
Figure 106 Vertical effective stresses at end of construction (HS, weak rockfill).
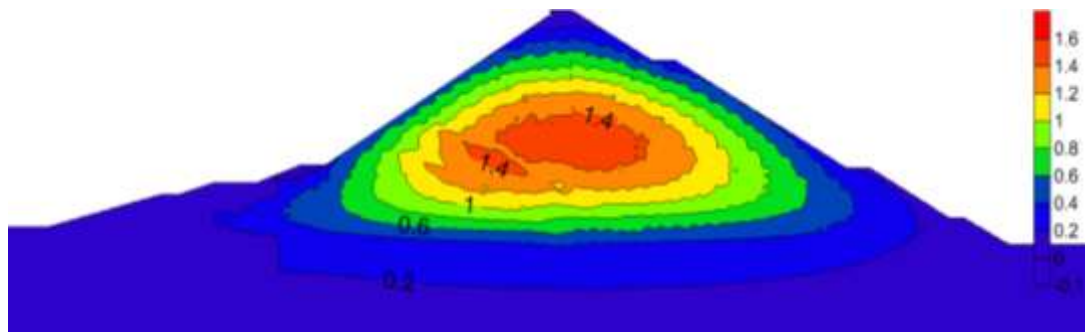
Figure 107 Total settlements at end of construction [m] (HS, weak rockfill).
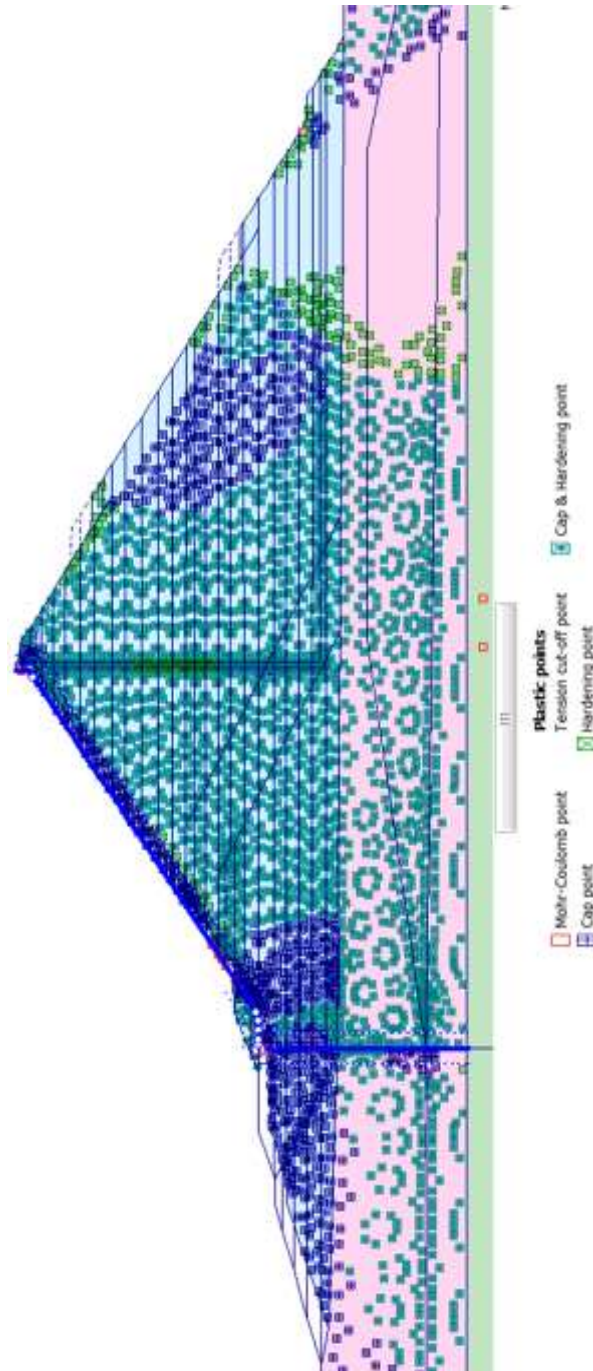
Figure 108 Plastic points in Sarigüzel embankment at end of construction (HS, weak rockfill).

10.6.2.1.2 First Filling

Maximum horizontal stress due to first filling (Figure 109) is located close the cut off wall at the weak rockfill to transition material change over and amounts to -1600kN/m². This is thought to be a local extreme value, due to the fact that the dam's design and stiffness of the transition zone have not been adapted to the weak rockfill material. This was done to ensure the results' comparability. In general, an upstream

fill consisting of weak rockfill material, does not provide sufficient support to the face slab and consequently should not be used in upstream shoulders.

Vertical stresses (Figure 110) do again concentrate to the lower parts of the vertical drainage and are in the order of -3500kN/m². Maximum deviatoric stress (Figure 111) amounts to 2500kN/m².
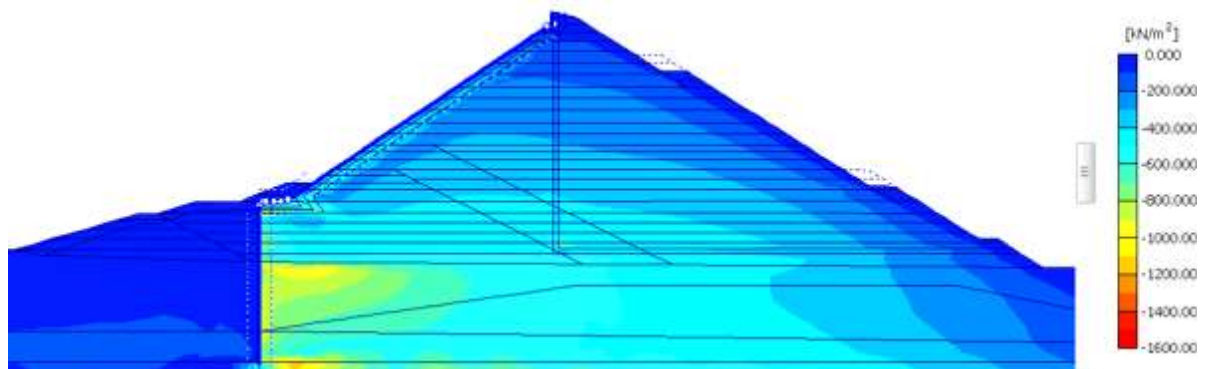
Figure 109 Horizontal effective stresses after first filling (HS, weak rockfill).
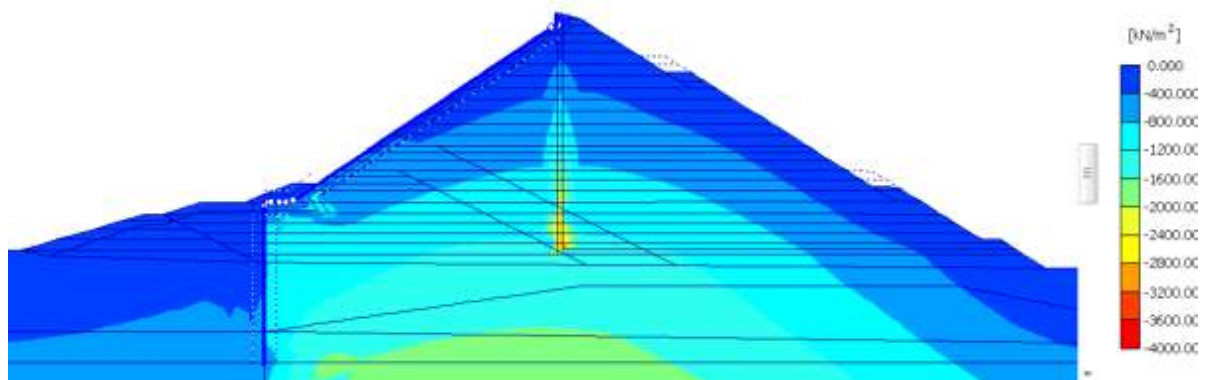
Figure 110 Vertical effective stresses after first filling (HS, weak rockfill).
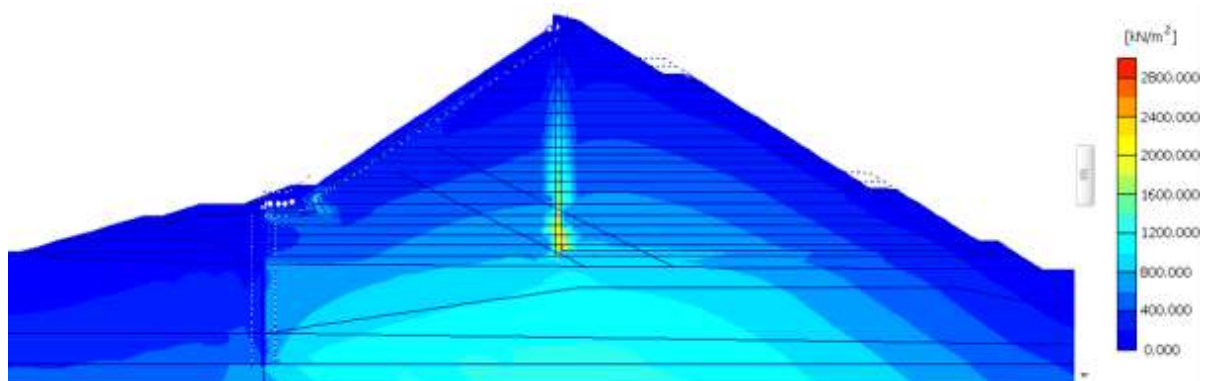
Figure 111 Total deviatoric stresses after first filling (HS, weak rockfill).

Maximum total settlement after first filling (Figure 112) amounts to 1.7m. Maximum total phase displacement due to first filling (Figure 115) results in 70cm, close to the cut off wall at the weak rockfill to transition material change over, respectively 55cm underneath the concrete slabs lower third. Figure 114 shows the differential vertical displacements. In general, the dam shows the same behavior during first filling as shown in HS SG analysis (cp. Figure 88), while the magnitudes of course are higher. Crest displacement due to first filling results in -22cm in vertical and 20cm in horizontal direction. Maximum horizontal displacement occurs close to the cut off wall and amounts to 65cm.
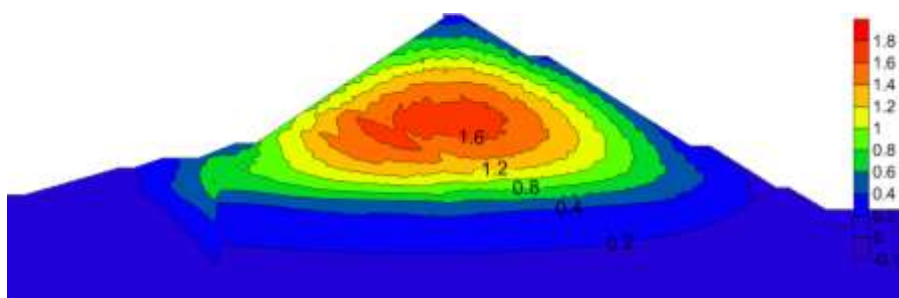
Figure 112 Total settlements after first filling [m] (HS, weak rockfill).
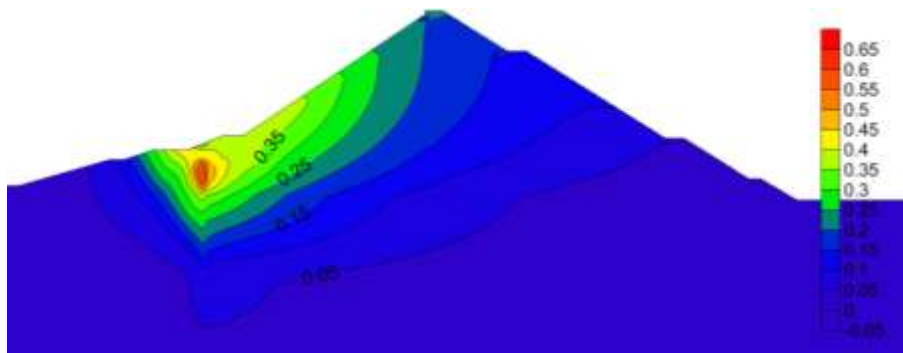
Figure 113 Horizontal phase displacements due to first filling [m] (HS, weak rockfill).
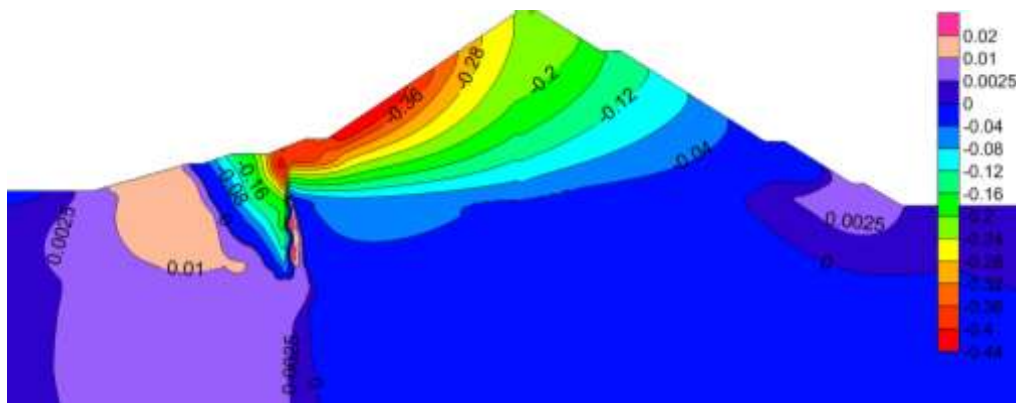
Figure 114 Vertical phase displacements due to first filling [m] (HS, weak rockfill).
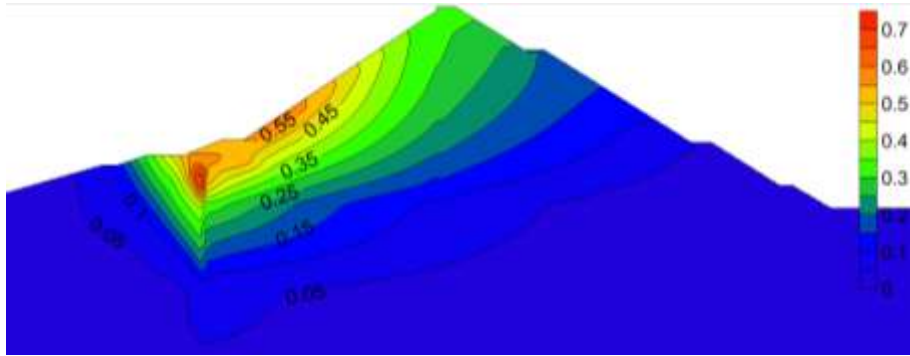
Figure 115 Total phase displacements due to first filling [m] (HS, weak rockfill).

10.6.2.2 Slab / Plinth Displacements HS-Analysis

10.6.2.2.1 Plinth

The Maximum displacement due to the selfhealing material's placement is in the order of -0.13cm in horizontal (towards upstream) and -2.5cm in vertical direction (downwards).

The maximum plinth displacement during impounding results in 37cm in horizontal and -41cm in vertical direction at the concrete slab connection and 37cm horizontally and -39cm vertically at the cut off connection.

10.6.2.2.2 Concrete Slab

As obvious in Figure 115 the maximum deflection due to first filling occurs at the slab's lower third, amounting to 59cm.

The slab is not subject to tensile stresses in all calculation phases. Maximum stress resultants for design result in:

- M= -350kNm/m; N= -52kN/m; V= 5kN/m.
- M= 306kNm/m; N= -2464kN/m; V= -51kN/m.
- M= -33kNm/m; N= -4540kN/m; V= 4.5kN/m.

Assuming a constant slab thickness of 40cm, the above mentioned stress resultants can be transmitted, if a two layered reinforcement layout with a rate of 0.85% is applied as upstream and downstream reinforcement. An overall steel rate of 1.70% is uneconomic and would result in further undesirable problems (from a technical point of view).

10.6.2.3 Stress-Strain-Behavior MC-Analysis

10.6.2.3.1 End of Construction

Maximum horizontal stress (Figure 116) in MC analysis of weak rockfill (MC WR analysis) results in -620kN/m^2 located at the rock to alluvium change over at the dam's axis. Compared to HS analysis, the extreme value is not located at the lowest part of the vertical drainage anymore. In common with HS analysis, MC analysis shows a significant reduction of horizontal stresses in the dams upper third as obvious from Figure 116. However, in MC analysis, the reduced horizontal stresses seem to be wider spread than in HS analysis.

Maximum vertical stress (Figure 117) results in -2200kN/m^2 located at the lowest part of the vertical drainage zone. MC WR analysis shows a maximum vertical stress that is 25% less than calculated in HS WR analysis. However, the weak rockfill "hangs up" on the stiffer drainage zone too, in MC WR analysis.
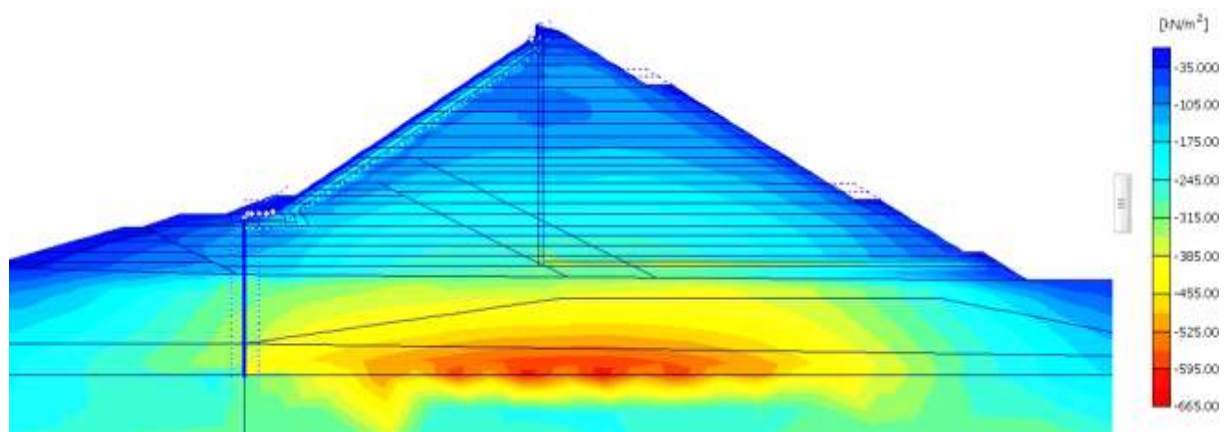
Figure 116 Horizontal effective stresses at end of construction (MC, weak rockfill).
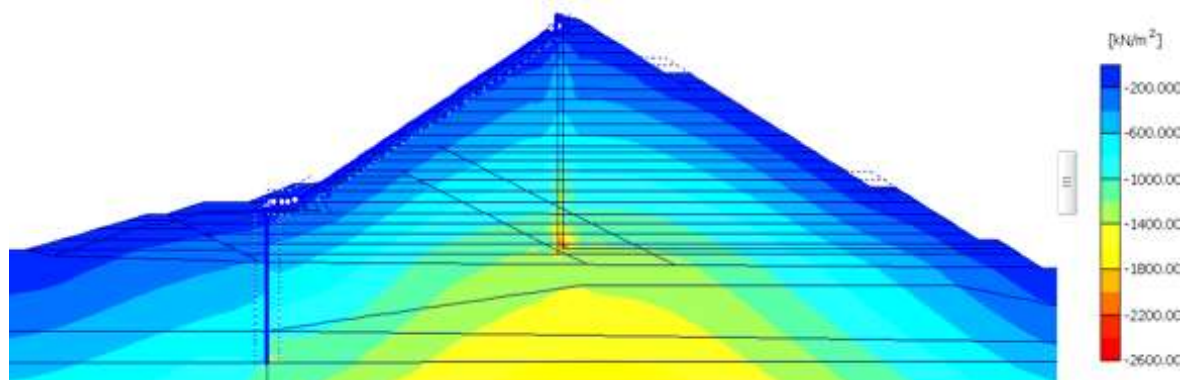
Figure 117 Vertical effective stresses at end of construction (MC, weak rockfill).

Maximum settlement at end of construction results in 1.10m at the embankment's middle. MC WR analysis result in 25% less deformation, compared to HS WR analysis. Which is quite surprising, as all deformations calculated by MC SG model always exceeded the deformations calculated by HS SG analysis. This behavior is further specified in the next chapter: 10.6.2.1.2 First Filling.

Figure 119 shows plastic points in Sarigüzel embankment at end of construction. Compared to HS WR analysis, the failure criterion is reached by several points at the embankment's center. Table 19 compares deviatoric, principal and minor stresses of HS WR and MC WR analyses observed in K, L and M (Figure 119). Generally the principal stresses remain relatively unaffected by the constitutive model. However, MC analysis yield smaller minor stresses, thus resulting in higher decviatoric stresses. Therefore the new stress distribution reaches the failure criterion in several points.

In general the drainage in MC analysis shows an overall stiffer behavior than the drainage in HS analysis. This is discussed in detail in chapter: 10.6.2.3.2 First Filling. The stiffer behavior results in a reduction of the horizontal stresses in the drainage's surrounding area.

Further plastic points occur on downstream surface due to small lateral pressures and close to the transition zone, where horizontal stresses reduce due to the stiff behavior of cushion and transition zone.
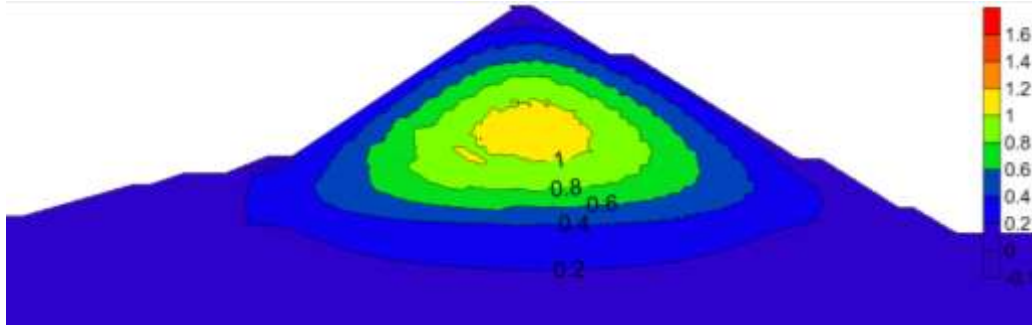
Figure 118 Total settlements at end of construction [m] (MC, weak rockfill).
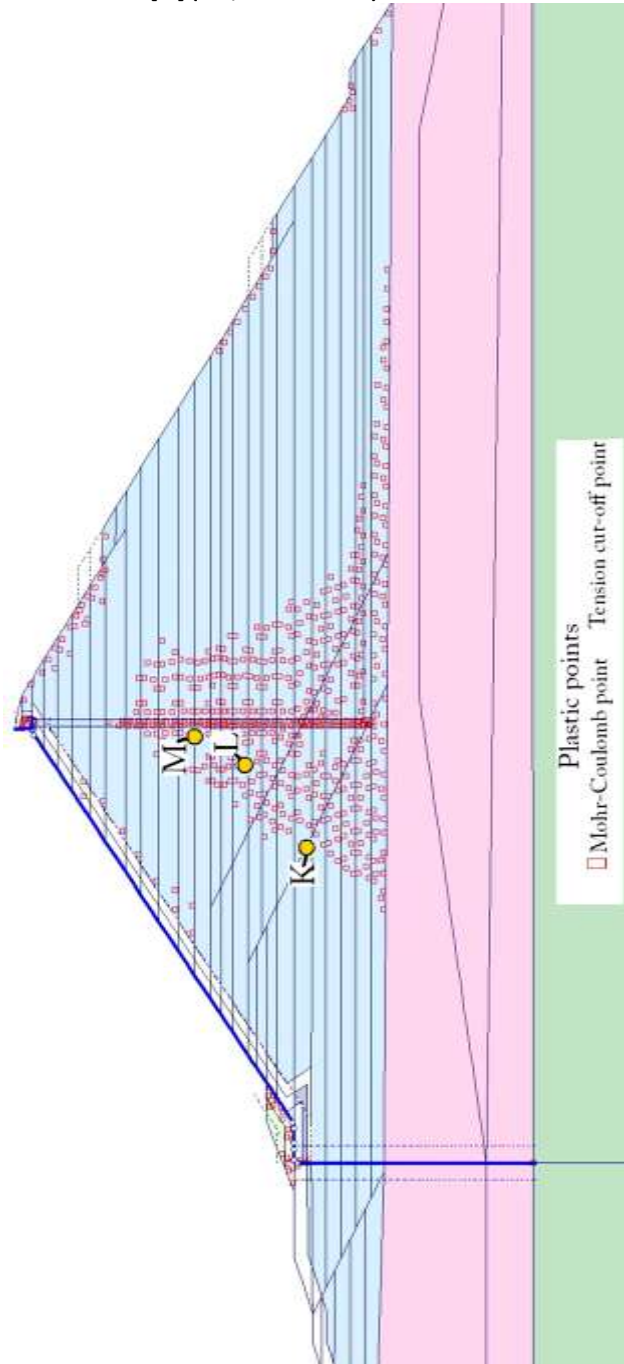
Figure 119 Plastic points and observation points (K, L, and M) in Sarigüzel embankment at end of construction (MC, weak rockfill).

Table 19 Stresses observed in HS WR and MC WR analyses.

Observa-tion point	HS WR analyses			MC WR analyses		
	Deviatoric stress q [KN/m^2]	Minor stress σ_3 [KN/m^2]	Principal stress σ_1 [KN/m^2]	Deviatoric stress q [KN/m^2]	Minor stress σ_3 [KN/m^2]	Principal stress σ_1 [KN/m^2]
K	610	289	899	691	207	898
L	494	246	740	574	171	745
M	392	195	587	455	135	590

10.6.2.3.2 First Filling

Maximum horizontal stress due to first filling amounts to -1200kN/m^2, 25% less than in HS WR analysis, but at same location. Maximum vertical stress is located at the lowest part of the vertical drainage, amounting to -2500kN/m^2, 30% less than calculated in HS analysis. Maximum deviatoric stress results in 1700kN/m^2, 30% less compared to HS analysis.
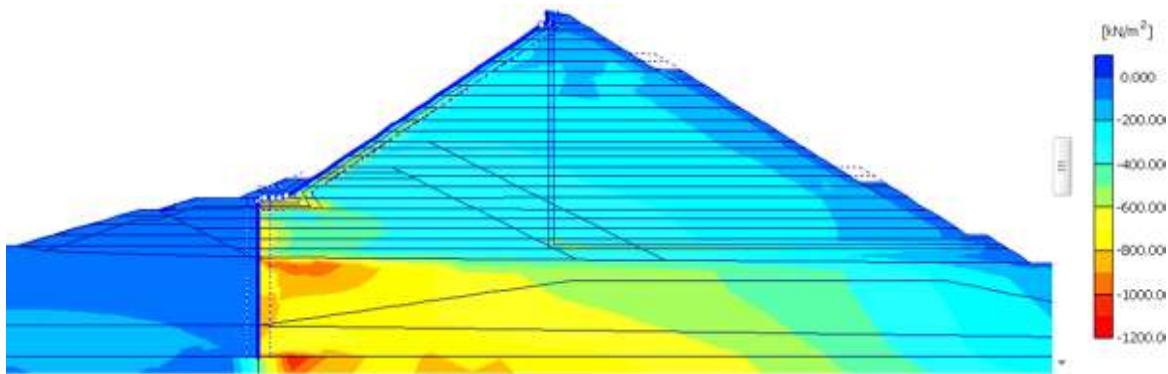
Figure 120 Horizontal effective stresses after first filling (MC, weak rockfill).
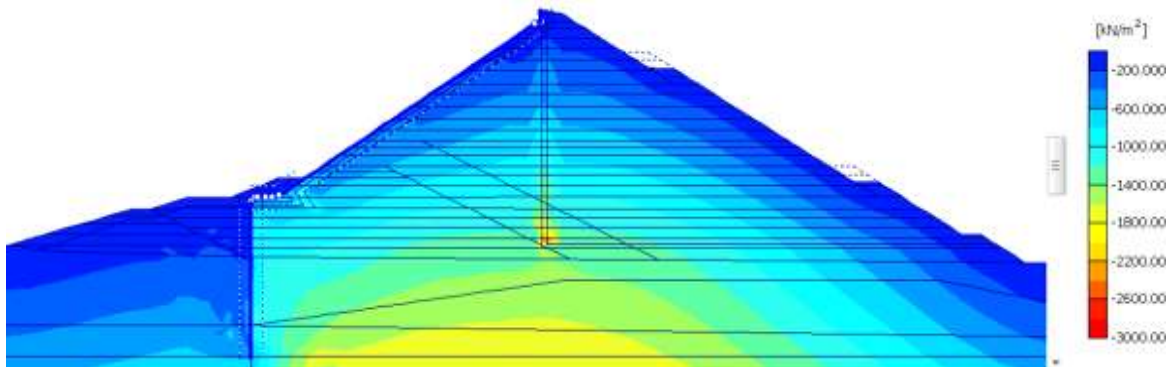
Figure 121 Vertical effective stresses after first filling (MC, weak rockfill).
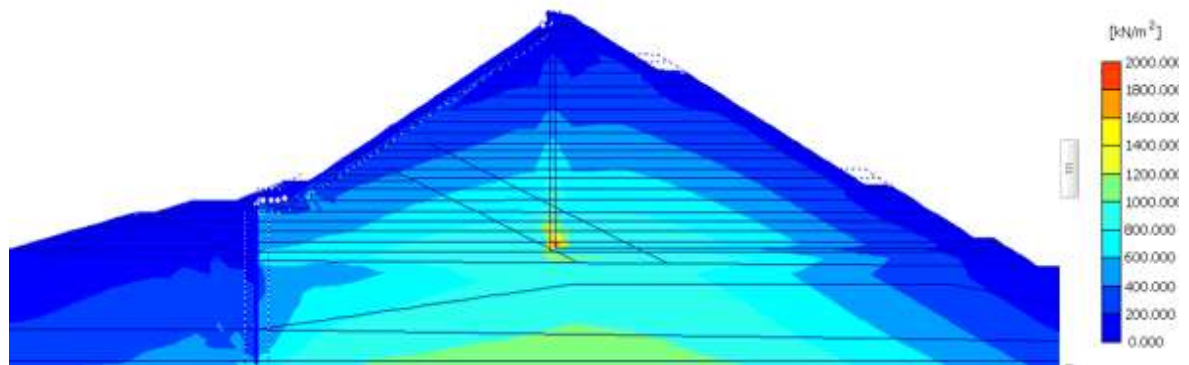
Figure 122 Total deviatoric stresses after first filling (HS, weak rockfill).

Maximum total settlement after first filling (Figure 122) results in 1.20m, 30% less than the result of HS analysis. As previously mentioned, all deformations calculated by MC SG analysis exceeded the deformations calculated by HS SG analysis. In weak rockfill analyses, it is the other way around. Maximum deviatoric stress in MC analysis results in 1700kN/m^2, however, this maximum value is concentrated to a small area of the dam's section. All other points of the dam's embankment undergo deviatoric stresses ranging from 0 to 1000kN/m^2 and confining pressures in the order of 0 to –500kN/m^2. Regarding Figure 123, the MC model underestimates axial strains in the majority of all cases. Assuming a deviatoric stress of 900kN/m^2 and a confining pressure of 300kN/m^2, MC model results in 3,75% axial strain, whilst HS model yields 8,25%. The strains are overestimated in cases of low deviatoric stresses and simultaneously exist-ing high confining pressures. But as most points show high deviatoric and high confin-ing pressures, the settlement in the embankment's center is mainly underestimated. In spite of the higher deviatoric stresses calculated by the MC model.

In general, MC model underestimates axial strains in marginal curved stress strain rela-tions, typically shown by weak rockfills. Whereas, MC model overestimates axial strains in highly curved stress strain relations, typically shown by rockfills of alluvial deposits or rockfills obtained from quarried, high strength rock.

Dashed lines = data obtained from triaxial tests on wetted Pancrudo gravel (shist) .
Solid lines = material behavior approximated by the HS model.
Dotted lines = material behavior approximated by the MC model.
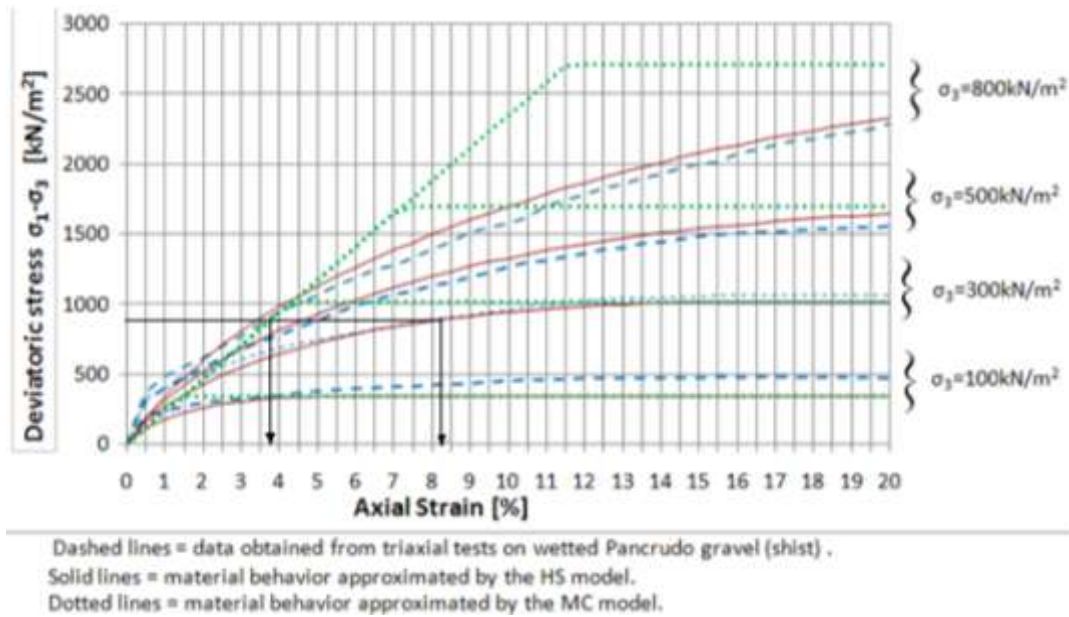
Figure 123 Strains yielded by MC and HS model for similar stress levels.

Figure 125 shows the horizontal phase displacements due to first filling. Maximum horizontal displacement amounts to 90cm (plus 38%) upstream of the cut off wall. Maximum vertical phase displacement (Figure 126) results in -70cm upstream of the plinth to cut off wall connection. Horizontal and vertical displacement of the crest due to first filling results in 52cm (plus 38%) and -5cm (minus 77%). Figure 127 shows the total phase displacements due to first filling with a maximum amounting to 1.1m (plus 64%) upstream of the cut off wall. Maximum face deflection results in 85cm (plus 65%) at the slabs lower third. In contrast to the above mentioned, the displacements of all concrete structures are significantly higher than obtained in HS WR analysis. This is thought to be due to the MC model's constant stiffness on un- and reloading.
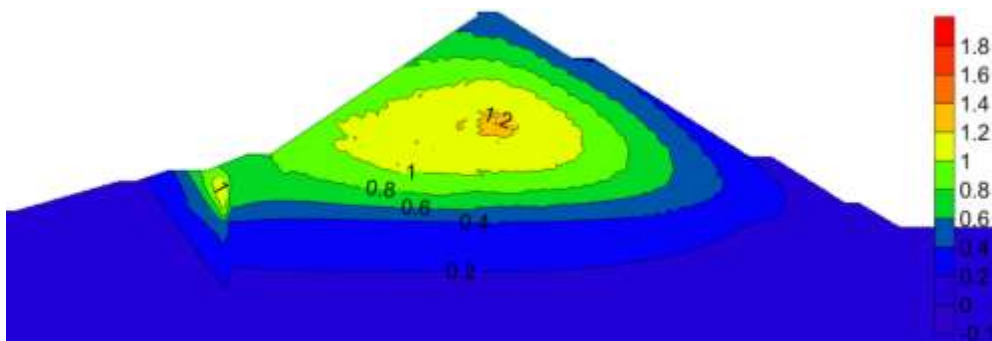
Figure 124 Total settlements after first filling [m] (MC, weak rockfill).
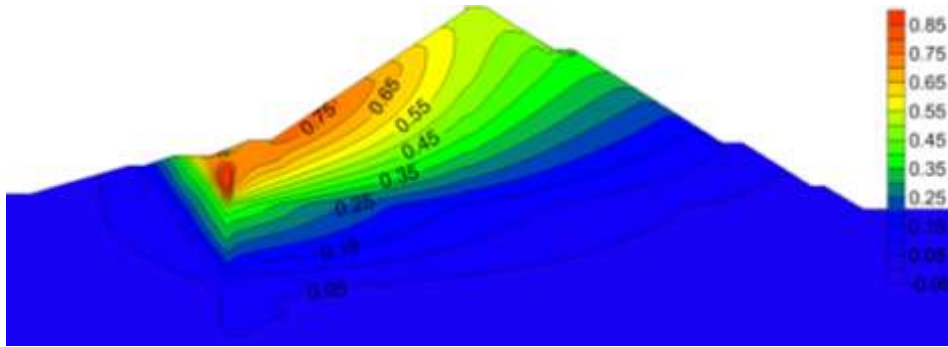
Figure 125 Horizontal phase displacements due to first filling [m] (MC, weak rockfill).
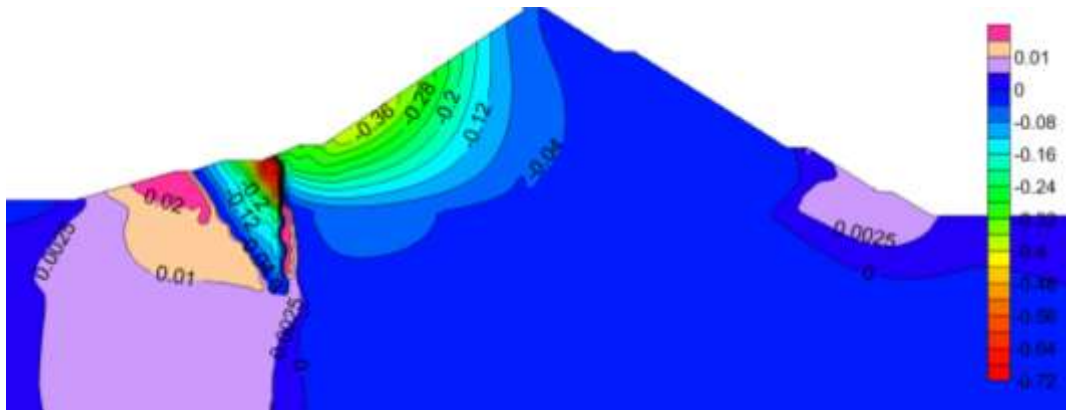
Figure 126 Vertical phase displacements due to first filling [m] (MC, weak rockfill).
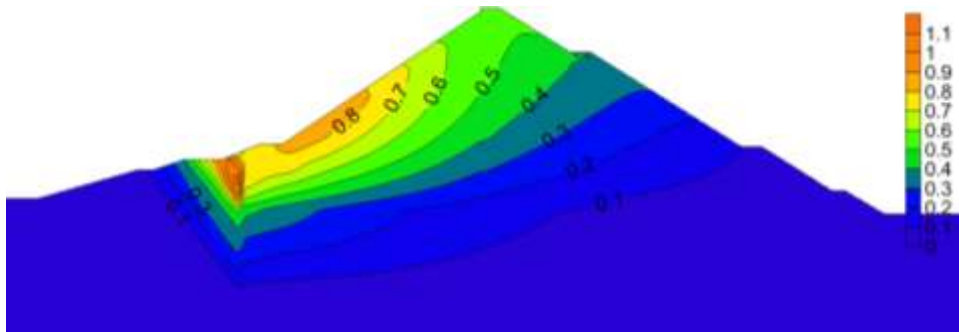
Figure 127 Total phase displacements due to first filling [m] (MC, weak rockfill).

10.6.2.4 Slab / Plinth Displacements MC-Analysis

10.6.2.4.1 Plinth

The maximum plinth displacement during impounding results in 71cm in horizontal and -30cm in vertical direction at the concrete slab connection and 71cm in horizontal and -24cm in vertical direction at the cut off connection. Compared to HS WR analysis, horizontal deformations increase (plus 35cm or 97%) whilst vertical deformation decrease (minus 11m or 27%).

The Maximum displacement due to selfhealing material's placement is 0.0 cm in horizontal and -3,5cm in vertical direction (downwards).

10.6.2.4.2 Concrete Slab

The maximum deflection due to first filling occurs at the slabs lower third, amounting to 78cm (+32% compared to HS WR analysis).

The slab is subject to tension in the lower third, when the selfhealing material is placed. Maximum stress resultants for design result in:

- M= -29kNm/m; N= 72kN/m; V= -5kN/m.
- M= -185kNm/m; N= -1500kN/m; V= -29kN/m.
- M= 42kNm/m; N= -576kN/m; V= 9,0kN/m.
- M= -81kNm/m; N= -1320kN/m; V=95kN/m.

The above mentioned stress resultants can be transmitted if a two layered reinforcement layout with 0,015% upstream and downstream reinforcement is applied.

11 Sensitivity Analysis

Sensitivity analysis were conducted for HS and MC analysis to estimate the impact of varying sand gravel fill material parameters on the dam's deformation behavior.

11.1 General Impact of Input Parameters on Dam Behavior

Herein the general impact of varying parameter sets on crest displacements and maximum face slab deflection after first filling is evaluated, to gain information about parameters highly affecting the dam's deformation behavior.

11.1.1 Mohr-Coulomb Model

The parameter set applied to MC analysis of sand gravel is varied in the same order of magnitude (±25%) for every particular parameter. It is commonly known, that the parameters do not vary within the same rated ranges. For, rockfills show a poisson's ratio normally ranging from 0,25 to 0,4 (i.e. ±25%) while the young's modulus ranges from 25000kN/m^2 to 300000kN/m^2 (i.e.± 85%). The following relations shall give a feeling about an appropriate accuracy in estimating input parameters.

The impact on the dam crest's displacement after first filling is shown in Figure 128. Thus it appears that in-/decreasing the parameters young's modulus (Eref) and dilata-

tion (psi) does not have significant effect on the crest's deformation if varied in a range of ±25%. Compared to the other input parameters in MC model, the internal friction angle (phi) seems to be the dominating parameter. The impact on the concrete slab's maximum deflection is shown in Figure 129. Again dilatation and young's modulus do not have significant influence on the face slab's deformation, whilst the poisson's ra-tion (nu) shows increasing significance.

Applying cohesion (cref) does always lead to discussions in dam society, especially in case of stability analysis. To investigate the general impact of cohesion in deformation analysis, an unrealistic high value (according to sand gravel) of 10kN/m^2 was applied, yielding that cohesion does not affect the dam's deformation behavior.

Figure 128 Impact of input parameters on crest deformation after first filling (MC, sand gravel fill).
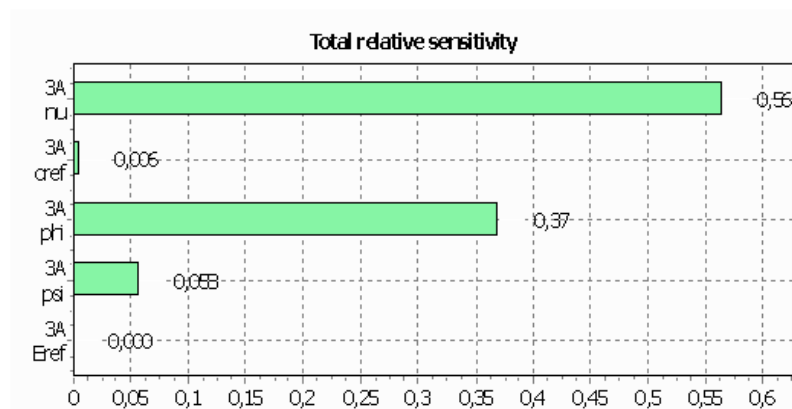
Figure 129 Impact of input parameters on face slab deformation after first filling (MC, sand gravel fill).

11.1.2 Hardening Soil Model

Unfortunately sensitivity analyses on HS model do not result in meaningful output. As HS model's input parameters E_{50}^{ref}, E_{oed}^{ref}, E_{ur}^{ref} and φ are associated parameters, they cannot vary independently. For example, the following terms have to be fulfilled: E_{oed}^{ref} > 0,8 E_{50}^{ref} and E_{ur}^{ref} > 2 E_{50}^{ref}. Consequently, within one calculation, a reduction of E_{50}^{ref} requires a reduction of E_{oed}^{ref} too. Thus, making it impossible to investigate the influence of E_{50}^{ref} separately. Due to this, the parameters E_{50}^{ref}, E_{oed}^{ref}, E_{ur}^{ref} and φ have to be excluded from sensitivity analysis.

Figure 130 shows the impact of power (m), dilatation (psi) and cohesion (cref) on crest deformation after first filling. Dilatation (psi) and power (m) are varied in a range of ±25%. Figure 130 indicates that dilatation, in relation to power, shows a significant impact.

To investigate the influence of cohesion in deformation analysis, an unrealistic high value of 10kN/m^2 was applied, yielding that cohesion does not affect the dam's deformation behavior. Figure 131 shows the impact of power, dilatation and cohesion on maximum slab deflection after first filling, yielding the same results, as apparent from Figure 130.

Figure 130 Impact of particular parameters on crest deformation after first filling (HS, sand gravel fill).
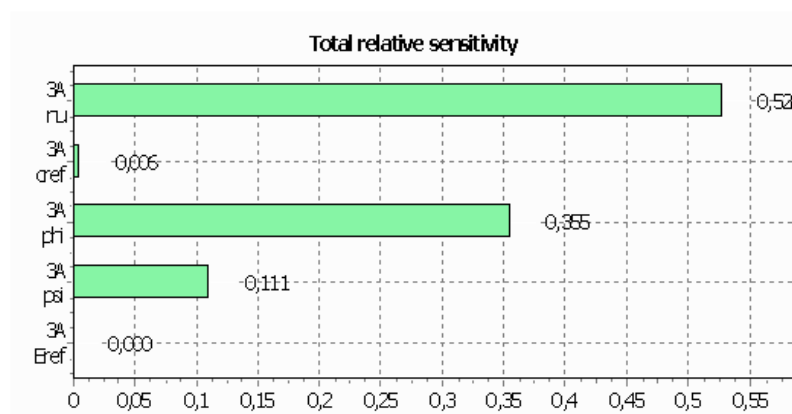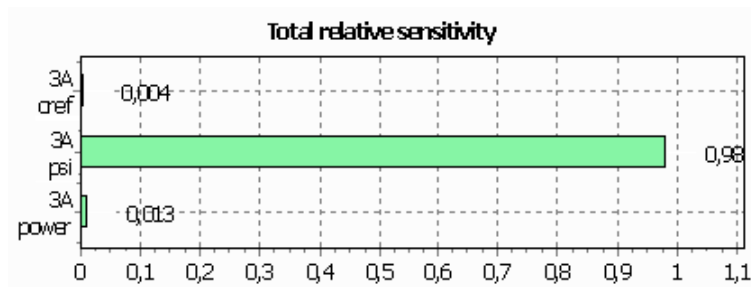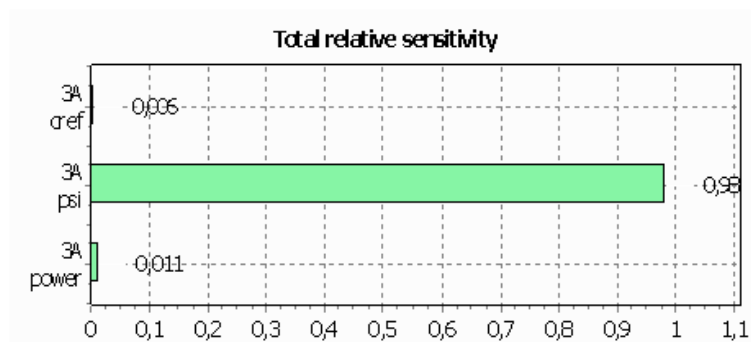

Figure 131 Impact of applied parameters on face slab deformation after first filling (MC, sand gravel fill).

11.2 Impact of Input Parameters on Slab Forces

Table 20 and Table 21 summarize the input parameters applied to sand gravel fill in HS and MC model. The impact on slab forces is studied by varying single parameters, while leaving the others unchanged. It should be noted, that the particular changed parameter varies in its natural range. The "natural" range of R_{inter} is discussed in detail.

Table 20 Sand gravel fill input parameters applied to HS model.

unsatu-rated specific weight	satu-rated specific weight	cohesion	inter-nal fric-tion angle	dila-tation	deforma-tion mod-ulus	un-/reloading mod-ulus	modulus	pow-er	fail-ure ratio	Stren-gth reduc-tion factor	refer-ence pressure
γ	γ_{sat}	c	φ	ψ	E_{oed}^{ref}	E_{ur}^{ref}	E_{50}^{ref}	m	R_f	R_{inter}	p_{ref}
[kN/m³]	[kN/m³]	[kN/m²]	[°]	[°]	[kN/m²]	[kN/m²]	[kN/m²]	[-]	[-]	[-]	[kN/m²]
21,5	23,3	0,2	45	9	55000	151000	73000	0,35	0,85	0,95	100

Table 21 Sand gravel fill input parameters applied to MC model.

Young's modulus	Poi-sons ratio	Unsatu-rated spe-cific weight	Saturated specific weight	Cohesion	Internal friction angle	Strength reduction factor	Di-lata-tion	According to a average later-al stress state of
E	ν	γ	γ_{sat}	c	φ	R_{inter}	ψ	σ_3
[kN/m²]	[-]	[kN/m³]	[kN/m³]	[kN/m²]	[°]	[-]	[°]	[kN/m²]
89100	0,30	21,5	23,3	0,2	45	0,95	9	200

11.2.1 Hardening Soil Model

Figure 132 shows the impact of a varying R_{inter} coefficient on the slab's stress resultants. R_{inter} controls the forces, transmitted by the concrete slab to the adjacent material. This is done, by reducing φ and c of the adjacent soil and applying the reduced parameter set to interface elements. Where: $c_i = R_{inter} \cdot c_{soil}$ and $\tan\varphi = R_{inter} \cdot \tan\varphi_{soil} \leq \tan\varphi_{soil}$. MC model is applied to the interface elements, however in case of HS analysis, the tangent stiffness is updated with increasing confining pressure. For further information, the reader is referred to Plaxis (2009, Reference Manual). As obvious from Figure 132, R_{inter} influences the compressive force (N_{min}) and bending moment (M_{max}) at end of construction (EoC). N_{min} EoC and M_{max} EoC reduce with increasing R_{inter}. Ten-

sile stresses due to the selfhealing material's placement increase in case of small R_{inter} coefficients. Due to the slab's general resistance, end of construction forces are of minor interest, while slab forces due to first filling are a matter of particular concern. If R_{inter} reduces, compressive forces decrease whilst bending moments increase. According to the slab's resistance, a reduction of R_{inter} results in negative impact on the slab's behavior. The bending moment (M_{max} FF) is unaffected by R_{inter} ranging from 1.00 to 0.70. Within this range, N_{min} FF reduces too, but without significant negative effects. Having in mind, that a two layered reinforcement layout turned out to be necessary in HS SG analysis (applied R_{inter} = 0.95), a R_{inter} lower than 0.7 will result in problematic slab behavior.

The above mentioned stands in contrast to recent efforts of reducing the shear transmission by applying bond breakers on the curb elements' surface. Pritchard (2008) reports that several high CFRDs located in steep valleys provided bond breakers in design with intend to reduce the slabs' horizontal stresses. At Kárahnjúkar dam, a 3mm thick asphalt emulsion was applied; at Bakun dam, sand asphalt and at Campos Novos and Barra Grande, plastic sheets. Campos Novos and Barra Grande showed massive face slab cracking and consequently high leakage values, which is found to be mainly caused by high horizontal stresses. The bond breakers gained no noticeable protection. Pritchard points out: "*A thin bond-breaker layer can be effective in eliminating or reducing adhesion but is not effective in cutting down friction.*"
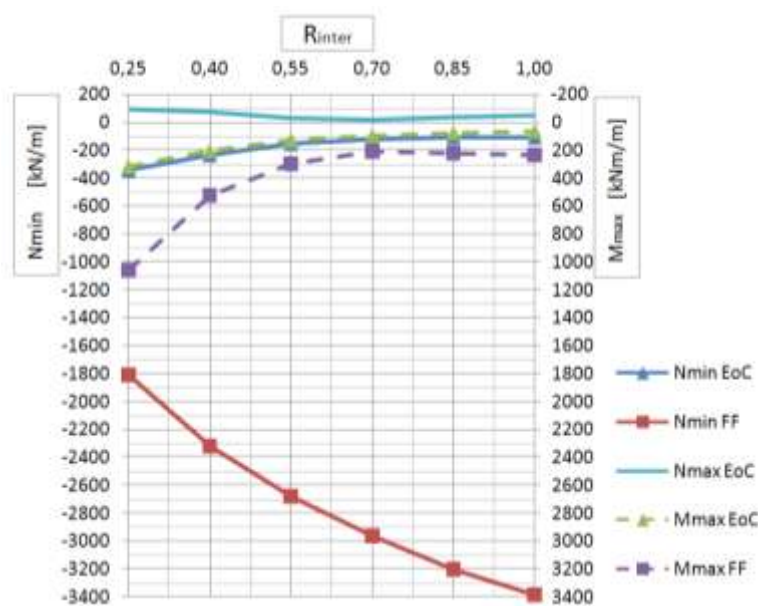
Figure 132 Impact of R_{inter} on slab forces in HS model.

Figure 133 shows the impact of an increasing E_{50}^{ref} on the slabs' stress resultants. Re-member, E_{oed}^{ref} and E_{ur}^{ref} were increases simultaneously within every E_{50}^{ref} step. Whilst tensile forces at end of construction and maximum bending moment after first filling remain unaffected, the maximum compressive forces decrease significantly with in-creasing moduli. The stress resultants M_{max} EoC and N_{min} Eoc (not displayed in Figure 133) are not affected by increasing moduli.
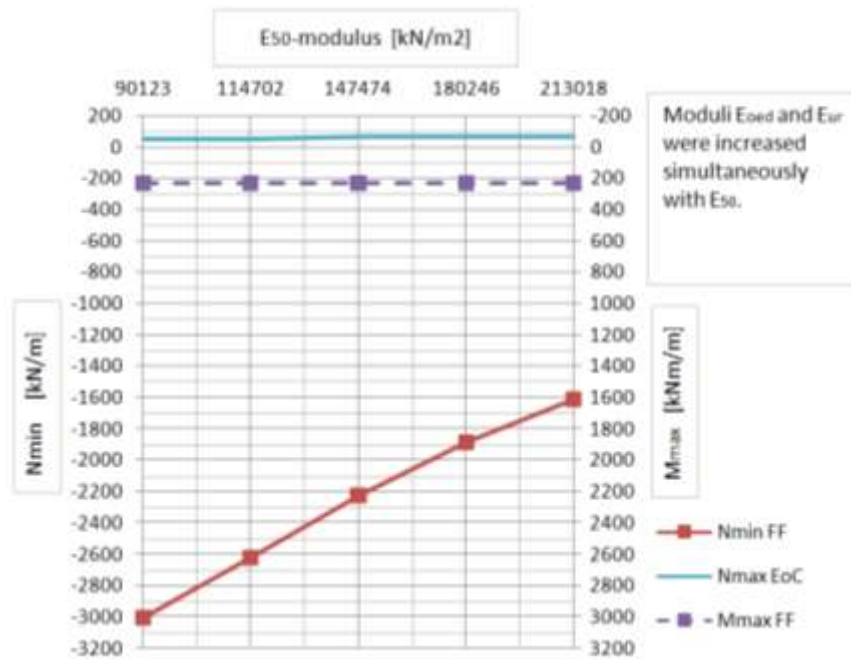
Figure 133 Impact of increased E-moduli on slab forces in HS model.

11.2.2 Mohr-Coulomb Model

Figure 134 shows the impact of R_{inter} on the slabs' forces in MC model. In general, MC model results the same trends as HS model did. Decreasing N_{min} FF and increasing M_{max} FF with decreasing R_{inter}. Compared to HS analysis, MC analysis results in generally smaller N_{min} FF, whilst N_{min} EoC, M_{max} FF, M_{max} EoC and N_{max} EoC remain almost unaf-fected.
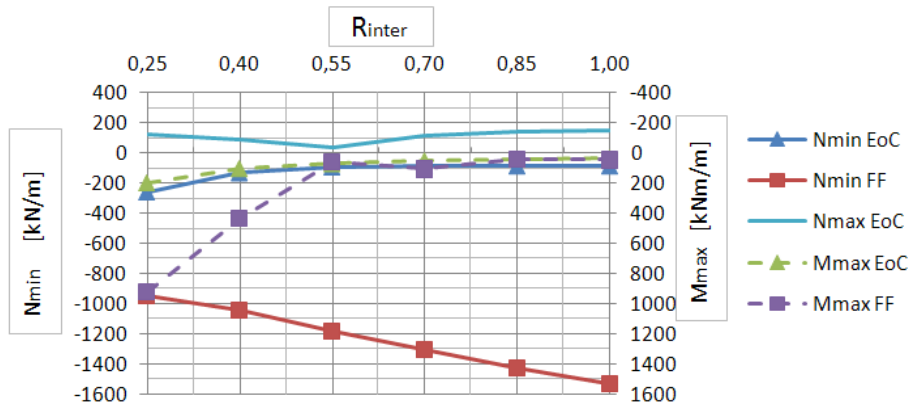
Figure 134 Impact of R$_{inter}$ on slab forces in MC model.

Figure 135 shows the impact of increasing E-modulus on the slabs' forces in MC analysis. The general trend of HS analysis is displayed in MC analysis too. Maximum compressive stress reduces with increasing modulus, whilst the other stress resultants remain unaffected.
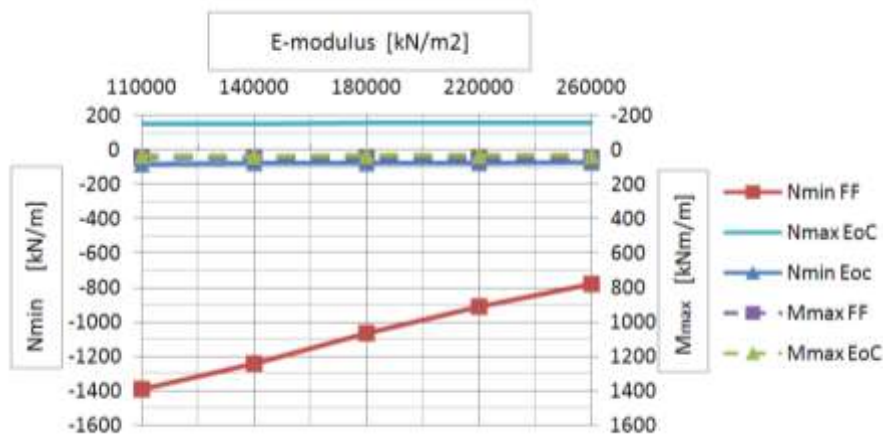
Figure 135 Impact of increased E-modulus on slab forces in MC model.

Figure 136 show the impact of varying poisson's ration on the slab's forces. M_{max} EoC, N_{min} EoC, N_{max} EoC (not displayed) and M_{max} FF are not affected, whilst N_{min} FF reduces with increasing poisson's ration.
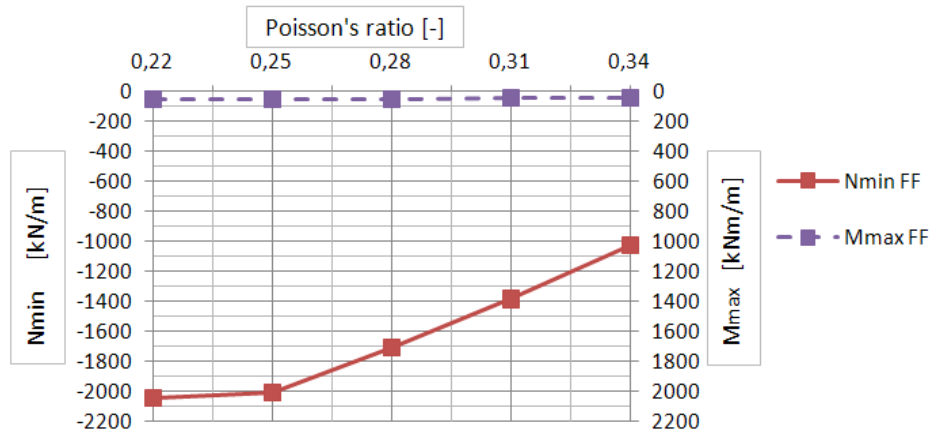
Figure 136 Impact of poisson's ratio on slab forces in MC model.

11.3 Impact of Input Parameters on Crest and Face Slab Deformation due to First Filling

11.3.1 Hardening Soil Model

Varying cohesion and dilatation does not affect the crest and slab displacements in HS analysis, by this reason the plots are not presented herein.

Figure 137 shows the impact of parameter power "m" on crest and slab displacement during first filling. The parameter power controls the material's stress dependency, or in other words, a decreasing m results in flatter stress paths in triaxial testing. The power m generally ranges from 0 to 1. With increasing m, the crest's settlement (crest delta v) decreases, whilst the horizontal crest displacement (crest delta h) remains un-affected. Maximum slab deflection is significantly affected by the parameter m, it decreases with increasing power.
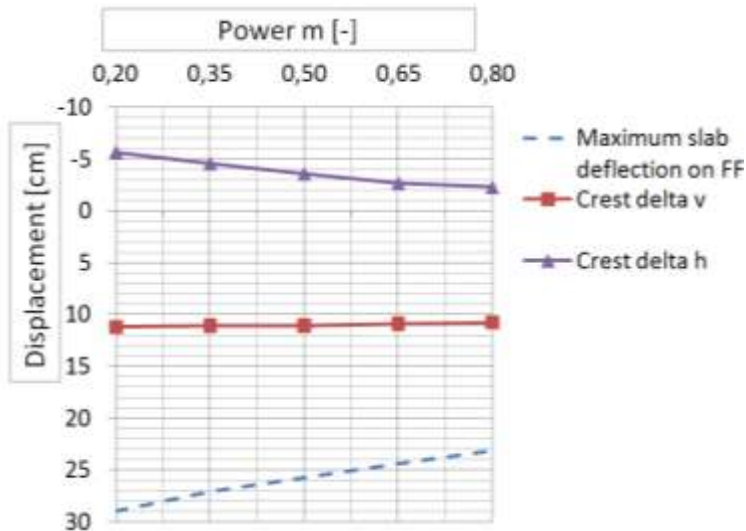
Figure 137 Impact of power "m" on slab deflection and crest displacement during impoundment in HS model.

Figure 138 shows the impact of a varying friction angle φ on crest and slab deformation due to fist filling. The internal friction angle is related to the actual stress dependent stiffness E_{50} (cp. formula 17) and hence, has a significant influence on the dam's behavior in HS model. The horizontal crest deformation remains almost unaffected. Either crest settlement is not significantly influenced. However, with increasing φ, the crest settlement decrease, whilst horizontal crest displacement increases. Surprisingly, maximum slab deflection increases with increasing internal friction angle. Figure 139 shows the deviatoric stress path from beginning of construction works till the end of the reservoir's impoundment. The stress paths are observed close to the point where the maximum face slab deflection due to first filling occurs. The deviatoric stresses calculated for a φ of 50° increase from 100 to 400kN/m^2 during impounding, whilst stresses calculated for a φ of 35° increase from 160 to 270KN/m^2. Figure 140 shows stress paths obtained from triaxial test on two sand gravel materials, one having a friction angle of 50° and the other having a friction angle of 35°. Both materials were tested for the above mentioned confining pressures (cp), occurring at beginning and at end of first filling. Thus it appears that, due to the higher stress conditions, the material having a φ of 35° shows an overall stiffer behavior than the material having a φ of 50°. By this reason, slab deflection increases with increasing internal friction angle.
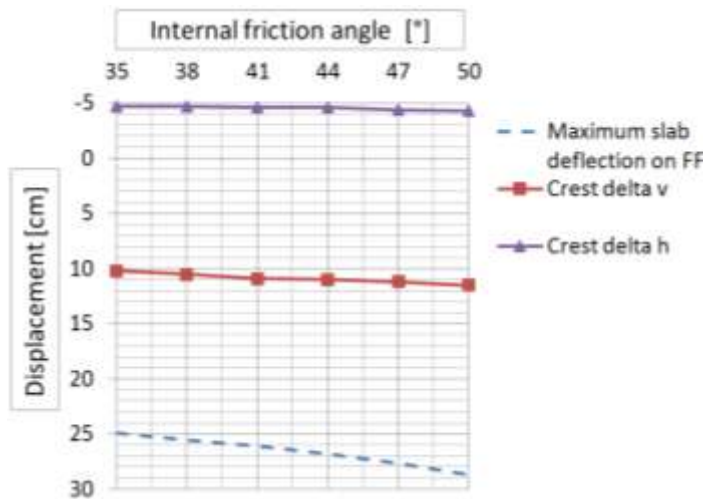
Figure 138 Impact of internal friction angle on slab deflection and crest displacement during impoundment in HS model.
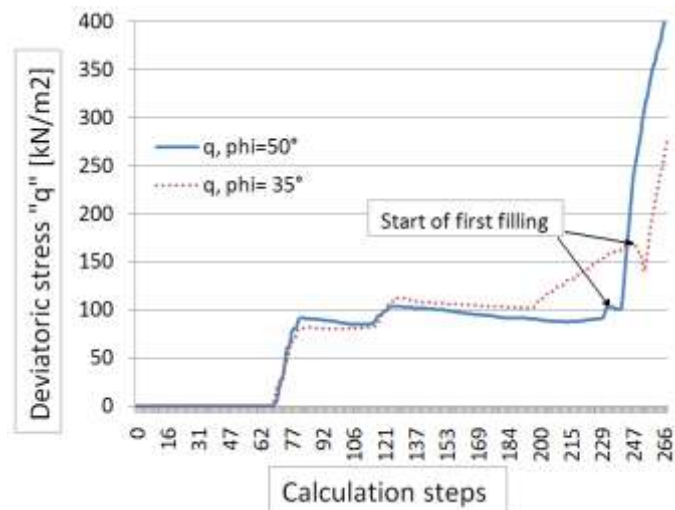
Figure 139 Deviatoric stresses close to the maximum slab deflection for two materials having different friction angles (HS model).
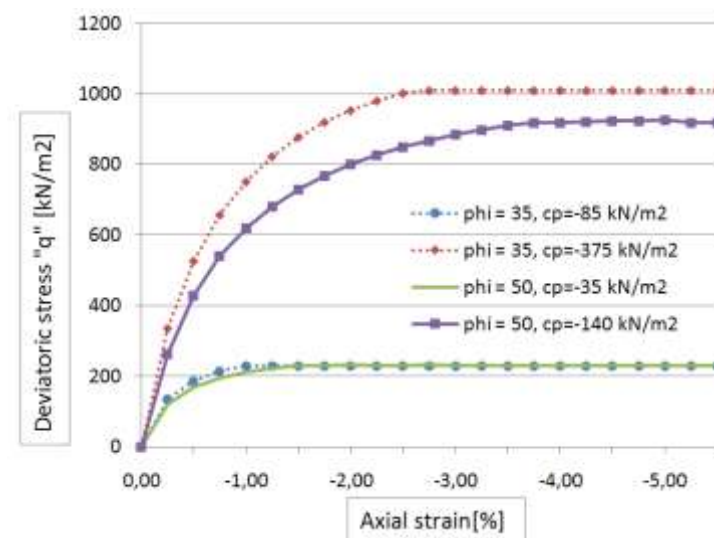
Figure 140 Triaxial tests on sand gravel with varying friction angles and varying confining pressures.

Figure 141 shows the impact of increasing moduli on general dam behavior during first filling. E_{oed}^{ref} and E_{ur}^{ref} increase simultaneously within every E_{50}^{ref} step. The horizontal and vertical crest displacements reduce with increasing moduli. The maximum slab deflection decreases with increasing moduli too.
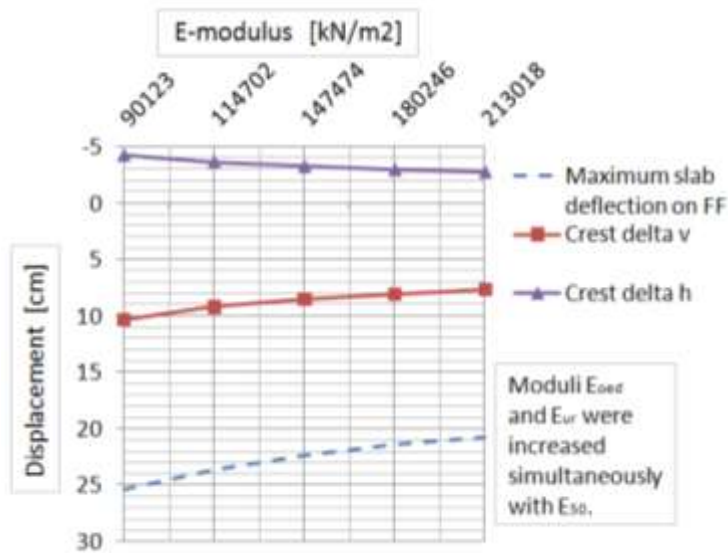
Figure 141 Impact of increasing moduli on slab deflection and crest displacement during impoundment in HS model.

11.3.2 Mohr-Coulomb Model

According to MC - model, a parameter variation of internal friction angle or dilatation, resulted in minor effects on crest and slab displacements. This is not in contrast to the output presented in chapter: 11.1, where the parameters were varied in a range of plus minus 25%. In this chapter, the parameters were changed within its natural boundaries, by this reason friction and dilatation play a minor part herein.

Figure 142 shows the impact of a increasing young's modulus on general dam behavior due to first filling. In general, the crest's settlement is almost unaffected, whilst horizontal crest displacement and maximum slab deflection decrease significantly with increasing modulus.
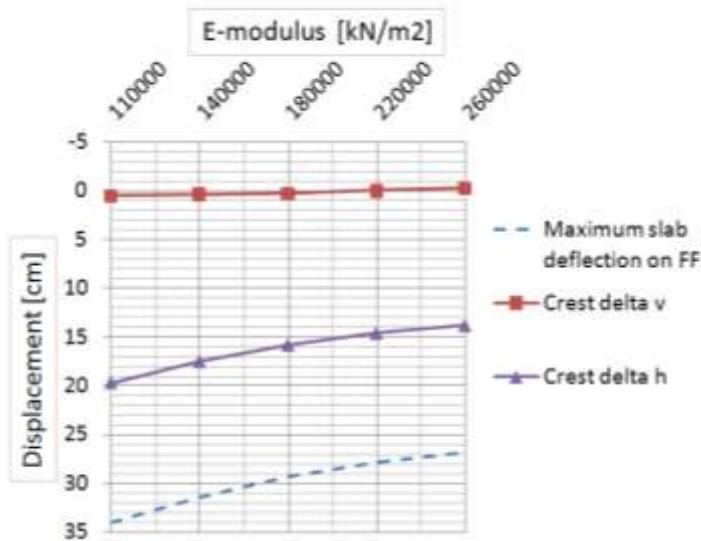
Figure 142 Impact of increasing young's modulus on slab deflection and crest displacement during impoundment in MC model.

Figure 143 shows the impact of varying poisson's ratio on general dam behavior due to first filling. The crest's horizontal displacement remains almost unaffected. The maximum face slab deflection decreases with increasing poisson's ratio. Of special interest is the relation of crest settlement versus poisson's ratio. A poission's ratio exceeding 0,28 result in the crest's uplift. To avoid wrong conclusions, one should bear in mind that the crest's uplifting is mostly due to tail water impoundment and the resulting unloading forces. However, Figure 143 highlights the general trend of decreasing crest settlement with increasing poisson's ratio.

Figure 143 Impact of poisson's ratio on slab deflection and crest displacement during impoundment in MC model.

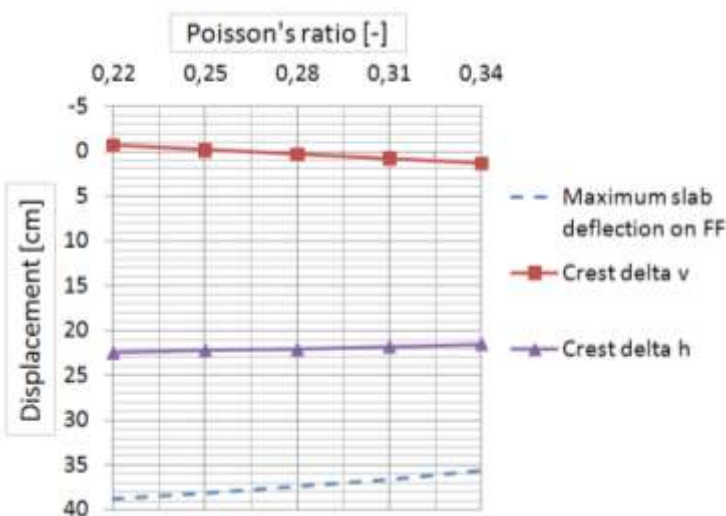# 12 Conclusions

The comparative research of Mohr-Coulomb and Hardening Soil analyses for high strength (i.e. sand gravel) and weak rockfills highlighted some aspects that should be considered in design and numerical modeling the deformation behavior.

According to sand gravel as main fill material and considering the fact, that the applied material parameters reflect its lower boundaries, no plinth/slab cracking as well as joint rupturing will occur during first filling. As long as a two layered reinforcement layout is applied in slab design. However, the analyses do only call for the highest dam sections were the embankment is constructed on alluvial deposits. They do not call for rupturing of the perimetric joint in areas with irregular plinth alignment as well as cracks potentially occurring in the cut off wall.

According to sand gravel fill, MC analyses in general yield in slightly higher deformations than HS analyses do. However, that's not the case for analyses of weaker rockfill, where MC analyses result in smaller settlements in the embankments central part, but lead to higher slab deformations during first filling.

Especially for analyses including weak rockfill, MC model will result in inaccurate results (especially when predicting the crest and slab deformation). This is to be due to the fact that strains are overestimated for small deviatoric stress states and are underestimated for high deviatoric stress states. Hence, utilizing more advanced constitutive models for weak rockfill analysis will result in a more reliable prediction of deformations.

It seams that, MC model underestimates axial strains in marginal curved (i.e. flat) stress strain relations, typically shown by weak rockfills. Whereas, MC model overestimates axial strains in highly curved stress strain relations, typically shown by rockfills of alluvial deposits or rockfills obtained from quarried, high strength rock (assuming that the young's modulus in MC analysis is calculated as 50% secant modulus to a stress strain relation according to the estimated average confining pressure, which is common practice).

Due to the MC model's constant stiffness on un- and reloading, the displacements of all concrete structures during impounding are probably overestimated, regardless if weak or stiff rockfill is modeled.

13 Research

Several very high CFRDs (higher than 140m) have shown large cracks and intensive rupturing of joints in recent years. CFRD construction is following an empirical approach and development is still on the way. There is a lack of information about the stress strain behavior of all sorts of rockfills. Extensive research was undertaken to study and test rockfills in the 1970's and 80's, mainly showing, that solitary laboratory tests cannot deliver sufficient data for deformation analysis. However, they provide general information about the stress-strain behavior, long term behavior or behavior on wetting. Due to the overwhelming amount of parameters affecting the soils behavior, an accurate prediction of a dam's real deformation is not possible to date.

Recent research focuses on wetting deformations, its modeling, statistical evaluation of dam behavior as on triaxial tests for super high CFRD construction (some of them providing a diameter of 30cm). Research on joint details is limited, especially regarding the maximum tolerated deformations of particular waterstops.

Currently an incredible amount of new constitutive models is available, some of them accurately describing the behavior of individual soil types, but all of them having the same problem: Not enough information about suitable input data.

To gain information about appropriate input parameters and to evaluate suitable constitutive models, extensive studies would have to be done. At first extensive information about a dam fill's general behavior has to be gained and class A analysis should be undertaken. Secondly deformation analysis should be updated by deformations observed during construction, to adjust the applied parameters or to back calculate the missing ones. In a last step, the improved parameters should again be modified to ensure the best fit to the observed deformations after impoundment (class C analysis). Frequently back calculated parameter sets for long term observation data or fluctuating reservoir levels could push the research in numerical modeling forward. As this is common practice for some trustworthy operators, publishing these results would push the whole dam society forward. Even publishing pure observation data of dams in operation could be helpful.

14 References

Astete, J., San Martin, L., Alvarez, L. 1992. The Santa Juana CFRD for Irrigation in Northern Chile. *IWP&DC*, April 1992, 42-44.

ATV–DVWK-M502, 2002. Berechnungsverfahren für Staudämme – Wechselwirkung zwischen Bauwerk und Untergrund. Deutsche Vereinigung für Wasserwirtschaft, Abwasser und Abfall eV.

Brandl, H., 1996. Slurry barrier walls for waste containment and contaminated land encapsulation. In: Kamon, M., ed. *Environmental Geotechnics.* Rotterdam, Balkeman, p. 459-466.

CFRD International Society, 2008. Guidelines for Design High Concrete Face Rockfill Dam, (Draft).

Cooke, J.B., (1984). Progress in rockfill dams (18th Terzaghi lecture). *Journal of Geotechnical Engineering*. Vol. 110 (10), pp. 1383-1414.

Cooke, J.B., Sherard J.L., 1987. *Concrete face rockfill dams: design, construction and performance*, USA: ASCE.

Cooke, J.B., 2000. The High CFRD. In: Concrete Face Rockfill Dams, J.Barry Cook Volume, Beijing, China. p. 1-4.

Douglas, K., 2002. *The shear strength of rock masses.* Thesis, (PhD). School of Civil and Environmental Engineering, The University of New South Wales, Sydney.

Duncan, J., Wong, K. and Ozawa, Y., 1980. FEDAM: A computer program for finite element analysis of dams. USA: University of California-Berkley.

EN-1992-1-1, 2004. Eurocode 2: Design of concrete structures – Part 1-1: General rules and rules for buildings.

Fell, R., MacGregor P., Stapledon D. and Graeme B., 2005. *Geotechnical Engineering of Dams*. The Netherlands: A.A. Balkema Publishers Leiden.

Feng, X., and Fu, J., 2009. Study on CFRD Construction Technology with Gravel and its Application in Siping CFRD. In: *1st International Symposium on Rockfill Dams, 20. September 2009 Beijing*. pp. 483-492.

Fitzpatric, M., Cole, B., Kinstler, F., and Knoop, B., 1985. Design of concrete faced rock-fill dams, USA: ASCE Geotechnical Engineering Division, 410-434.

Frutuoso da Silva, A., 2007. *Analises Tridimensionalis de Barragens de Enrocamento com Face de Concreto com Objetivo de Otimizar os Criterios de Projeto*. Thesis, (PhD). Brasil University.

Guidici, S., Herweynen, R. and Quinlan, P. 2000. HEC experiences in concrete faced rockfill dams – past, present and future, *In*: *International Symposium on Concrete Faced Rockfill Dams*, 18.September 2000 Beijing. ICOLD, 2000

Hall, E., and Gordon, B., 1963. Triaxial Testing with Large-Scale High Pressure Equipment. *Laboratory Shear Testing of Soils*. ASTM, p. 329-339.

Holzmann, M., 2008. *Studie zur Anwendbarkeit verschiedener Materialmodelle in der FE-Berechnung von Staudämmen*. Thesis, (MSc). Fakultät für Bauingenierwesen, University of Technology Innsbruck.

Hunter, G., Fell, R., 2002. The Deformation Behavior of Rockfill. Australia: The University of New South Wales.

ICOLD. 1989. Rockfill dams with concrete facing. State-of-the-art. International Commitee on Large Dams, Paris. Bulletin 70.

ICOLD, (2005). Concrete Face Rockfill Dams Concepts for Design and Construction. Draft.

IWP&DC., 2008. CFRD under pressure. *IWP&DC*, Febr. 2008, 27-29.

IWP&DC International Hydro Power & Dam Construction, Yearbook 2009

Kai, W. and Duncan, J., 1974. Hyperbolic stress strain parameters for nonlinear finite element analysis of stresses and movements in soil masses. USA: University of California-Berkley.

Kovacevic, N., 1994. *Numerical Analysis of rockfill dams, cut slopes and road embankments*. Thesis, (PhD). Imperial College of Science, Technology and Medicine, Faculty of Engineering. London.

Kulhawy, F., Duncan, J. and Seed, H., 1969. Finite element analyses of stresses and movements in embankments during construction. USA: University of California, Berkley.

Mackenzie, P. and McDonald, L., 1985.Mangrove Creek Dam: Use of soft rock for rockfill. *In:* Cooke, J. and Sherard, J*., ed. Concrete Face Rockfill Dams, Design, Construction and Performance,* ASCE Geotechnical Engineering Division, p. 208-230.

Marsal, R., 1973. Mechanical properties of rockfill. *In:* Hirschfeld, R. and Poulos, S., ed. *Embankment-dam engineering Casagrande volume.* USA: John Wiley & Sons. p. 109-199.

Marulanda, A. and Pinto, N., 2000. Recent experience on design, construction and performance of CFRD dams. In: Concrete Face Rockfill Dams, J.Barry Cook Volume, Beijing, China. p. 279-315.

Meißner, H., 1991. Recommendation of the Committee on Numerical Methods in Geotechnics of the German Geotechnical Society [in German]. Geotechnik , 1991-14, 1-10.

Montanez-Cartaxo, L.E., 1992. The Perimetric Joint Design for Aquamilpa Dam. *IWP&DC*, April 1992, 22-28.

Mori,R.T., 1999. Deformations and Cracks in Concrete Face Rockfill Dams. *In: Concrete Face Rockfill Dams, Proceedings, Second Symposium on CFRD, October 1999 Florianapolis, Brazil.*

Nobari, E. and Duncan, J., 1972. Effect of reservoir filling on stresses and movements in earth and rockfill dams. Report TE-72-1, University of California, Department of Civil Engineering.

Noguera, G., Bellet, A., Vidal, L., 1999. Design and Construction of Chile's Puclaro Dam. *IWP&DC*, September 1999, 16-19.

Oldecop, L. and Alonso, E., 2007. Theoretical investigation of the time–dependent behavior of rockfill. *Geotechnique 57*, No. 3, 289-301.Thomas, M., (1988). Rockfill Dam Design and Analysis. In: Jansen, R.B., Advanced Dam Engineering. New York: Van Nostrand Reinhold, 372-381.

Palmi, J.and Sixtus, L., 2007. Lessons learned from Mohale. *IWP&DC*, Aug. 2007, 16-25.

Pinto, N.L.S and Filho Marques, P.L. 1998. Estimating the maximum face slab deflection in CFRDs. *Hydro Power & Dams*, Volume 5, No. 6, 28-31.

Pinkerton, I.L., Soetomo, S. and Matsui, Y., 1985. Design of Cirata concrete face rockfill dam. In: Cooke, J.B. and Sherard, J.L., ed. Concrete Face Rockfill Dams. Design, Construction and Performance*,* ASCE Geotechnical Engineering Division, p.642-656.

Plaxis,. 2009. Plaxis 2D material models manual version 9.0

Potts, D., Zdravkovic, L. 2001. Finite element analysis in geotechnical engineering Application. UK: Thomas Telford Publishing.

Potts, D., Zdravkovic, L. 1999. Finite element analysis in geotechnical engineering Theory. UK: Thomas Telford Publishing.

Pritchrad, S., 2008. Taking the Empirical Approach. *IWP&DC*, Febr. 2008, 22-25.

Resende, F., Materon, B., 2000. Ita Method-New Construction Technology for the Transition Zone of CFRD's. *In: CFRD 2000, Proceedings, International Symposium on Concrete Faced Rockfill Dams,* 18 September 2000 Beijing, China. p. 459-470.

Schanz, T., Vermeer, P.A., Bonnier, P.G., (1999). The hardening soil model: Formulation and verification. In: R.B.J. Brinkgreve, Beyond 2000 in Computational Geotechnics. Balkeman, Rotterdam: p. 281-290.

Sherard, J., 1985. The upstream zone in concrete faced rockfill dams. *In:* Cooke, J.B. and Sherard, J.L*., ed. Concrete Face Rockfill Dams, Design, Construction and Performance,* ASCE Geotechnical Engineering Division, p. 618-641.

Terzaghi, K., 1960. Discussion on: I.C. Steele and J.B. Cooke, Rockfill dams: Salt Springs and Lower Bear River concrete face dams. *In: American Society of Civil Engineering Proceedings, vol. 86, No. Pol*. p. 65-74.

United States Society on Dams, 2007. Strength of Materials for Embankment Dams.

USBR. 1961. Laboratory tests of rock cores from the foundation of Shihmem dam Taiwan, Formosa. *Concrete Laboratory Report No. C-1157*, United States Department of the Interior Bureau of Reclamation.

Valencia, G.F. and Sandoval, E.M. 1997. Aquamilpa Dam Behavior. In: *Proceedings of Seventeenth Annual USCOLD Lecture Series, Non Soil Water Barriers for Embankment Dams.* San Diego, California, 133-147.

Wang, Y., andQu, L., 2000. Design Principle and Method of Seepage Control of Wuluwati High Concrete Faced Sandy Gravel Rockfill Dam. *In*: *International Symposium on Concrete Faced Rockfill Dams, 18.September 2000 Beijing*. ICOLD, 2000. pp. 425-437.

Yan, L. 20. Construction of the Concrete-Faced Sand-Gravel Dam of the Wuluwati Water Pivotal Project. *In*: *International Symposium on Concrete Faced Rockfill Dams*, 18.September 2000 Beijing. ICOLD, 2000. pp. 519-530.

Zeping, Xu., 2000. Three dimensional stress and deformation analysis of Wuluwati CFRD. *In*: *International Symposium on Concrete Faced Rockfill Dams*, 18.September 2000 Beijing. ICOLD, 2000. pp. 381-425.

15 Certification

I certify that the ideas, designs and experimental work, results, analyses and conclusions set out in this master thesis are entirely my own effort, except where otherwise indicated and acknowledged.

I further certify that the work is original and has not been previously submitted for assessment in any other course or institution, except where specifically stated.

_____   _____

Place, Date   Signature